THE PROTEOMIC RESPONSE OF THE *CARCINUS MAENAS* Y-ORGAN OVER THE COURSE OF THE MOLT CYCLE

A Thesis

presented to

the Faculty of California Polytechnic State University,

San Luis Obispo

In Partial Fulfillment

of the Requirements for the Degree

Master of Science in Biology

by

Mark Stephen Hamer

February 2015

COMMITTEE MEMBERSHIP

TITLE:	The proteomic response of the *Carcinus maenas* Y-organ over the course of the molt cycle
AUTHOR:	Mark Stephen Hamer
DATE SUBMITTED:	February 2015
COMMITTEE CHAIR:	Lars Tomanek, PhD Associate Professor, California Polytechnic State University
COMMITTEE MEMBER:	Donald Mykles, PhD Associate Professor, Colorado State University
COMMITTEE MEMBER:	Kristin Hardy, PhD Assistant Professor, California Polytechnic State University

ABSTRACT

The proteomic response of the *Carcinus maenas* Y-organ

over the course of the molt cycle

Mark Stephen Hamer

Molting in arthropods is a complex process governed by regulatory mechanisms that have evolved and adapted over millennia to allow these animals to grow, despite being confined by a hardened exoskeleton. We isolated the molt-regulating Y-organs (YO) from the common shore crab *Carcinus maenas* at molt stages B, C_{1-3}, C_4, and D_0 to assess how changes in protein abundances might underline the unique physiology of each of these stages. We found that changes in protein abundance were most notable in the postmolt stages (B and C_{1-3}), where an increase in energy metabolism and the reactive oxygen species stress (ROS) response proteins was observed. An increase in triosephosphate isomerase and transketolase suggest that the postmolt YO is participating in triglycerides storage and is also actively recycling excess ribose sugars manufactured during the YO's previously activated state. We also propose as mechanism through which ROS-induced release of cyclophilin A may contribute to YO atrophy during postmolt through the remodeling of structural proteins such as collagen. We support the standing observation of YO atrophy during postmolt by drawing attention to hemolymph protein abundances, especially those of cryptocyanin isoforms, which dropped precipitously in intermolt (C_4) and remained at low abundances into early premolt (D_0). Finally, though our evidence is preliminary, we propose that future investigations into the YO proteome address the significance of the protein glutamate dehydrogenase. Glutamate dehydrogenase, a key enzyme involved in the formation of glutamate, represents a potential nutrient-sensing checkpoint that might be involved in YO activation. Historically, most attention has gone to the acute molt stages, where signaling mechanisms involved in the activation of the YO have been the focus. Here, we present data suggesting that other regulatory mechanism may be governing the atrophy the postmolt YO. A better understanding of crustacean physiology has the potential to benefit ecosystems and economies worldwide.

Key Words: *Carcinus maenas*, molting, Y-organ, ROS

AKNOWLEDGMENTS

I would like to first and foremost thank my family for their unending support through all of life's ups and downs. I have been so fortunate to have so much love in my life from Mary, Paul, and Kailey Hamer. I can't imagine of a better group of people to have on my side as I've grown. Thank you for always inspiring positivity and a sense of wonder in the world around me. I love you.

To Tori, thank you for your support and patience. You have been such a positive influence on me the past five years of my life. You've opened my mind to so many new experiences and our adventures together have been only the best. Je t'aime ma petite crevette.

To all of my friends, "they were the best of times, and they were the worst of times, but mostly they were the best of times." I love you guys.

I would also like to thank Don Mykles for including me as a part of his NSF proposal and to Lars Tomanek for his invitation to Cal Poly and the introduction to the field of proteomics.

TABLE OF CONTENTS

LIST OF TABLES

LIST OF FIGURES

Figure Page

Figure Page

Figure Page

Figure Page

I. INTRODUCTION

In this study we explore the crustacean growth mechanisms using *Carcinus maenas,* the common green shore crab, as our model. *Carcinus maenas* has been used in studies of crustacean growth (e.g. molting) and population dynamics for over a century. Many of the preliminary physiological observations made concerning crustacean growth were performed on *C. maenas*. The extensive background information that exists on its physiology, along with its worldwide invasive distribution, makes it an ideal candidate for exploration of the molecular mechanisms that control crustacean growth.

In *C. maenas* growth occurs through a process termed molting. The molting process is characterized by the shedding of the old exoskeleton. The animal then emerges with a new soft exoskeleton capable of growth though the uptake of water. This process is regulated by a pair of endocrine/autocrine organs called Y-organs (YO). When activated, these organs produce hormones that stimulate the physiological cascade that ends in the molt. The work of other labs has helped to identify and explore the roles of various signaling molecules and isolated pathways, but to our knowledge none have addressed the proteome of the Y-organ as a whole. Thus, our goal in this study to define the proteome of the YO in an attempt to better understand its function over the course of the molt cycle, in both a molecular and physiological context. Over the past 20 years, proteomics has developed into an extremely powerful exploratory tool. It is especially useful in its ability to provide detailed, unbiased results from which novel hypotheses about tissue function can be derived. In this study we have employed the use of proteomic techniques to assess changes in protein abundance as they occur over the course of the molt cycle in the Y-organ of *C. maenas*.

The purpose of this introductory chapter is to provide the reader with the background to the ecology, physiology and molecular processes known to regulate molting of the study organism. We will also describe the analytical tools we employed to identify changes in the proteome of the Y-organ. The first section will discuss *C. maenas* ecology and physiology. The next will give a detailed account of what is currently known about the regulation of growth and the activation state of the Y-organ. We will conclude with a section on the proteomic workflow, including a review of MALDI-ToF/ToF tandem mass spectrometry. The results of this study provide evidence supporting the roles of unique intracellular mechanisms accompanying individual molt stages, and thus growth of the organism as a whole. Elucidating the physiological mechanisms that determine growth in crustaceans through analysis of the proteome will provide insights into the processes that affect the developmental successes of crustaceans

Carcinus maenas ecology and general physiology

The European green shore crab, *Carcinus maenas*, belongs to the phylogenetic infraorder Brachyura (McLaughlin, 2005). Its native range spans from the Atlantic coast of Scandinavia to northern Africa (Roman, 2004). Today, this eurythermic decapod crustacean thrives in intertidal zones worldwide (Figure 1), a result of anthropogenic introduction events recurring over the past 200 years (Darling et al., 2008; Klassen et al., 2007). It is a highly mobile and adaptable predator with opportunistic feeding habits determined by availability of other littoral prey items (Roman, 2006). Still, its preferred food source consists predominantly of mollusks and other crustaceans (Klassen et al., 2007). High fecundity and extraordinary resilience to a fluctuating physical environment

result in larvae that may be carried long distances in the ballast water of ships or even in contaminated airplane cargo (Roman and Palumbi, 2004). This has lead to the establishment of *C. maenas* populations on the coastline's of the Americas, Asia, South Africa, and Australia (Darling et al., 2008). The combined environmental resilience and pervasive availability of this species makes it a suitable model organism for the study of invasion dynamics, thermotolerance assessments, and investigations into hormonally regulated intracellular pathways (Chang and Mykles, 2011; Kelley et al., 2011; Roman and Darling, 2007; Skinner, 1985a).

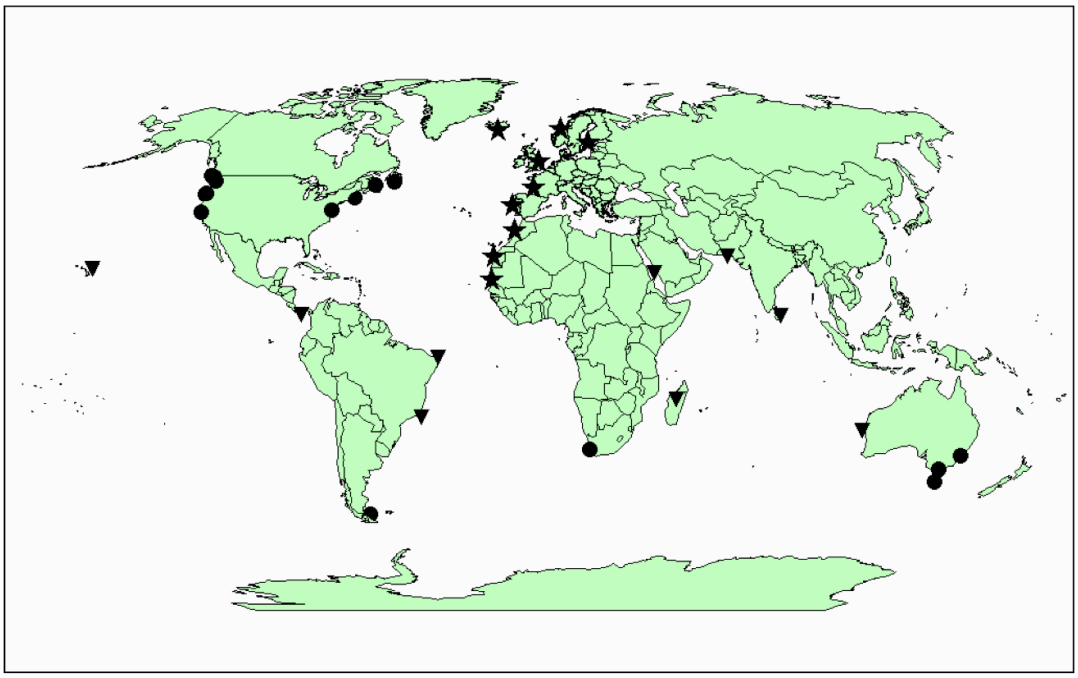

Figure 1. Worldwide distribution of green crabs. Stars indicate native range. Circles indicate successful establishment of an introduced population. Triangles indicate failed introductions (Adapted from Klassen et al., 2007).

The exoskeleton of arthropods consists of a chitinous matrix that, once hardened, is incapable of further growth (Lachaise et al., 1993). Thus, for the animal to achieve growth, it must escape the confines of its old exoskeleton and temporarily allow the soft

underlying tissue to uptake water and expand (Chang and Mykles, 2011). This process, termed ecdysis, is the culminating event in the crustacean molt cycle and was first defined by the French biologist Pierre Drach in 1939 (Drach and Tchernigovtzeff, 1967). The entire process must be performed succinctly and is thus under tight regulatory control. The exoskeleton remains pliable for about a week following ecdysis, but the chelipeds, cutting mandibles, and maxillipeds are targeted for immediate hardening due to the self-evident roles in feeding and defense (Spees et al., 2003). The process is primarily regulated through a tropic hormonal mechanism involving molt-inhibiting hormone (MIH) and the pro-molting hormone, ecdysteroid (Skinner and Graham, 1972).

A basic understanding of crustacean growth processes is fundamental for those involved in crustacean aquaculture (Gillespie and Station, 2007). Given the importance of many crustacean species in structuring food webs, it is also of great interest to those involved in ecosystem management and conservation (Pascoal et al., 2009). Negative economic impacts of *C. maenas* invasions on marine aquaculture have already been predicted and will only worsen in coming years (Grosholz and Ruiz, 1995; Walton et al., 2002). Likewise, native species living in fragile marine ecosystems that have been invaded are under constant threat from *C. maenas* populations (Roman and Palumbi, 2004; Walton et al., 2002). In either case, informed decision-making requires detailed understanding of the regulatory aspects of crustacean growth.

In this section we take a closer look at three major aspects of *C. maenas* biology as they relate to our investigation. The focus will initially be on describing the fundamental aspects of *C. maenas* ecology, exploring attributes that make it so successful as an invasive species. This will segue into a discussion on the population biology of this

species – again, key to its success as a global invader. We will end with a general introduction of this species' physiology, with a focus on defining terminology related to molting and a review on the intricate aspects of this fascinating biological process.

Carcinus maenas ecology and invasive propensity

Today, *Carcinus maenas* exists as a cosmopolitan species stemming from a native population that continues to thrive along the north Atlantic coastlines of Africa and Europe (Klassen et al., 2007). Considerations of the development, ecology, genetic diversity, feeding strategies, and inhabitable ranges can help explain the invasive successes experienced by *C. maenas* over the past two centuries.

To make inferences about potential impacts that developmental life stages have on the successful establishment of invasive *C. maenas* populations, we should first describe its life cycle. The mating season for this species is widely variable, ranging anywhere from a couple of months to year-round (Klassen et al., 2007). Most of the variation seen in length of mating season have been attributed to seasonal water temperature fluctuations (Dawirs et al., 1986). Like other brachyuran crab species, female *C. maenas* release a potent sex pheromone in their urine just prior to molting (Berrill, 1982). This attracts males, the largest of which will guard her until she has finished molting, when he will then copulate with her (Berrill and Arsenault, 1982). This mating ritual not only offers protection to the vulnerable postmolt female but also ensures mating rights to a single male, who will diligently guard her by exercising a copulatory embrace that lasts long after the actual event of copulation occurs (Berrill and Arsenault, 1982).

Female *C. maenas* can yield multiple egg clutches producing upwards of 200,000 total eggs per year (Domingues et al., 2011). Once fertilized, the female carries these eggs on her abdominally located pleopeds (swimming legs) for the next couple of months until free-swimming larval zoeae hatch and are released into the open sea (Klassen et al., 2007). Zoeae represent a series of non-reproducing planktonic larvae that develop through a total of four stages over the next four to six weeks (Nagaraj, 1993). They inhabit coastal open water and can be found at depths ranging from 20 to 45 meters, depending on the time of day (Queiroga, 1998). Abiotic conditions such as water salinity and temperature are important factors that affect the survival and growth of the animal during these life stages (Nagaraj, 1993). The zoeae protect themselves from unfavorable water conditions via vertical migration within the water column (Queiroga et al., 1997). Once development through all zoeae stages is complete, a final metamorphosis into a post-larval megalopa stage begins. At this point the animal settles to the ocean floor where it prepares itself for a final transformation into the benthic adult stage (Baeta et al., 2005). This adult will continue to grow via molting for the rest of its life. The process from hatchling to benthic adult can take anywhere from 27 to 54 days, depending primarily on water temperature (Dawirs et al., 1986; Klassen et al., 2007).

Pelagic zoeal larvae continue to be the primary source of invasive *C. maenas* populations (Gillespie and Station, 2007). Ballast water taken on by ships in shallow harbors and ports where *C. maenas* zoeae are present facilitate their transportation of animals in this life stage over great distances and time spans (Cohen and Carlton, 1995). Once on-board, survival rates are relatively high due to their resilience to stresses like temperature, dissolved oxygen and salinity (Cohen and Carlton, 1995; Nagaraj, 1993).

In 1996 the United States passed H.R. 4283, "The National Invasive Species Act" into law. The act was designed to specifically address the subject of invasive species' sullying the ballast water of ships. Unfortunately, the act expired in 2002 and is no longer enforceable by law. Recent private campaigns have attempted to maintain awareness of the hazards involved with improper ballast expulsion, but the lack of legislation makes any formal legal regulation impossible. Regardless of past or future regulation, *C. maenas* has already established permanent populations in bays, estuaries and other coastal marine areas worldwide. (Cohen and Carlton, 1995).

The genetic structure of introduced populations of *C. maenas* provides further evidence of this species' strength in establishing, maintaining, and even expanding upon new non-native populations (Pringle et al., 2011). Successful colonization of a new locale is often hindered by the founder effect, where genetic diversity within the smaller colonizing population is significantly reduced compared to that of the original population. Thus, species that are established through single introduction events usually suffer in their ability to adapt to the new environment, especially if conditions are more extreme than the phenotypes present have evolved to cope (Roman, 2006). For *C. maenas*, repeated (or multiple) (re-)introductions through fouled ballast water, as well as other anthropogenic sources, have allowed invasive populations to retain a reasonable amount of genetic diversity (Roman and Darling, 2007). In addition, zoeal migrations made possible by ocean currents provide this species with a natural source of genetic drift that further connects populations that would otherwise be reproductively isolated (Pascoal et al., 2009; Roman and Darling, 2007). What's more, even populations that do display relatively low genetic diversity have shown a remarkable ability to persist in non-native

environments (Tepolt et al., 2009). In the American Northwest, a large cold-water adapted population may have already arisen as a result of a phenotypic divergence from the founding population (Kelley et al., 2011).

The introduction of a species to a non-native habitat does by no means imply it will persist there, let alone thrive and expand. The evolutionary relationship an organism shares with its environment is one that establishes a framework of conditions through which survival is possible. For some species these conditions might overlap with the conditions of other geographical regions, allowing for invasions to occur. *Carcinus maenas* is one such species. The native range of *C. maenas* is composed of vast areas of coastline with widely varying topography ranging from calm marshy estuaries to weatherworn rocky outcroppings (Domingues et al., 2011). Regardless of the geography, adults inhabit the intertidal zone and can be found from the high tide mark to a depth of 5 to 6 meters (Klassen et al., 2007). Water temperature and salinity in its native environment also vary considerably. It can survive temperatures ranging from 0°C to 35 °C, though it is only reproductively viable between 18°C and 26°C (Klassen et al., 2007). A fantastic example of a euryhaline organism, it can tolerate salinities ranging from 4 to 52 psu (practical salinity units) (Klassen et al., 2007). The dynamic nature of its native environment must surely be considered as another important aspect *C. maenas*' inclination to invade foreign coastlines.

If we might add yet another reason for the success of *C. maenas* as an invader then it should be a brief mentioning of its diet. The ability for an invasive species to acquire food in its new environment is imperative to its perseverance there. Native *C. maenas* populations are opportunistic predators that show rank-ordering preference for

molluscs, crustaceans, polychaetes, and green algae (Grosholz and Ruiz, 1996). The feeding habits and preferences of these invasive populations seem to correspond with those living under native habitat conditions (Grosholz and Ruiz, 1996; Klassen et al., 2007). Of course, introduced populations are also presented with novel prey items, some of which are economically vital to those whose livelihoods are based on aquaculture and fishing. The feeding preferences of *C. maenas* have been highlighted as a concern for communities since many bivalves are preferentially targeted as prey (Yamada et al., 2005).

Any ecological analysis of an invasive species is a daunting task, especially when that species is continually presented as one of the world's top 100 alien invaders (Gillespie and Station, 2007; Grosholz and Ruiz, 1996; Klassen et al., 2007). Though the life cycle and reproductive strategies employed by *C. maenas* are relevant to its invasive proclivity, they are not at all unique from other marine organisms. In fact, species that employ alternative reproductive strategies, such as broadcast spawning, might theoretically make more effective invaders (Huxel, 1999). It is for this reason that we have taken into consideration other relevant aspects of *C. maenas* ecology. Genetic structure, a general resilience to the external environment, and dietary plasticity have all significantly contributed to the expansion of this species into intertidal zones worldwide (Grosholz and Ruiz, 1996; Kelley et al., 2011; Klassen et al., 2007).

General C. maenas physiology and introduction to molting physiology

One of the attractive aspects of using *C. maenas* as a study organism is the substantial amount of background information available on this organism's physiology.

In fact, fundamental descriptions of its anatomy and physiology can be traced back as far as the 19th century and have been undergoing continual refinement ever since (Crothers, 1967). In this section we will review the basic anatomy and physiology of the infraorder Brachyura, placing as much specificity on *C. maenas* as the available literature will allow. This necessitates an initial discussion on gross anatomy to familiarize the reader with the terminology that will be used throughout the remainder of the section. After this, the focus will turn to a description of crustacean growth. In this chapter we will focus on the physiological aspect of molting, saving the cellular and biochemical mechanisms of this process for the following chapter, where they will be explored in-depth.

Like other arthropods, *C. maenas* shares the developmental three-part super-structural segmentation pattern seen in all other members of this phylum, which consist of a head, a thorax, and an abdomen (VanHook and Patel, 2008). As with other members of Crustacea, the body plan of adult *C. maenas* has somewhat diverged from that of other arthropods. Most notably, the head and thorax are fused into a cephalothorax, which makes up the majority of the animal's body (Crothers, 1967). The abdomen is reduced and ventrally tucked against the posterior of the thorax. As the name implies, this decapod crustacean has a total of ten bilateral "walking legs", two of which, termed chelae, are specialized for tasks like feeding and defense (Crothers, 1967). The remaining legs, which really are used for movement, are termed pereiopods. Other specialized appendages include sensory antennae, cutting mandibles, food-handling maxillipeds and maxillae, flow-inducing respiratory scaphognathites, and copulatory/egg carrying pleopods (Figure 2) (Crothers, 1967).

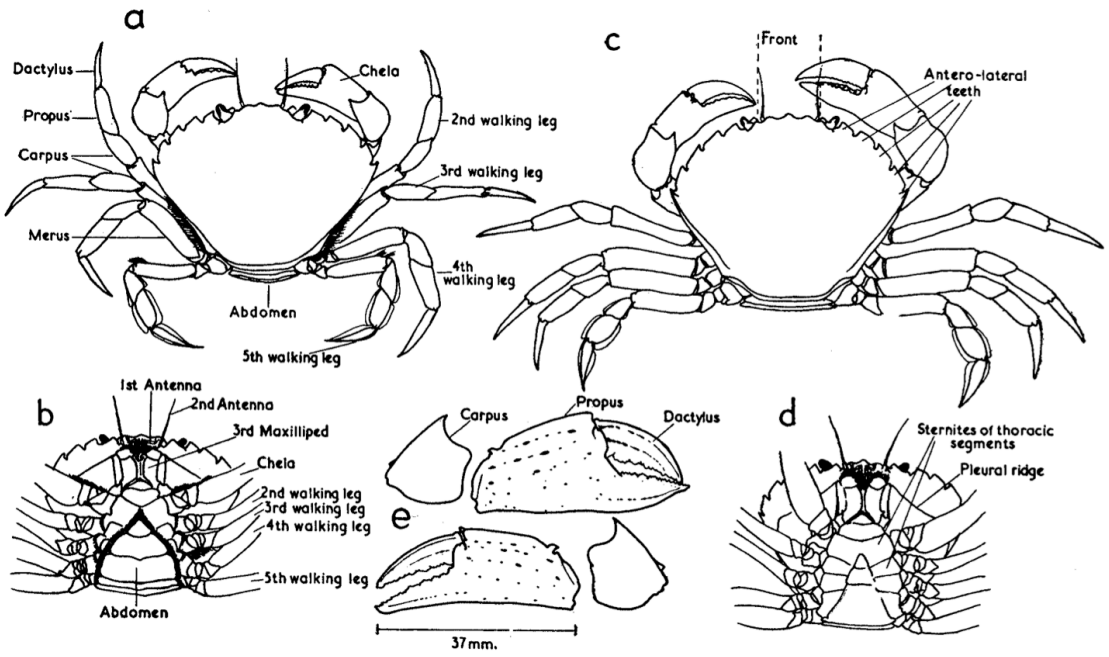

Figure 2. A) Female dorsal surface B) Female ventral surface C) Male dorsal surface D) Male ventral surface E) Chelae of a large male specimen (adapted from Crothers, 1968). Not pictured, but very near to the maxillipeds shown, are the maxillae and mandibles. Also in the region, but internal and positioned laterally, would be the flow-inducing respiratory scaphognathites. Copulatory/egg carrying pleopods are hidden beneath the tucked abdomen.

The exterior of *C. maenas* is covered in a hard exoskeleton composed of equal parts protein and chitin (Skinner, 1962). The most notable structure, called the carapace, covers the entire dorsal side of the animal and houses the animal's main body cavity. The primary structure of the exoskeleton is that of a superficial calcified cuticle with a basally located living epidermal layer (Skinner, 1962; Terwilliger and Ryan, 2006). The exoskeleton is composed of three primary layers; the epicuticle, which comes in direct contact with the environment followed the more basal exocuticle, endocuticle, and membranous layer (Skinner, 1962). Beneath these non-living layers is the epidermis, which functions in the synthesis and repair of the more superficial layers throughout the crustaceans' life.

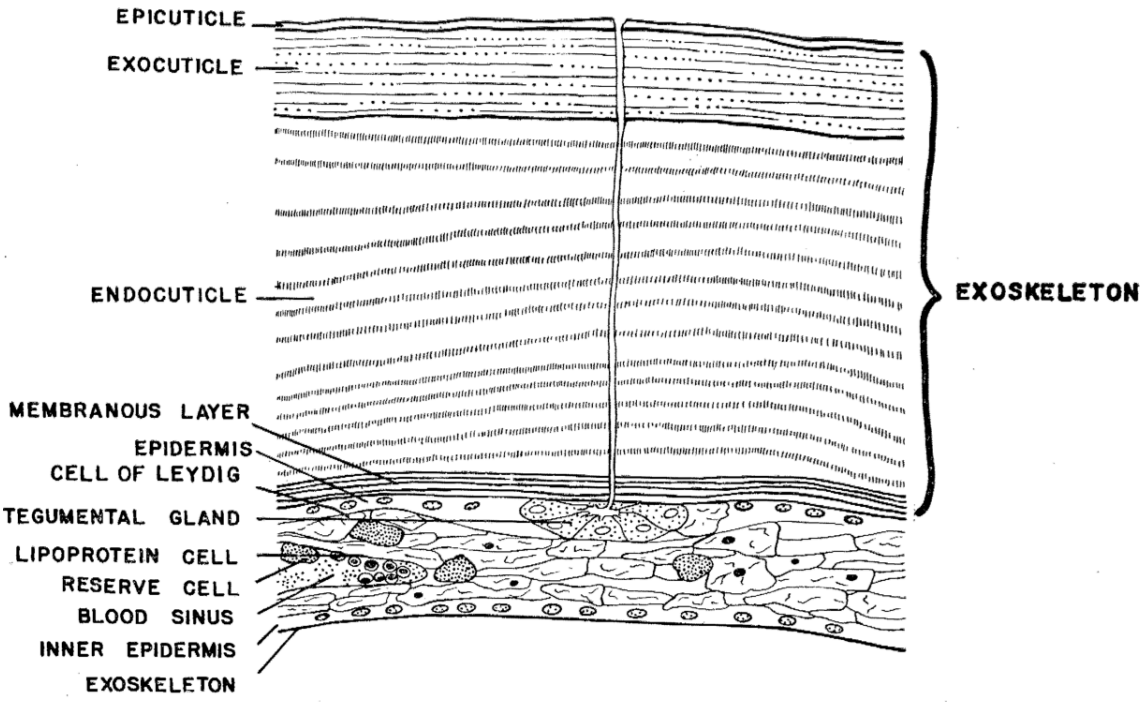

Figure 3. Diagrammatic cross-section of the integumentary tissue of an intermolt *Gecarcinus*, drawn to scale. The epidermal layer described is the one adjacent to the thick outer exoskeleton. 100 X magnification (Adapted from Skinner, 1962).

The carapace of *C. maenas* can provide other useful information to those observing it. Degradation of the pigment molecules present in the carapace progresses in animals that have endured longer periods between molts (Reid et al., 1997). The coloration in the species can range from dark green, in newly molted animals, to bright red in later stages of the molt cycle. Newly molted animals show greater resilience to environmental stressors at the cost of reduced chelae and carapace thickness (Reid et al., 1997). Thus, coloration can be used as a proxy for survival and mating success across individuals (Reid et al., 1997; Todd et al., 2005). Studies addressing the significance of color morph often times contradict each other and leave the reader with more questions

than answers (Abuhagr et al., 2014; Tepolt et al., 2009; Todd et al., 2005). Future studies might address the issue by comparing the two color morphs using proteomics, or even metabolomics, over transcriptomics where a physiological difference such as carapace color may not be apparent.

Size in this species is usually expressed in terms of carapace width (CW). During the first few molt cycles adults are fairly small, having a CW of only a couple millimeters, but grow significantly larger as they age (Berrill and Arsenault, 1982). Males as large as 9 cm CW have been recorded (Klassen et al., 2007). Regardless of gender, the average sexually mature adult crab's CW is likely to fall with the range of 30-60 mm (Crothers, 1968, Baeta et al., 2005; Berrill and Arsenault, 1982). On average, males are 1 cm larger than sexually mature females of the same age (Baeta et al., 2005; Berrill and Arsenault, 1982). This is reflected by observations of copulatory pairs in which the male is always measurably larger than the female (Berrill and Arsenault, 1982). That said, temperature has a drastic effects on global growth patterns throughout *C. maenas* development (Berrill and Arsenault, 1982; Dawirs et al., 1986; Yamada and Gillespie, 2008). This is supported by studies showing that populations inhabiting colder climates show significantly longer generational times and lifespans and exhibit slower growth rates (Berrill and Arsenault, 1982).

Up until this point we have avoided discussing the internal anatomy of *C. maenas*. We will now turn our attention to the molting process along with its physiology, which will require the introduction of certain organs and organ systems. Due to its important role in the transport of the pro-molting hormone, ecdysteroid, we will initially describe the crustacean circulatory systems. Next, the organ responsible for synthesis of this

hormone will be described. The remainder of these systems will be described, as is necessary, within the context of our discussion. Still, the primary goal of this section is to introduce the process of molting, one of the most extraordinarily fascinating and complex events any organism can undertake.

Nutrients and oxygen are delivered to the internal organs of *C. maenas* through a circulatory system whose primary component is the copper-containing, oxygen-binding protein hemocyanin (Lachaise et al., 1993; Reiber and McGaw, 2009; Terwilliger and Ryan, 2006). This protein, along with nutrients and other blood proteins make up a blood-like fluid known collectively as the hemolymph. Unlike insects whose complex branched tracheal network allows for direct diffusion-based oxygen transport, crustaceans rely on a circulatory system that is rather unique. Recent use of a specialized casting technique has allowed for the mapping of what has now been termed an "incomplete" closed circulatory system (Reiber and McGaw, 2009). In this system hemolymph is circulated through tissues in one of two ways. In the brain and antennal complexes hemolymph passes through complete capillary beds, as it would in any typical closed circulatory system. In other tissues, hemolymph is pumped through arterial extensions that end in collecting sinus structures, eventually leading to heart-bound veins. The lack of endothelium in these sinuses explains the historical presumption of a "sluggish and poorly regulated" circulatory system (Reiber and McGaw, 2009). In fact, the well-defined structure of these sinuses (see Figure 3) form lacunae that are functionally and morphologically similar to capillaries, despite their histological dissimilarity (Reiber and McGaw, 2009). The circulatory systems of decapod crustaceans, including that of *C. maenas* should be appreciated not just for their complexity though. This system, and the

hemolymph that flows through it, also play an important role in the transport of oxygen, nutrients, and hormones to tissues and organs throughout the organism.

As alluded to, ecdysteroid is a hormone that plays a central role in the entire *C. maenas* molt cycle. Before introducing the molt stages in more depth, I will introduce the organ responsible for the synthesis of ecdysteroid, the Y-organ (YO). The YO is a small globular endocrine/autocrine organ located within the anterior region of the cephalothorax, near the brain (Figure 4) (Hopkins, 2012). In all brachyuran crabs its primary purpose is the synthesis and subsequent release of the steroid pro-hormone, ecdysone, into the hemolymph. Once released, ecdysone is immediately converted into the functional molting hormone ecdysteroid, specifically 25-deoxyecdysone in *C. maenas*, by periphery tissues. It is then transported to integumentary tissue where it stimulates processes involved in ecdysis (Mykles et al., 2010).

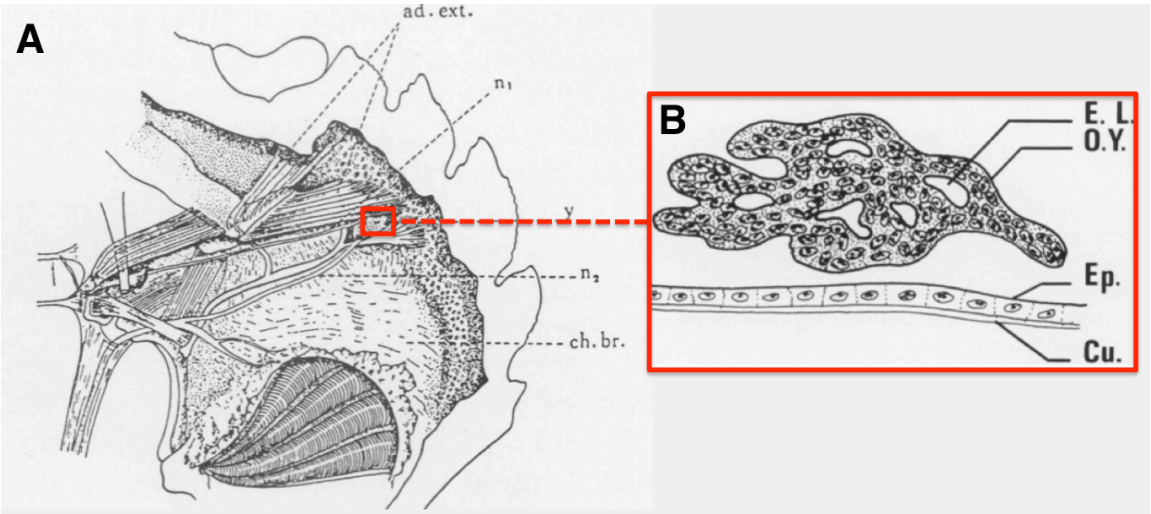

Figure 4. A) Dorsal view of the *Carcinus maenas* gross anatomy showing the location of the Y-organ. The top of the figure represents the anterior of the animal. Ad. ext. = external adductor muscle of mandible, ch. br. = branchial chamber, nl&n2 = nerves; Y = YO. B) Y-organ structure of *C. maenas*; Cu = cuticle, EL = blood sinus, Ep = epidermis; OY = YO. (Adapted from Skinner, 1985)

Synthesis and release of ecdysone from the YO is regulated through the actions of another hormone called molt-inhibiting hormone, or MIH. A peptide hormone, MIH is produced by neurosecretory cells of the X-organ/Sinus Gland (XO/SG) complex located in the animal's eyestalks (Lee et al., 2007a). MIH acts to inhibit molting by binding to its receptor located on the surface of the YO and inhibiting transcription of genes involved in ecdysteroid synthesis (Nakatsuji et al., 2009). In most decapod crustaceans, eyestalk ablation (ESA) removes the primary source of MIH and the animal molts. *Carcinus maenas*, however, does not follow this general trend (Abuhagr et al., 2014). We will return to the molecular and biochemical pathways involved in MIH and YO activation in the next section. Hemolymph ecdysteroid titers are the primary driving force behind the crustacean molt cycle. We will now examine the different stages of this cycle and their physiological outcomes.

The rigid exoskeleton of decapod crustaceans requires the animal shed its extracellular cuticle in order to grow (Skinner, 1966). The end result of this molting process is ecdysis, where the animal emerges from the confines of its old cuticle with a fresh soft cuticle capable of temporary growth through the absorption of water (Mykles, 1980). In order for ecdysis to occur it is compulsory that the connective tissue between the old and new exoskeleton be relaxed and broken down (Skinner, 1985b). Over the course of several molt stages crustaceans activate or suppress the release of a range of molt-regulating hormones, including MIH and ecdysteroid, into the hemolymph. The terminal step in this process is the release of ecdysteroid from the YO (Chang and Mykles, 2011). As the name implies, ecdysteroid binds to and activates an intracellular

ecdysteroid receptor (EcR/RXR), facilitating processes required for the culminating step of ecdysis (Kim, 2005; Skinner, 1962; Mykles 2011).

Ecdysis itself happens over a very brief period of time; sometimes in only a few minutes (Chang, 1995). Nevertheless, before it can occur, the animal must first pass through a series of discreet molt stages that have been assigned alphabetical labels. It should be noted that much of the past work on molting physiology has been performed using another decapod crustacean, *Gecarcinus lateralis* (Skinner, 1985b). The time periods we provide are taken from these studies, so they should only be used as a proxy for those in *C. maenas*. Stages A, B and C_{1-3} represent the postmolt stages following ecdysis. Stage C_4, intermolt, is a period of anecdysis during which the crab spends the majority of its life. YO activation, discussed later, marks the beginning of premolt, a series of preparatory stages leading to ecdysis. Premolt is separated further into three distinct stages: early premolt (D_0), mid premolt (D_{1-2}) and late premolt (D_{3-4}). Ecdysis marks the end of premolt and the completion of the molt cycle (Chang and Mykles, 2011). As has already been mentioned, much of the regulation involved in the advancement through these molt stages is under the control of the YO. Consequently, as we explain each molt stage we will pay special attention to the morphological and physiological changes occurring in the YO.

Immediately following ecdysis, the animal enters a series of three postmolt stages (Stages A and B and C_{1-3}). During these stages the animal is most vulnerable to predators. It is therefore crucial that it rapidly advances through the necessary water-absorption phase, then, immediately begin hardening its most crucial body components. Stage A, which lasts only a day, is noted by a reduction in size of the epidermal cell layer that sits

just basal to the newly forming exoskeleton. The cuticle itself has "the consistency of a soft membrane" during this stage and is actively absorbing water from the environment (Drach and Tchernigovtzeff, 1967). The rapid absorption of water at this stage causes observable growth – up to 30% in carapace width (Crothers, 1967). The YO, having just gone through its most active ecdysteroidogenic phase, atrophies (Chang and Mykles, 2011). As it does, it re-enters a basal state and it once again becomes sensitive to the inhibitory effects of MIH (Asazuma et al., 2009). The result is a precipitous drop in the YO's ecdysteroidogenic capacity and a transcript-level reduction of ecdysteroidogenic genes (Chang and Mykles, 2011).

The next post molt stage, stage B, picks up where stage A ends and proceeds over the course of the next month or so (Skinner, 1985b). The joints proximal to the chelae are much smaller than the claws themselves. Thus, if the crab is to successfully molt with intact chelae, it must degrade the muscles in these appendages to allow clearance as the animal escapes the confines of its old exoskeleton (Chang and Mykles, 2011; Skinner, 1966). The degradation of these muscles, while necessary, requires that new muscle be synthesized during postmolt (Skinner, 1966). This process begins here in stage B and continues through the remainder of postmolt. The YO remains in its basal state during this stage as it will throughout the rest of postmolt and intermolt (Chang and Mykles, 2011). Stage B is also noted by synthesis of the endocuticle. Continual synthesis and calcification of the endocuticle by the epidermis, occurs at a rate of approximately 7 μm per day (Skinner, 1985b). Preference is given to tissues most crucial to defense and feeding, so that the hardening process begins at the tips of the appendages and works its

way inwards (Crothers, 1967). Even at the end of stage B, the main carapace remains soft in certain places (Drach and Tchernigovtzeff, 1967).

It is over the course of the final postmolt stage, C_{1-3}, that the animal completely hardens the remainder of its exoskeleton. Progression through C_1 and C_2 shows continued hardening of the tegument (Skinner, 1985a). Synthesis of new muscle tissue also continues over the course of this stage (Drach and Tchernigovtzeff, 1967; Skinner, 1966). In C_3, final tegument rigidity is achieved but the membranous layer separating it from the basal epidermis has not yet formed. The eventual formation of this layer marks the final transition into intermolt, stage C_4 (Skinner, 1985a).

The crab now enters the longest period of the molt cycle, intermolt. During C_4 the YO remains highly sensitive to MIH, thus keeping it in an inactive state (Chang and Mykles, 2011). The inactivity means that ecdysteroid titers in the hemolymph remain low over the entirety of this stage. This stage can last over half a year and is a time during which the crab's primary focus is on survival and feeding; especially in an attempt to store lipids and glycogen, which will be needed during the acute stages of molting (Skinner, 1985a). The intermolt period, then, is one of generally little concern to the molt cycle in and of itself. Instead, we will take this as an opportunity to briefly introduce a couple of new topics that are best described before we continue on to descriptions of the different premolt stages. The first is a method of externally measuring progression through intermolt and premolt. The other is an introduction to the methods that can be utilized to induce molting in some species.

In most cases Brachyura that have lost walking legs, either experimentally or naturally, will begin to regenerate these limbs in a two-stage process that begins during

intermolt (Skinner and Graham, 1972). The first stage of growth, termed basal growth, is marked by the formation of a differentiated and innervated primary limb bud (1º LB) (Hopkins, 2001). If the 1º LB is autotomized at this point, the animal will regenerate a 2º LB to take its place (Skinner, 1985a). Secondary LBs are characterized by their ability to inhibit progression through early premolt directly via the production of a MIH-like hormone termed Limb Autotomy Factor-Proecdysis (LAF_{pro}) (Mykles, 2001). Once the animal has allowed itself to enter early premolt, the LB will undergo a second stage of growth called proecdysial growth (Hopkins, 2001). It is during this stage that the LB, will expand to nearly three time its size, fully regenerating the limb (Hopkins, 2001). The R index is a numerical value that is based on a measurement of the regenerating LBs length and the animals CW, such that R=100LB/CW (Chang and Mykles, 2011). In general, the value calculated using this measure increases as the animal progresses through intermolt and premolt (figure 5).

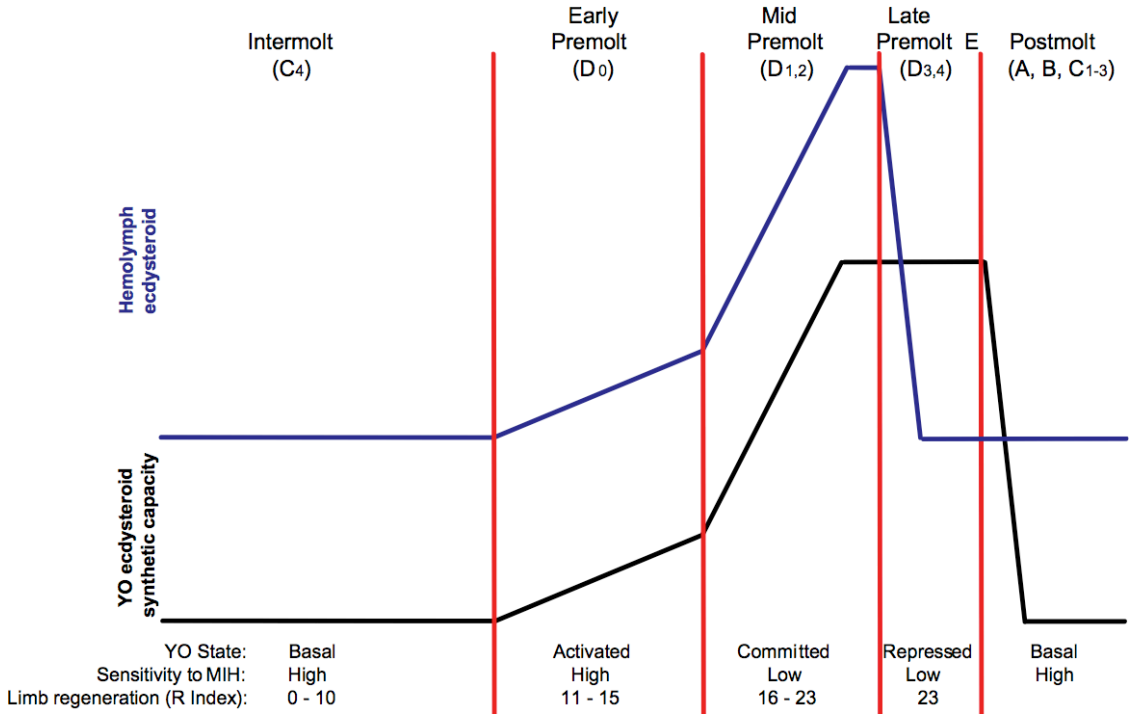

Figure 5. As the crustacean progresses through the molt cycle, YO activation triggers a series of intracellular events that initiate the synthesis and release of ecdysteroid into the hemolymph. The initial activation of the YO occurs through a reduction in circulating MIH. However, the YO remains sensitive to MIH and will revert back to the basal state if exogenous MIH is added. As the animal progresses through the committed state the YO becomes insensitive to MIH, ecdysteroidogenic capacity increases, and hemolymph ecdysteroid titers reach a maximum. During late premolt, and immediately preceding ecdysis, hemolymph ecdysteroid titers begin to drop precipitously. Following ecdysis the YO will return to a basal state, inhibited by MIH. If the animal has been subjected to MLA, the R index may be used to judge the progression through premolt (Adapted from Chang and Mykles, 2011)

The loss of too many legs can actually induce molting itself in some animals (Skinner and Graham, 1972). In fact, this makes the artificial induction of molting possible in some species of decapod crustaceans. For example, in *Gecarcinus lateralis* multiple leg autonomy (MLA) of more than five walking legs will stimulate the animal to molt (Chang and Mykles, 2011). In a natural setting *G. lateralis* that have lost less than five legs due to predation or trauma will sometimes intentionally autotomize additional legs in order to molt and thus regenerate a full set (Skinner, 1985; Mykles, 2001). For

reasons, currently not fully understood, *C. maenas* does not respond to MLA. This is one reason why more recent research on crustacean molting has been as focused on the more easily manipulated *G. lateralis* (Skinner and Graham, 1972).

Though MLA can be effective as an inducer of precocious molts, it does not always induce immediate or predictable results in all species (Hopkins, 2001; Skinner and Graham, 1972). An alternative, based on the knowledge that YO ecdysteroidogenic activity is under persistent inhibitory control by MIH, involves the complete resection of the eyestalks. Eyestalk ablation (ESA) has thus seen widespread use as a method of molt induction in research involving the crustacean molt cycle, especially those assessing the cellular and molecular mechanisms in control YO activation and function (Chang and Mykles, 2011). Unfortunately, ESA does not induce molting in all crustaceans, including *C. maenas*. This has lead to the theory that MIH is being produced in other areas of the brain and thoracic ganglion (Abuhagr et al., 2014).

One of the possible consequences of studying YO animals that have been induced to molt, especially through ESA, is that the YO shows different response patterns than that of a naturally activated YO (Covi et al., 2009). For example, YOs that are induced to molt via ESA remain sensitive to MIH throughout the activated state (Lee et al., 2007a). Different patterns in the abundance of key signaling molecules have also been observed in naturally activated YOs versus those that have been induced via ESA (Lee et al., 2007b). This is by no means an attempt to discredit the finding of past studies that utilized ESA animals. Rather, it is being addressed to support the findings of this current study. In fact, most researchers now use *in vitro* methods for studying the YO (Covi et al., 2009).

As we return to our explanation of molt cycle physiology we enter a series of stages marked by the activation of the YO. Whether this activation is induced experimentally or naturally, these premolt stages represent the most well studied aspects of the cycle. Throughout the intermolt stage, R index values range from zero to ten. At the end of premolt, however, R index values will reach as high as twenty-three (Chang and Mykles, 2011). Figures 5 and 6 offer two graphical depictions of molting and how the YO changes over the course of this cycle.

We begin at stage D_0, early premolt, which is initiated by a reduction in the amount of MIH released from the XO/SG (Chang and Mykles, 2011). Consequently, the YO becomes uninhibited and enters an activated state, the cellular and molecular details of which will be discussed in-depth in the next section. Activation results in measurable increases in both the ecdysteroidogenic capacity of the YO and in hemolymph ecdysteroid titers (Chang and Mykles, 2011). The effects of this initial release of ecdysteroid are felt throughout the organism, affecting calcium storage, muscle degradation, and LB growth (Hopkins, 2001; Skinner, 1966; Skinner, 1985a).

One of the first effects that this newly synthesized and secreted ecdysteroid has on the physiology of the animal occurs in a rather unlikely place, the epithelial cells of the stomach (Ueno et al., 1992). Here, these cells begin to secrete hard calcium filled deposits called gastroliths (Skinner, 1985; Mykles 1997). These calcium stores will continue to grow over the remainder of premolt (Glazer et al., 2013). Following ecdysis these calcium stores will be reabsorbed by the animal as formation of the new cuticle occurs (Glazer et al., 2013).

Another physiological event that coincides with early premolt YO activation is the initiation of somatic muscle degradation in the chelae (Skinner, 1966; Mykles 1997). Over the course of the next one to two months, an animal's chelae will lose approximately 60% of its maximal intermolt muscle mass – a necessity if it is to squeeze these large appendages through the much smaller proximal joints during ecdysis (Skinner, 1966). Thus, to ensure successful limb escape, this crucial process is initiated here in early premolt.

The last major physiological change observed in D_0 is that of proecdysial growth, of limb regenerates which has already been discussed (Hopkins, 2001). Together with gastrolith formation and somatic muscle atrophy, we begin to see just how extensive and tightly regulated the events preceding ecdysis are (Skinner, 1966; Ueno et al., 1992). Early premolt marks the last stage at which progression through ecdysis can be postponed. This is supported by experiments showing that exogenous introduction of MIH or LAF_{pro} will inhibit the animal from entering mid-premolt (Yu *et al*., 2001). If such inhibition does not occur, and conditions are suitable, the animal will next enter mid-premolt.

One of the hallmarks of a naturally committed mid-premolt animal is not the complete cessation of MIH secretion by the XO/SG complex, but rather a reduction in YO's sensitivity to MIH (Chang and Mykles, 2011). Myostatin, a member of the transforming growth factor beta (TGF-β) family of signaling proteins has also been implicated in the transition of the YO from the activated to the committed state (Covi et al., 2009). The committed YO of mid-premolt is thus characterized by an increase in ecdysteroid synthetic capacity, leading to a precipitous rise in hemolymph ecdysteroid

titers throughout the organism (Chang and Mykles, 2011). Entrance into D_1 implies, definitively, that the animal will proceed through ecdysis within the next month (Skinner, 1985a).

The increase in hemolymph ecdysteroid titers indicates that any tissue expressing the ecdysteroid receptor can begin to translate that signal into a physiological change. It should be of no surprise then that one of the primary locations of change during D_1 is at the boundary between the old and new exoskeleton (Skinner, 1985a). The cells of the epidermis begin to grow and separate from the old exoskeleton, a process called apolysis (Skinner, 1962). Recovery of minerals and other biologically valuable compounds occurs through reabsorption of the old exoskeleton (Skinner, 1985a). The processes of readying the new exoskeleton continues into stage D_2, when synthesis of the epicuticle and exocuticle occurs.

In stages D_3 and D_4 YO ecdysteroidogenic capacity plateaus but circulating ecdysteroid titers soon begin to plummet, reaching basal levels by the time ecdysis occurs. This is the result of a negative feedback mechanism induced by ecdysteroid itself (Nimitkul, 2011). During the latter stages of D_3 the old epidermis becomes "friable" in preparation for ecdysis. Stage D_4 is denoted by a pink coloration to the hemolymph, a product of the reabsorption of the keto-carotenoid, astaxanthin, from the old exoskeleton (Skinner, 1962). The progression through these stages is relatively rapid, and together are achieved in about a week (Skinner, 1985a). By the end of D_4 the R index will reach its maximum value, which in *G. lateralis* is 23 (Chang and Mykles, 2011).

The terminal step of ecdysis is truly fascinating to observe. All of the physiological preparations made by the animal during the preceding proecdysial stages

have led to a point where it can now literally crawl out of its old exoskeleton. Depending on the species, this process can take anywhere from 30 minutes to an entire day (Abuhagr et al., 2014; Chang and Mykles, 2011). This marks the conclusion of another round of growth in the crustacean molt cycle and entrance back into the postmolt stages.

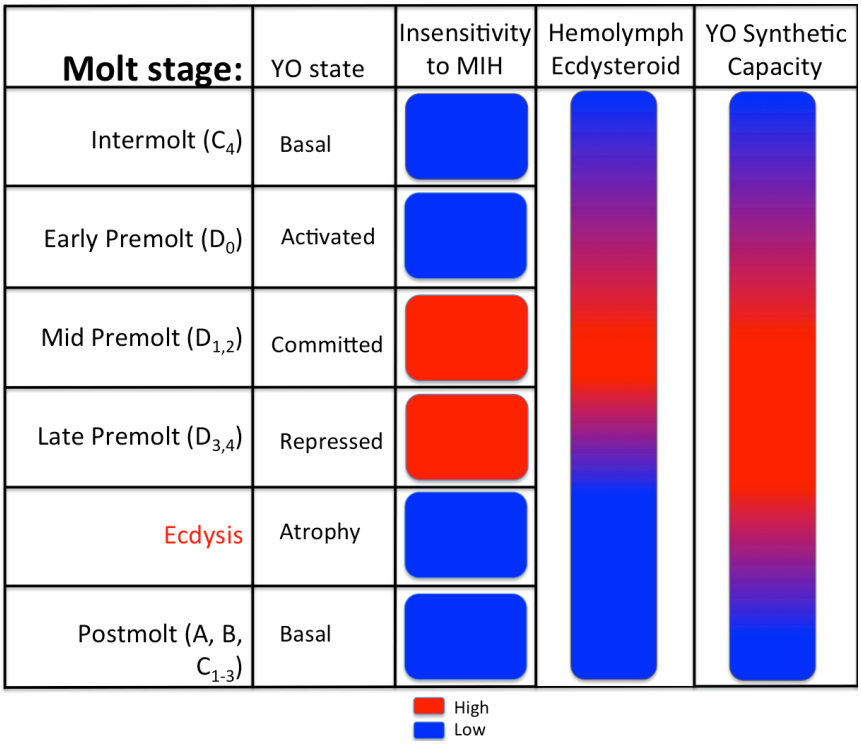

Figure 6. An alternative diagram showing the progression of the YO through the molt cycle. As described in figure 5, the YO progresses through an activated, committed and repressed state during premolt. After ecdysis the YO atrophies and eventually returns to its basal MIH-sensitive state.

We now reach the conclusion of our discussion on decapod crustacean ecology and basic physiology. Research that has been performed on various species showed that the process is largely conserved across decapods (Mykles et al., 2010). So far we have covered the crucial terminology and physiological processes required for further in-depth discussions on the molting process. In the next section we will revisit this process, paying

special attention to the complex cellular and molecular signaling pathways involved in the activation state of the YO itself.

Regulation of the Y-organ activation state

As molting is equivalent to growth in crustaceans, it is a process that is tightly regulated. In this section we will explain how molting is regulated at the cellular and molecular level. More specifically, we will discuss the various signaling pathways involved in each of the YO's physiological states, including the inhibitory role of MIH, the activation by mechanistic target of rapamycin (mTOR), the entrance to the committed state through a putative TGF-β, and the negative feedback via ecdysteroid itself. Some of these pathways are well defined, while the involvement of others are putative and require further confirmation.

The Y-organ, through the production and secretion of ecdysteroid during premolt, represents the primary growth-regulating organ in crustaceans (Chang and Mykles, 2011). During postmolt and intermolt periods the YO is under continuous repression by the inhibitory peptide hormone MIH. MIH is synthesized and released by the neurosecretory cells and enlarged glandular termini of the XO/SG complex located in the eyestalks and brain tissue (Chang, 1995). The XO/SG complex is a neurohemal organ complex, thus, release of MIH occurs directly into the hemolymph, through which it is then transported to its target organs (Chang, 1995).

When MIH comes in to contact with its receptor, a putative G protein-coupled receptor located on the surface of YO cells, it transduces downstream inhibitory signals that prevent the transcription, translation, and/or post-translational activation of

ecdysteroidogenic genes and proteins (Figure 7) (Chang and Mykles, 2011). The initial event in the signaling cascade, termed the triggering phase, involves the conversion of ATP to the second messenger cAMP by adenylyl cyclase (AC) (Lee et al., 2007a). In turn, cAMP binds to protein kinase A (PKA), activating it through removal of regulatory subunits that otherwise block its catalytic domains. Activated PKA regulates the transcription/translation of ecdysteroidogenic genes/proteins both directly and indirectly (Chang and Mykles, 2011). The indirect method involves the opening of Ca^{2+} channels on the cell surface. The subsequent influx of calcium into the cell activates calmodulin (CaM), and in turn the Ca^{2+}/CaM-dependent protein phosphatase, calcineurin (CaN) (Rusnak and Mertz, 2000). This point marks the point of transition from the "triggering" phase into the second "summation" phase of the MIH signaling cascade (Chang and Mykles, 2011).

The summation phase is initially characterized by the activation of a Ca^{2+}/CaM-dependent soluble nitric oxide synthase (NOS) through CaM/CaN-mediated dephosphorylation (Covi et al., 2008; McDonald et al., 2011). NOS activation triggers an increase in intracellular nitric oxide (NO) which in turn activates a soluble NO-sensitive guanylyl cyclase (GC-1) (Kim et al., 2004). As a result, GTP is converted to the signaling molecule cGMP, which activates cGMP-dependent protein kinase (PKG)(Lee et al., 2007b). Like PKA, the activation of PKG inhibits transcription and translation of ecdysteroidogenic genes (Lee et al., 2007b).

Overall, sensitivity of the YO to MIH can be regulated internally through the activity of the cyclic nucleotide phosphodiesterases PDE1 and PDE5, which are capable of degrading cAMP and cGMP, respectively (Nakatsuji et al., 2009). The implications of

such a finding shows that YO activation state is not dictated solely through external MIH hemolymph concentration. Instead, it may also be controlled intracellularly through mechanisms implicating cyclic nucleotide ratios and even calcium concentrations (Covi et al., 2008; Nakatsuji et al., 2009). The regulatory implications of these enzymes within the YO is supported by the observation that addition of MIH during the committed YO state has little effect on ecdysteroidogenic synthesis and secretion (Chang and Mykles, 2011)

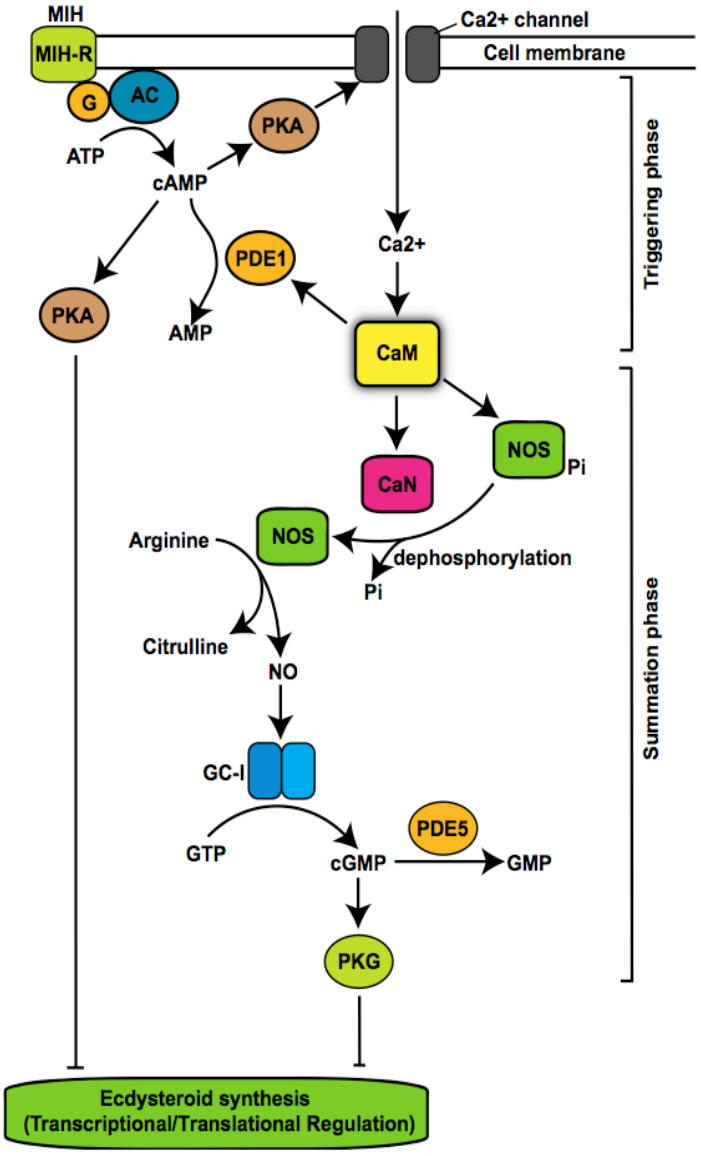

Figure 7. MIH binds to specific transmembrane receptors on cells of the YO resulting in a signaling cascade beginning with the conversion of ATP to cAMP by adenylyl cyclase. Increasing intracellular cAMP concentrations mediate protein kinase A (PKA) activity resulting in the opening of Ca^{2+} channels on the cell surface. This leads to the activation of nitric oxide synthase (NOS) through calmodulin (CaM) and calcineurin (CaN). Guanylyl cyclase-I (GC-1), which converts GTP to cGMP, is dependent on NO. As a result, protein kinase G activity increased and inhibits ecdysteroidogenesis at the transcriptional and translational level. The major downstream transcriptional and translational regulator being inhibited is hypothesized to be the mTOR complex (Figure 8). Adapted from (Chang and Mykles, 2011).

The MIH signaling pathway (Figure 7) represents the upstream regulatory mechanism believed to be partially in control of a highly conserved transcription/translation factor regulator called metazoan target of rapamycin (mTOR) (Layalle et al., 2008). Rapamycin, an immunosuppressive molecule from which the protein's name is derived, is a potent inhibitor of the mTOR (Inoki and Guan, 2006). *In vivo* mTOR forms a complex along with three additional proteins, Raptor, GβL, and Rheb. This complex called mTORC1, is highly conserved across all animal taxa, and represents an important regulator of nutrient-dependent cell growth (Inoki and Guan, 2006; Layalle et al., 2008). Processes associated with mTORC activity range from cell-cycle regulation in yeast to cancer growth rates in humans (Inoki and Guan, 2006). As would be expected for a protein complex with such vast implications for growth, the inputs capable of affecting mTORC1's activation state are numerous. Growth factor concentration, environmental stress, and nutrition status have all been shown to be involved in the activation state of mTORC1 (Inoki and Guan, 2006; Layalle et al., 2008). Given the connection between molting and growth, it is little surprise that mTORC1 plays a significant role in the ecdysteroidogenic capacity of the YO. The importance of mTORC in molting in *C. maenas* is demonstrated by the inhibitory effect of exogenously added rapamycin on the secretion of ecdysteroid by the YO (Chang and Mykles, 2011; Abuhagr *et al.,* 2014*).*

One of the key regulatory factors of mTORC activity is a small GTPase of the RAS superfamily – Rheb (Inoki et al., 2003). In its GTP-bound state, Rheb associates with mTORC1, allowing it to phosphorylate the translational regulators S6K and 4E-BP1. However, hydrolysis of Rheb-bound GTP by Rheb GTPase activating protein

(Rheb-GAP) disassociates Rheb from mTORC, leaving mTORC in a dephosphorylated and deactivated state (Inoki et al., 2003). Another common inhibitory pathway is initiated when rapamycin binds to FKBP12, an immunophilin with cis-trans prolyl isomerase activity (Peterson et al., 2000). This protein complex interacts directly with mTOR, inhibiting its ability to phosphorylate S6K and 4E-BP1. Inhibited phosphorylation of S6K and 4E-BP1 results in decreased mRNA translation through decreased activity of the elF4G:40S ribosome complex.

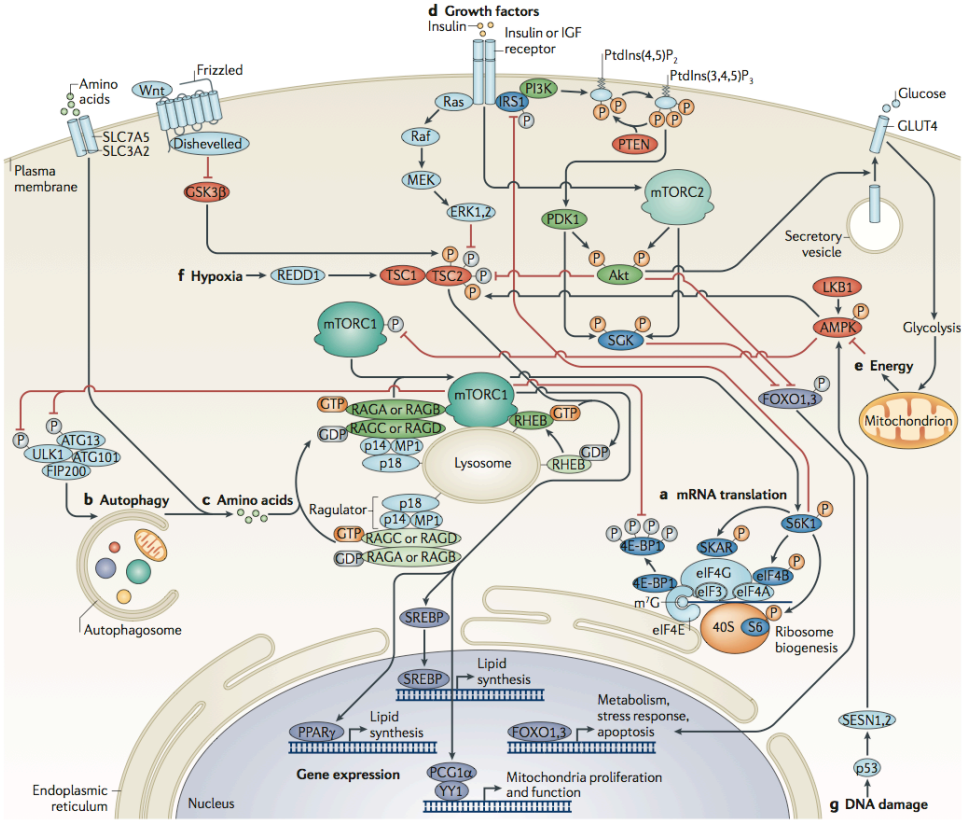

Figure 8. The complexity of the mTOR regulatory pathway. mTOR is capable of integrating a vast number of internal and external signals. The activation state of mTOR is determined through the relative contribution of these signals and ultimately affects cell growth (Adapted from Zoncu et al., 2011).

As we continue upstream in the signaling pathways responsible for mTORC activation state, we begin to realize the true complexity of this regulatory network (Figure 8). Recent work has shown that MIH signaling might be integrated as an input within this system at several points (Figure 9). Thus, the basal-state YO of intermolt and postmolt may be, in part, the result of mTOR inhibition through MIH signaling (Chang and Mykles, 2011). The details of this regulatory paradigm are yet to be fully understood. It has been proposed that MIH signaling inhibits mTORC via interactions with AKT, Rheb, and/or FKBP12 (Figure 9) (Abuhagr et al., 2012).

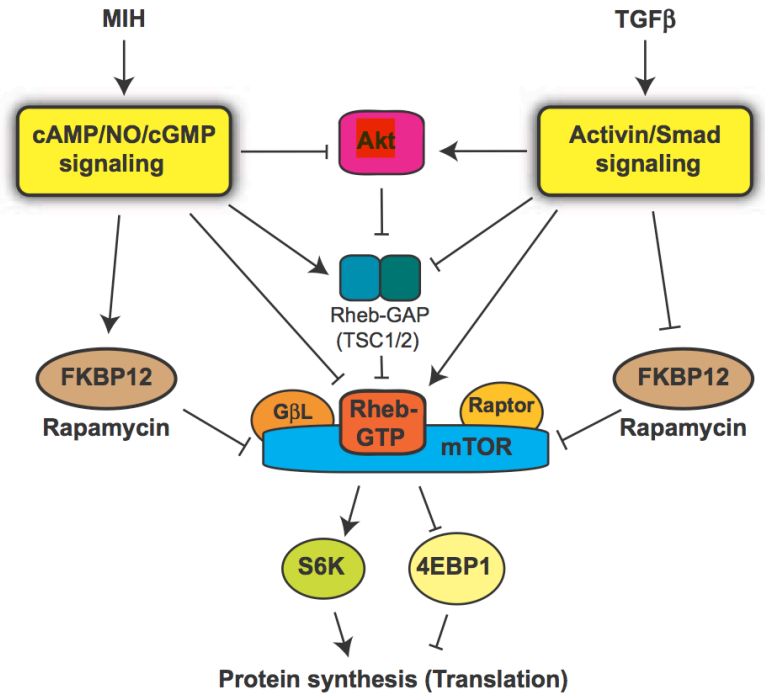

Figure 9. Proposed upstream pathways affecting the activation state of mTORC in the crustacean YO (Adapted from Abuhagr et al., 2012).

YO-specific mTORC activation state is also coordinated through the actions of Activin/Smad signaling through a putative TGFβ. Though the exact mechanism is still under investigation, the TGFβ receptor antagonist, SB431542, inhibits the transition of the YO from the activated to committed state (Abuhagr et al., 2012). The most immediate downstream target to be affected by TGFβ activation of the Activin/Smad signaling cascade is Akt, which in turn regulates mTOR function (Trendelenburg et al., 2009). As of now, we can only say that this TGFβ acts as a YO differentiation factor (Chang and Mykles, 2011)

Our knowledge of the pathways leading to YO activation is still developing, but there is more certainty about the consequences downstream of its activation. The activated YO is one of high biosynthetic potential. The activation of ecdysteroidogenesis potentiates an increase in hemolymph ecdysteroid concentrations to nearly 40 times those of their basal levels (Chang and Mykles, 2011). The process of ecdysteroidogenesis involves a multi-step biosynthetic pathway that has been thoroughly explored and will now be described in detail.

The YO achieves ecdysteroidogenesis via the conversion of cholesterol to ecdysone (Figure 10) or 25-deoxyecdysone (25dE), both of which are direct precursor molecules to the functional molting ecdysteroids 20-hydroxyecdysone (20E) and ponasterone A, respectively (Mykles, 2011).

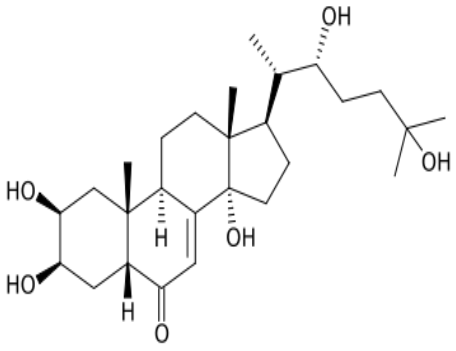

Figure 10. The molecular structure of ecdysone.

Like other arthropods, *C. maenas* relies on dietary sterols for ecdysteroid biosynthesis, as it is unable to synthesize them *de novo* (Lachaise et al., 1993). The first stage of ecdysteroid synthesis is conserved across arthropods and involves a multistep conversion of cholesterol to 5β-Diketol (Figure 11) (Mykles, 2011). Initially cholesterol is converted to 7-dehydrocholesterol by 7,8-dehydrogenase, which is encoded for by the neverland (nvd) gene (Niwa et al., 2010). The following steps leading to formation of 5β-Diketol have proved difficult to resolve and have therefore become aptly labeled as the "black box" of ecdysteroidogenesis (Mykles, 2011). Recent work suggests that a mitochondrial-associated cytochrome P450 mono-oxygenase encoded by spook, and the short-chain dehydrogenase/reductase encoded by non-molting glossy/shroud have significant functional roles within the black box process, but the exact mechanisms remain elusive (Niwa et al., 2010; Pondeville et al., 2013). In the final step of this first stage Δ^4-diketol is reduced to 5β-Diketol by 5β[H]-reductase (Blais et al., 1996).

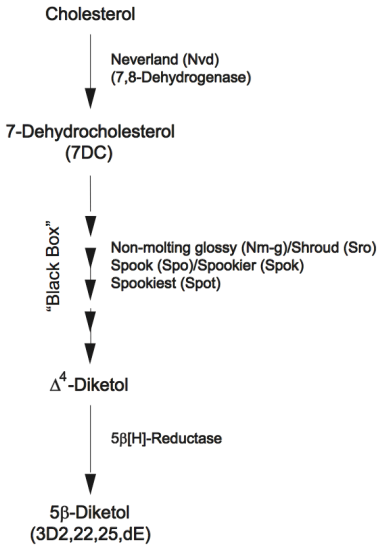

Figure 11. The initial conversion of cholesterol to 5β-Diketol is conserved across all arthropod species. The formation of various short-lived intermediates has made resolving the exact details of these biosynthetic steps very difficult. They have therefore been called the "black box" reactions. The enzymes that carry out the "Black Box" reactions are Non-molting glossy (Nm-g)/Shroud (Sro), Spook (Spo)/Spookier (Spok), and Spookiest (Spot). (Adapted from Mykles, 2011).

The biosynthetic steps following formation of 5β-Diketol occur primarily within the inner membrane of the mitochondria and are much better understood (Smagghe, 2009). In *C. maenas*, 5β-diketol is initially converted to 5β-Ketodiol by 3-Dehydroecdysteroid-3b-reductase (Dauphin-Villemant et al., 1997). Next, selective hydroxylation reactions catalyzed by several unique cytochrome P450 mono-oxygenases modify the pro-ecdysteroid to its secreted form. These hydroxylase enzymes are encoded by the Halloween genes phantom (phm), disembodied (dib), shadow (sad), and shade (shd) and are responsible for the modification of 5β-Diketol into any of four possible end products: ecdysone, 3-dehydroecdysone (3DE), 25-deoxyecdysone (25dE), and 3-dehydro-25-deoxyecdysone (3D25dE) (Mykles, 2011). As a general rule, no more than two ecdysteroid products are secreted from the YO of a given species (Mykles, 2011).

In *C. maenas* ecdysone and 25dE are the primary ecdysteroids secreted into the hemolymph by the YO. Formation of these products is a result of systematic hydroxylation of steroidal core and side chain carbons by the Halloween hydroxylases (Figure 12). Selective hydroxylation occur such that once a hydroxylation pattern has been established further manipulation of the product by other hydroxylase enzymes is hindered, thus providing directionality to the process (Lachaise et al., 1993). These lipophilic products are then released from the YO through simple diffusion across the cell membrane (Birkenbeil, 1983; Lachaise et al., 1993; Savigny et al., 2007).

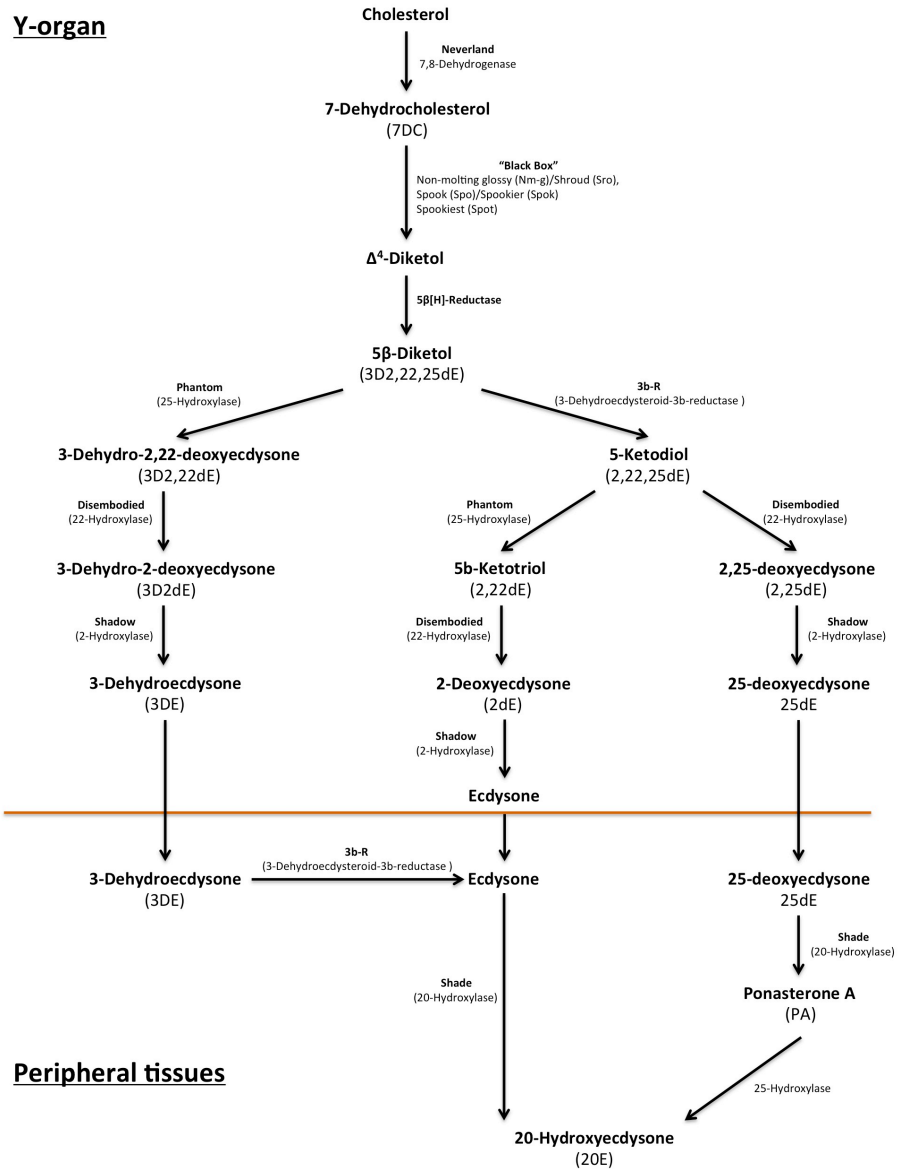

Figure 12. Biosynthetic pathway from cholesterol through to the production of the active ecdysial hormone 20E (Modified from Mykles, 2011).

Secretion of these YO end products does not necessarily mark the end of the ecdysteroid synthetic mechanism. Peripheral tissues including the gonads, hindgut, abdominal ganglia, eyestalk ganglia, hepatopancreas, antennal gland, and epidermis all play a crucial role in the final biosynthetic step of ecdysteroidogenesis (Mykles, 2011).

Specifically, these periphery tissues are responsible for a final hydroxylation of carbon 20, which in *C. maenas*, converts ecdysone and/or 25dE into the active ecdysteroid 20E (Figure 13) (Chang and Mykles, 2011; Mykles, 2011). The active ecdysteroid end product 20E is then dispersed throughout the body of the *C. maenas* via the hemolymph. Whether or not the transport of ecdysteroid occurs freely or by way of carrier proteins is unclear. The amphipathic nature of ecdysteroid suggests that such carrier proteins would be unnecessary. However in, in some spider species ecdysteroids are found bound to the common hemolymph protein hemocyanin (Jaenicke et al., 1999).

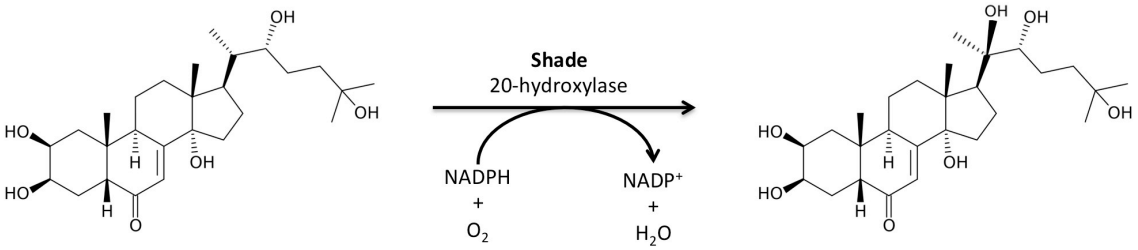

Figure 13. The final hydroxylation step carried out by the cytochrome P450 monooxygenase, Shade (20-hydroxylase). Though this reaction occurs outside the YO, similar hydroxylation reactions are carried out by other Halloween family P450 monooxygenases inside the YO. These reactions are responsible for the selective hydroxylation of steroidal core carbons responsible for ecdysteroidogenesis.

Connective tissue degradation and muscle atrophy in preparation for ecdysis are, historically, two of the most notable and well-studied physiological effects exhibited by ecdysteroid. However, ecdysteroid receptors are found in almost every organ and tissue, suggesting the existence of potentially undiscovered functions (Spindler et al., 2009). For example, it has recently been suggested that an ecdysteroid-induced negative feedback

mechanism may be responsible for directing the YO into a repressed state following its activation in mid premolt. (Kim et al., 2005; Chang and Mykles, 2011).

We made mention of the observed physiological changes seen in a few ecdysteroid sensitive tissues in the first section of this chapter. In somatic muscle, signaling through a ecdysteroid receptor is responsible for the tissue degradation that allows chelae to escape through their proximal joints (Kim et al., 2005; Skinner, 1966). The same signaling event also initiates connective tissue degradation, limb regeneration, and preparation for cuticular separation during premolt stages (Hopkins, 2001; Skinner, 1962). Ecdysteroid signaling has also been implicated in the stimulation of gastrolith formation during premolt (Ueno et al., 1992). The signal that induces change in these tissues is initiated through binding of ecdysteroid to an intracellular ecdysteroid-specific receptor. In reality, the functional ecdysteroid receptor forms a heterodimeric receptor complex containing both EcR and retinoid X receptor (RXR) (Smagghe, 2009; Wang and LeBlanc, 2009). In insects, a RXR ortholog called ultraspiracle (USP) exists (Kim et al., 2005). The EcR:RXR/USP complex acts as a transcription factor that initiates transcription of tissue specific genes in response to signal reception. The pathways involved in this feedback mechanism may involve mTOR and Activin/Smad, but are likely more complex. A description of the consequences of this feedback mechanism is currently the target of investigations being carried out by our collaborators.

The YO is a highly complex endocrine organ. The amount of regulation needed to maintain an animal in an appropriate growth state is of obvious importance to its survival. Here we have described the current state of knowledge of YO regulatory control. When the inhibitory effects of MIH are absent, either through decreased extracellular MIH

signaling or intracellular PDE mediation, the YO enters a state of de-repression. This marks the beginning of YO activation and thus the entrance in to early premolt. A second signal, believed to be transmitted mediated through Activin/Smad causes the YO to further increase its ecdysteroidogenic output, marking the entrance to the committed state. Ecdysteroidogenesis is the result of transcriptional and translational activation of pro-ecdysteroidogenic genes such as those of the Halloween family. Eventually, during late premolt, ecdysteroid titers reach a level where they will begin to act through a negative feedback mechanism, repressing the YO and slowing ecdysteroidogenesis. At this point the animal has synthesized enough of the hormone to orchestrate molting on a whole organism level. The animal undergoes ecdysis and the YO enters back into its MIH-mediated basal state of ecdysteroid synthesis repression.

Using Proteomics to uncover changes in the YO over the course of the molt cycle

Molecular biology is a young discipline. In fact, it was less than 80 years ago that Warren Weaver, director of science at the Rockefeller Foundation first coined the term "molecular biology" to describe to his contemporaries the newly developing field that integrated the studies of physics, chemistry, and biology (Weaver, 1970). Since that time it has been an area of explosive and continual growth. The characterization of DNA's molecular structure, mapping of the human genome, and genetic modification of plants and animals all owe their existence to developments within this field (Collins et al., 2003; Uzogara, 2000; Watson and Crick, 1953). Today, we understand that complex molecular processes are what drive life's existence. During the mapping of the human genome, it was believed by many that successful completion of the project would hold the keys to

unlocking some of the most complex biological questions (Collins et al., 2003). However, as is more often the case than not, the conclusion of this project only left the scientific community with more unanswered questions. Most importantly, it planted the seed of realization that there is much more to an organism than its DNA.

Of course, DNA's fundamental role is to encode genetic information (Watson and Crick, 1953). However, it is the spatial and temporal expression of these genes that allows for the differentiation and specialization of different organs and tissues. The distinct expression of proteins within various tissues is what makes them unique, but it is also what determines their activity, productivity, and general vigor. Mapping the human genome gave rise to a new way of thinking; one that encouraged large-scale investigations into massively complicated biological questions (Collins et al., 2003). From the thriving study of genomics budded the new and exciting fields of transcriptomics, proteomics, and metabolomics - each of which hoped to address some of the questions left unanswered by genomic studies alone (Lovric, 2011).

Of course, each of these fields also has its limitations. Compared to genomics, transcriptomics suffers from the fact that mRNA concentrations are in a constant state of flux, and some transcripts are never actually translated into proteins (Lovric, 2011). Still, transcriptome mapping provides extremely useful information on the expression patterns of genes, giving us better insight into regulatory aspects of the cell's function. The field of proteomics aims to resolve some of the shortfalls from which both genomics and transcriptomics suffer. By observing only translated proteins, one is able to capture a temporal representation of the exact mechanisms being employed by the cells of a given tissue (Lovric, 2011). Metabolomics may also be used to make assumptions about which

processes and reactions are actively occurring in a tissue by observing the metabolites present. Both proteomics and metabolomics inherently suffer from problems rooted in sample degradation and loss during the obligatory processing and identification steps (Lovric, 2011).

By no means are the "-omics" mutually exclusive. In fact, they are often used together in parallel to make significant findings regarding the function of a tissue (Kültz et al., 2007). For example, this current study will utilize a proteomic approach to assess changes in the YO over different molt stages. This data, along with collaborative work currently being performed on the YO transcriptome will help elucidate the internal functions and the regulatory mechanisms at play in this organ over its various states of activation. In this section we will describe the proteomic workflow and how it can be used to assess cellular function in tissues such as the YO. But first, we must define proteomics itself.

An all-encompassing definition of the proteome is easy to imagine, yet in practice may be impossibly ambitious to generate. It would essentially require that every protein, along with each of its possible isoforms and post-translational modifications, be identified and quantified in each tissue of the entire organism (Lovric, 2011). In realty, the methods used to extract, isolate and process samples intended for proteomic analysis limit the extent to which proteins will remain viable for later identification (Lovric, 2011). Even if it were possible for these methods to be one hundred percent efficient in maintaining protein integrity with zero loss, cells do not express all possible proteins at all times (Rabilloud, 2002). This differential expression of proteins actually provides a route through which meaningful observations can be made about the proteome and,

through interpolation, tissue physiology itself. We must therefore work within the more realistic scope of comparative or "differential" proteomics, relying on the assessment of temporal changes in the observable proteome of a specific tissue under controlled experimental conditions (Lovric, 2011).

We have used the beginning of this section to shed some light on the discipline of proteomics. It should be noted that there is no standardized protocol though which a proteomic investigation if performed; nor is one method decidedly better for every situation (Yates et al., 2009). Instead, a range of approaches may be enlisted so far as they are capable of meeting three basic criteria. They must: 1) isolate protein from the sample so that individual proteins can be 2) quantified 3) and identified (Lovric, 2011; Rabilloud, 2002). As we will see, Weaver's original definition of molecular biology is beautifully exemplified through the multifaceted techniques required to obtain results in the field of proteomics.

For the past thirty years, proteomic investigations have largely relied on the separation of proteins using two-dimensional gel electrophoresis (2-D GE) (Rabilloud, 2002). The discipline has been used to answer a broad range of scientific questions, ranging from the effects of environmental stress to the discovery of cell-surface biomarkers present on breast cancer cells (Morrison et al., 2012; Tomanek, 2011). Advancements in protein identification techniques may one day antiquate the need for gel-based protein separation, but for now it remains the most widely used and versatile tool for protein separation in the field (López, 2007; Magdeldin et al., 2014). The advantages and disadvantages of other methodologies have been extensively reviewed and discussed elsewhere, and so do not need to be reiterated here (López, 2007;

Rabilloud, 2002; Yates et al., 2009). Instead, we will focus on a description of our proteomic workflow, which utilizes 2-D GE for separation and quantification, followed by a soft ionization technique known as matrix-assisted laser desorption/ionization (MALDI) for identification (Yates et al., 2009).

The initial processing of a sample is of utmost importance to the remainder of the proteomic workflow. Not only must proteins be isolated from other cellular and extracellular constituents like DNA and lipids, but endogenous proteases must also be deactivated so that protein degradation is minimized (Lovric, 2011). Furthermore, this step should leave proteins in a denatured state, free of protein aggregates and undesirable aberrant protein modifications (López, 2007). Conveniently, these goals are achieved jointly through the use of a single specialized homogenization/lysis buffer. Our particular solution consisted of urea, thiourea, ASB-14, Tris-base, bromophenol blue, dithiothreitol (DTT), and immobilize pH 3-10 gradient (IPG) buffer. Both urea and thiourea serve as solubilizing chaotropic agents, helping to destabilize inter/intra-molecular bonds (López, 2007). The ideal result is complete protein denaturation and solubilization (Magdeldin et al., 2014). Thiourea in particular was used to destabilize intramolecular disulfide bonds through reduction, while addition of DTT helps to maintain them in this reduced state (Garfin and Heerdt, 2002; Rabilloud, 1998). A CHAPS alternative called ASB-14, is used and acts as a zwitterionic detergent to increase membrane protein solubility while simultaneously reducing gel streaking during later isoelectric focusing (IEF) steps (Garfin and Heerdt, 2002; López, 2007). In addition to a general Tris-base buffer, a pH-specific ampholytic IPG buffer is added to maintain solubility of proteins through later steps.

Bromophenol blue is added as well, but acts purely as a visual aid during IEF and is not required for solubilization (Garfin and Heerdt, 2002).

Mechanical force through trituration can be used to help accelerate the process of YO solubilization during homogenization (Wang et al., 2003). The entire process must be performed on ice to limit the potential actions of endogenous proteases before being denatured and deactivated by the homogenization solution. Protease inhibitors should be considered conditional to the sensitivity of the samples (Thongboonkerd et al., 2004). Once uniformity of the homogenate is achieved the samples are spun in a centrifuge to fractionate the denser undesirable cellular constituents from the solubilized protein. A final purification step utilizing trichloroacetic acid (TCA) and acetone is used to remove any additional salts, lipids, or nucleic acids from the protein. By definition, this step dehydrates the sample and thus a rehydration solution must be used to reconstitute the proteins into a salt-free solution ready for further 2D gel electrophoresis. As a final step, a product such as the "GE Healthcare 2D Quant kit" must be used to obtain protein concentrations prior to IEF. The kit, which follows the principles of a standard Bradford assay, is useful in that it allows protein concentration to be determined using only a few μL of rehydrated sample (Bradford, 1976). Unlike a Bradford assay, the GE Healthcare kit remains sensitive to protein concentrations in the presence of detergents and reducing agents like those in the homogenization/rehydration buffers.

The isolated and quantified protein samples are now ready for first dimensional separation, which is achieved through the exploitation of each individual protein's intrinsic isoelectric point (pI). This procedure, known as isoelectric focusing (IEF) is founded on the basis that amino acids, and thus proteins, are amphiprotic and have

distinct pIs related to the charge state of their R-groups. The system works by establishing a fixed pH gradient within the medium (i.e. gel) through which the proteins will flow when subjected to an induced electrical current, e.g. by attaching the R-groups to the acrylamide monomers before polymerization. These immobilized pH gradient (IPG) strips function such that when a protein resting at a pH below its pI (i.e. positively charged) is subjected to an electrical current, it will travel towards the cathode until it reaches a "pH zone" on the IPG strip at which its net charge is neutral. Likewise, a protein resting at a pH above that of its pI will carry a net negative charge, travelling instead towards the anode. Thus, assuming isolation of a collection of dissimilar proteins with unique amino acid structures, this method will ensure separation through attainment of net neutral charges at different points on the pH scale (Figure 14).

After IEF is complete, the IPG strip, which now contains all of the proteins separated by their respective pI, is removed and placed on top of a polyacrylamide gel for standard sodium dodecyl sulfate polyacrylamide gel electrophoresis (SDS-PAGE), which will further separate proteins by their molecular masses. The end result is a gel containing all of the solubilized proteins isolated in the homogenization/isolation steps, and separated by their charges in one dimension and masses in the other (Berth et al., 2007). "Spots" on the gels can be visualized using a Colloidal Coomassie Blue stain that doubles as a fixative allowing cold storage of the gels that extends their utility for weeks (Berth et al., 2007; López, 2007). Each spot, of which there might be hundreds or even thousands of on a single gel, (see Figure 15) represents a single protein (Berth et al., 2007).

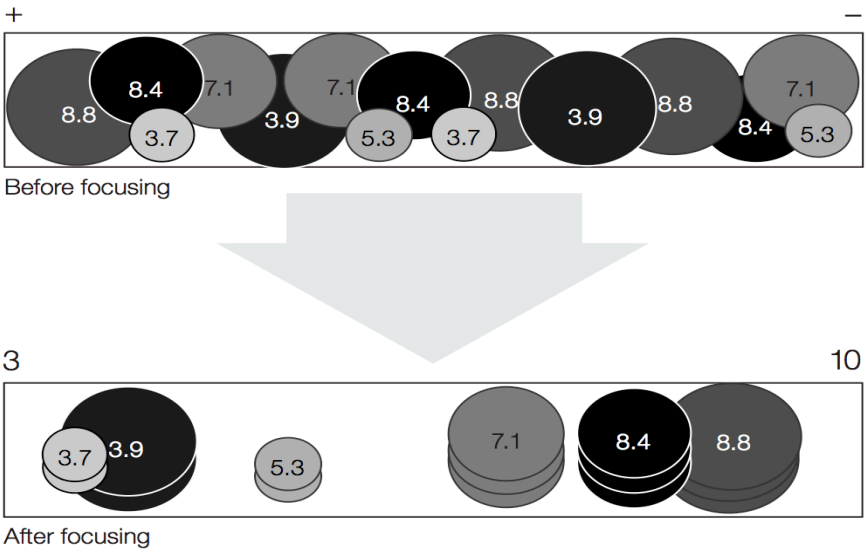

Figure 14. The basis for isoelectric focusing is founded in a protein's unique isoelectric point (pI), which enables it to be separated from others when exposed to an electric current along a pH gradient (Adapted from Garfin and Heerdt, 2002).

Each gel processed in the above manner may contain proteins from either a single treatment replicate or a pooled sample comprised of the tissue of multiple organisms subjected to identical treatments. The physical gels are next digitized for software-based analysis, which is handled within a specialized program called Delta 2D (DECODON). Delta 2D and analogous programs such as Decyder 2D (GE Healthcare) play a crucial role in a process termed "image warping" (Berth et al., 2007). One of the consequences of utilizing a gel-based separation method is the occurrence of minor protein migration discrepancies. This, along with the inherent proteomic variation within individual organisms, results in minor incongruences between corresponding spot locations on each gel (Lovric, 2011). Thus, even the raw gels within the same treatment group differ enough such that spots must be warped in order for comparisons between groups to be made.

The term warping refers to the super-positioning of spots from corresponding false colored raw 2-D gel images to create a single treatment-level corrected image representative of that treatment's net proteome (Berth et al., 2007). Expanding upon this process allows for the creation of a "fused-gel" image, which contains all of the proteins of the experiment on a single normalized gel image known as a proteome map (Berth et al., 2007). This fused-gel image generates a "consensus spot pattern" allowing for statistical comparisons to be made between treatment groups once normalized spot volumes have been established (Berth et al., 2007). To accomplish this, Delta 2D takes into account spot volume, a function of spot boundaries and pixel densities relative to background "noise" and other spots (Berth et al., 2007). Once complete, each individual spot can be compared to its corresponding spot on the gels of other treatment groups to assess changes in the expression of that protein.

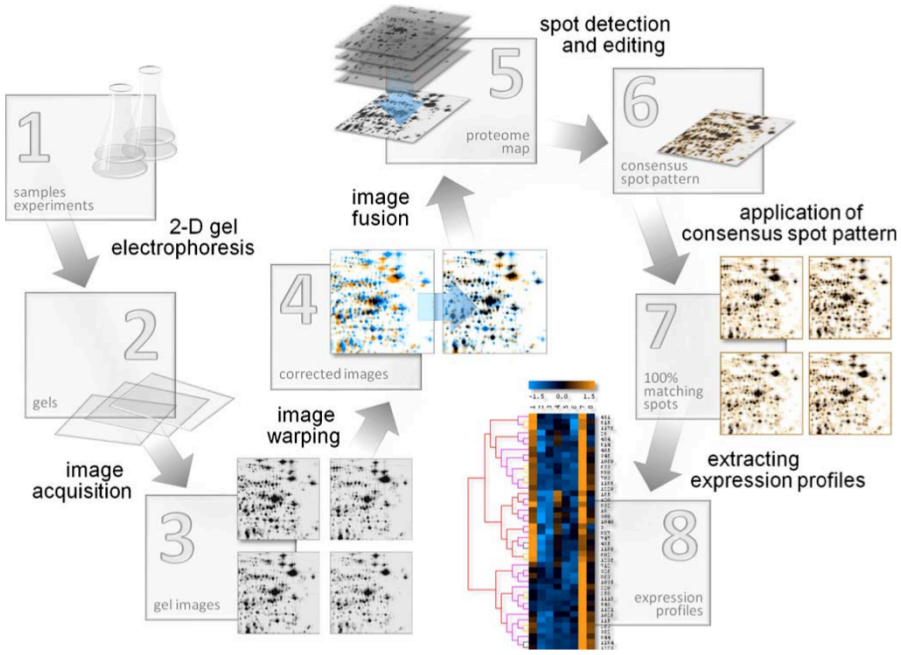

Figure 15. Outline of the process from gel acquisition to production of preliminary results using an "image warping first" approach and the creation of a consensus spot pattern (Adapted from Berth et al., 2007).

The aim of a Delta 2D analysis is the production of expression profiles and heat maps depicting quantified protein expression patterns across the treatment groups (Lovric, 2011). From the normalized spot volume data, statistical analyses can be performed to determine the significance of protein abundance patterns across treatments. Once protein identification is completed, these abundance patterns will provide valuable insights into the cellular processes being activated or deactivated in the tissue of interest (Berth et al., 2007). Heat maps are then generated in a hierarchically clustered fashion by assigning each protein Pearson correlation value, which allows proteins exhibiting similar trends in abundance to be clustered together. These heat maps can be later manipulated to depict all spots or only those deemed significant through the statistical analysis (Berth et al., 2007).

Delta 2D provides self-contained statistical tools capable of performing the most common statistical analyses. Using the program itself, rather than a third-party statistical package, is the preferred method as the data remains directly associated with the image analyses (Berth et al., 2007). One powerful statistical tool contained within Delta 2D is that of the principal component analysis (PCA). PCA, which is a fundamentally multivariate statistical approach, can be simplified into a graph containing only the two most explanatory dimensions. This two-dimensional graph separates treatments according to changes in protein abundance patterns. The x-axis (principal component 1). in this representation represents the axis along which most of the variation in the data is explained. An axis perpendicular to it separates treatments further and explains the second-most percentage of the variation in the data (PC2). Loading values assigned to each protein indicate the relative contribution each has on the separation of one treatment

cluster form another. When used in parallel with heat maps and expression profiles, PCA data can provide excellent insight into the effect that each protein has on the treatment as a whole. Specifically, it can be used in addition to analytical techniques like ANOVA to assess the contribution of individual proteins to significant differences observed between treatment groups. Overall, the statistical approach taken to a given data set can vary widely by experiment and should be considered before experimentation even begins as it may substantially influence its structure (Berth et al., 2007).

With heat maps and abundance profiles complete, the samples must next be readied for the third and final step in the proteomic workflow: identification. Different methods of identification must be considered as success relies on proper sample preparation specific to the identification strategy being employed (Yates et al., 2009). The separation and quantification strategies explained above were chosen knowing that the final identification step would apply MALDI-ToF/ToF, a form of tandem mass spectrometry (MS/MS) (Rabilloud, 2002; Yates et al., 2009). MALDI-ToF/ToF is ideal for use on samples that have been pre-separated, such as those that have been processed by 2D GE (Lovric, 2011).

As the name implies, MALDI-TOF/TOF utilizes a laser-induced ionization technique to create charged tryptic protein fragments whose masses can be determined via their time of flight (TOF) as they are reflected through a region of space of highly controlled conditions (the drift region) (Lovric, 2011; Yates et al., 2009). Before samples can be submitted to analysis via MALDI-TOF/TOF, they must first be isolated from the gels in which they are fixed, digested (fragmented) into peptides using trypsin, and then co-crystalized within a matrix on a stainless steel target plate. These plates allow for

hundreds of samples to be plated and analyzed over the course of a single experiment, or "run" (Neumann, 2004). The matrix is chosen to preferentially absorb the specific wavelength of laser light used so that the protein itself is not degraded in the process (Lovric, 2011). It is also designed to be a strong proton donor to promote ionization of the protein (Lovric, 2011). If the right amount of laser energy is fired at the target plate, the co-crystallized matrix and peptides are vaporized, and enter the gas phase where protonation of the protein fragment, e.g. peptides, occurs through a yet unresolved mechanism (Lovric, 2011).

Once the ionized protein fragment is vaporized from the target plate, its newly acquired charged gaseous state is utilized to accelerate it away from the plume of the explosion using a strong induced electromagnetic field (Lovric, 2011). A delayed ion extraction (DE) technique ameliorates differential acceleration patterns produced by the laser-induced explosion, which can otherwise have drastic effects on detection accuracy (Lovric, 2011). The ionized protein fragments can then be accelerated through a collision induced disassociation (CID) chamber containing an inert gas, e.g. argon, that slows, heats, and further fragments the peptide before reaching an ion gate (mass selection gate or precursor ion selection gate) where the fragment can then be further selected for based on its TOF (Lovric, 2011). This mass selection system essentially functions by deflecting all ionized protein fragments from the flight path, using a perpendicular electromagnetic field, until the expected time when ions of a desired mass enter, at which point it is momentarily switched off to allow their passage (Lovric, 2011).

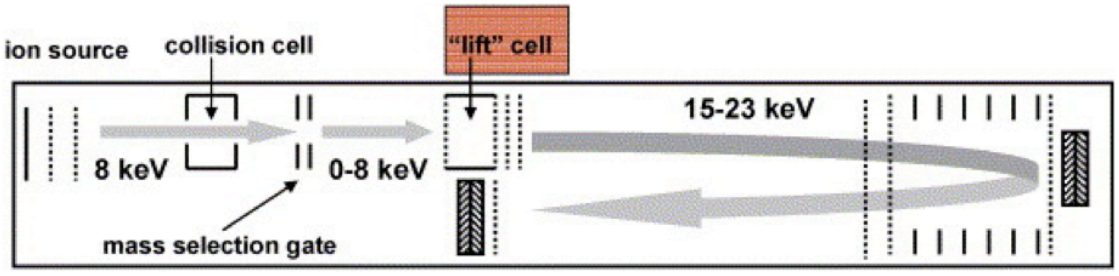

Figure 16. Schematic of the Bruker's ultraflex II^{TM} TOF/TOF machine used in the current study. Proteins are ionized via matrix-assisted laser desorption/ionization (MALDI), accelerated through space towards detectors, and are then identified using properties unique to each fragments mass/charge (m/z) ratio. Two detectors are utilized to increase resolution and accuracy of identification by analyzing both peptide mass fingerprint (PMF) and peptide fragment fingerprints (PFF) (Adapted from Cotter et al., 2007).

Once passed through the collision chamber and mass selection gate, the selected ions enter a lift cell which functions to increase accuracy by re-accelerating them through a vacuous drift region, towards a reflectron. The reflectron is composed of a series of electrostatic lenses, with electromagnetic potential increasing as a function of distance (Lovric, 2011). At the end of this electromagnetic "tunnel" lies a detector capable of taking an initial m/v (mass/velocity) measurement of the sample. The field is designed to be of slightly higher power than that of the LIFT re-accelerator (Lovric, 2011). Thus, the ions slingshot back into the drift region, undergoing secondary TOF during which they will be further separated and finally be recorded by another detector located near the LIFT cell. The result is higher resolution and thus a better chance of identifying a protein from the fragment.

The above method allows for TOF measurements to be taken in tandem (MS/MS). Initially, a peptide mass fingerprint (PMF) is recorded as the m/z of the complete ionized protein fragment. Because protein fragments created by the CID and LIFT process originate from a single ionized peptide, they can be used in parallel to

further fragment and select for peptide fragment fingerprints (PFF) (Lovric, 2011). Thus, the PMF fragments provide insight into the putative sequence of amino acids making up the peptide. The PMF provides an estimate of the distribution of peptide masses and a putative identification. The PFFs can then be used to cross-check if the peptide masses of the putative protein ID, and the amino acids composition of the peptide, match those of the theoretical peptides from an in-silico digestion of peptides from that putative PMF ID. The secondary fragmentation, when used with a post-CID LIFT accelerator, thus allows for greater identification accuracy to be achieved when compared to MS that relies solely on PMF (Lovric, 2011).

The data collected through TOF/TOF MS/MS is visually represented on a graph; the x-axis being mass (Da) and the y-axis intensity. PMFs with the greatest intensity are those chosen for further PFF. The intensity and mass data of these "hits" is used to identify the protein by comparing it with data in online databases. The term resolution is applied to represent the height of the peak divided by the width at half its intensity and is a unitless absolute measurement (Lovric, 2011). Higher resolution measurements are more likely to be deemed significant when searched against online databases such as Mascot (Matrix of Science), as these databases use statistical probability to determine if the peptide resolved in the experiment matches those of established expressed sequence tag (EST) libraries for PMF and PFF data (Tomanek and Zuzow, 2010). A MOlecular Weight SEarch (MOWSE) score is assigned using a logarithmic transformation of the probability that the match is occurring by chance alone. In this way, higher MOWSE scores are more likely to be deemed significant. Matching of more than one PFFs is used to ensure accurate protein identification (Tomanek and Zuzow, 2010).

Protein identities recovered using the MALDI-TOF/TOF MASCOT identification strategy can now be assigned to the heat maps and statistical analyses completed earlier in Delta 2D. Finally, the results of the comprehensive proteomic workflow have produced data that can be interpreted and analyzed within the context of biological systems. The explorative nature of proteomics allows for hypotheses to be generated about the proteins and their role in any number of cellular processes (Lovric, 2011). Usually, proteins are assigned a broad functional category (e.g. metabolic proteins, cytoskeletal elements, etc.) to help in assessment what physiological trends can be observed in response to the treatments (Tomanek, 2011).

II. MANUSCRIPT

Abstract

Molting in arthropods is a complex process governed by regulatory mechanisms that have evolved and adapted over millennia to allow these animals to grow, despite being confined by a hardened exoskeleton. We isolated the molt-regulating Y-organs (YO) from the common shore crab *Carcinus maenas* at molt stages B, C_{1-3}, C_4, and D_0 to assess how changes in protein abundances might underline the unique physiology of each of these stages. We found that changes in protein abundance were most notable in the postmolt stages (B and C_{1-3}), where an increase in energy metabolism and the reactive oxygen species stress (ROS) response proteins was observed. An increase in triosephosphate isomerase and transketolase suggest that the postmolt YO is participating in triglyceride storage and is also actively recycling excess ribose sugars manufactured during the YO's previously activated state. We also propose a mechanism through which ROS-induced release of cyclophilin A may contribute to YO atrophy in postmolt through the remodeling of structural proteins such as collagen. We support the standing observation of YO atrophy during postmolt by drawing attention to hemolymph protein abundances, especially those of cryptocyanin isoforms, which dropped precipitously in intermolt (C_4) and remained at low abundances into early premolt (D_0). Finally, though our evidence is preliminary, we propose that future investigations into the YO proteome address the significance of the protein glutamate dehydrogenase. Glutamate dehydrogenase, a key enzyme involved in the formation of glutamate, represents a potential nutrient-sensing checkpoint that might be involved in YO activation. Historically, most attention has gone to the acute molt stages, where signaling

mechanisms involved in the activation of the YO have been the focus. Here, we present data suggesting that other regulatory mechanism may be governing the atrophy the postmolt YO. A better understanding of crustacean physiology has the potential to benefit ecosystems and economies worldwide.

Key Words: *Carcinus maenas*, molting, Y-organ, ROS

Introduction

One of the fundamental requirements for any animal is the need to grow and develop over the course of its life. Different strategies have evolved that include everything from abrupt events of metamorphoses to slow and steady growth patterns that maintain the original body shape over the entire life cycle. Just as in other arthropods, crustaceans have evolved an extraordinary means of growth that circumvents the inherent obstacle that results from living within the constraints of a non-pliable exoskeleton. To do this, the animal must molt, a process that is governed by a complex series of regulated stages that eventually lead to the emergence of the live intact animal from its old exoskeleton (i.e. ecdysis).

There are a number of reasons why understanding the importance and complexity of the molting process should be considered. Firstly, fisheries and aquaculture facilities that are involved in the capture and rearing of crustaceans will undoubtedly benefit from a better understanding of growth in these animals. Secondly, and as is the case with the study organisms of the present research, crustaceans can be veracious invaders that disrupt the non-native habitats to which they are introduced (Roman and Palumbi, 2004; Walton et al., 2002). Consideration of their growth and development may not only help curb the effects of populations that have already been introduced, but may help to prevent the occurrence future introductions. In fact, the two reason listed are not mutually exclusive and a reduction in introduction events will benefit fisheries by decreasing stress on the system and increasing production of the more desirable species (Walton et al., 2002).

Understanding the regulatory mechanisms that govern crustacean molting has been a decades-long process that has provided results demonstrating that molting is under tight regulatory control by a tropic hormone system involving multiple organs and a number of upstream signaling inputs (Chang and Mykles, 2011). Recent progress has been made to elucidate the cellular pathways that regulate the biosynthesis of ecdysteroid, the molting hormone that signal for the downstream physiological events that lead to ecdysis (Chang and Mykles, 2011). Additionally, studies observing the enzymes involved in ecdysteroidogenesis have shown that a group of cytochrome p450 mono-oxygenases present in the primary molt-regulating Y-organ (YO) are responsible for the sequential hydroxylation of cholesterol into ecdysteroids (Mykles, 2011). Despite these advancements, there remain aspects of crustacean molting that are less well understood and warrant further investigation.

One aspect of the molting process that has been somewhat overlooked has been the sequence of events that occur in the postmolt YO. During these stages the YO is no longer biosynthetically active and undergoes a period of atrophy, eventually returning to a basal repressed state (Chang and Mykles, 2011). Though the physiological observations of this event have been well established for decades, no work has been performed to provide evidence for the molecular mechanisms that govern the atrophy of this postmolt YO. In this study we address this lack of information by developing hypotheses concerning the cellular mechanisms of YO atrophy using a proteomic approach.

Proteomics is a discovery-based method wherein testable hypothesis are formed only after the proteome has been elucidated (Tomanek and Zuzow, 2010). The method has become an invaluable tool utilized either in standalone applications or in addition to

transcriptomic studies, to provide additional insight into intracellular function of tissues and organs. Because the analysis of the proteome offers the ability to select specific time-points at which cellular protein constituents can be assessed it represents an ideal method for evaluating the changes occurring in the YO over the molt cycle. In this study we assess changes in the proteome of the green shore crab *Carcinus maenas* through the use of two-dimensional gel electrophoresis followed by tandem mass spectrometry in order to examine changes to the YO proteome of this species over the course of the molt cycle.

Carcinus maenas is an invasive crustacean species that has now established populations worldwide. Its adaptability to a wide range of environments along with its predatory nature have had the consequence of disrupting many fragile ecosystems to which it has been introduced. As discussed prior, understanding the development and growth of this organisms is warranted so as to reduce future invasions and to help manage those that have already occurred. Furthermore, many arthropods grow through a molt-cycle that is more or less the same as that of *C. maenas*. Any discoveries made here will help to shed light on the process as it occurs in other arthropods.

In our study, we harvested YOs from a total of 36 animals representing four discrete molt stages; intermolt (C_4), early premolt (D_0) and postmolt (B and C_{1-3}). Due to the small physical size of these organs we pooled samples so that each of the 2-dimensional gels run represented the average protein expression of three animals in a given molt stage. We then compared protein abundances across molt stages to uncover molt stage-specific processes that were being enhanced or inhibited as the animal progressed through the molt cycle. These findings provide support for the development of

hypotheses and allow us to make connections between cellular physiology and the physiology of the organisms as a whole.

Our findings revealed numerous protein-level changes across the molt cycle, however the two primary constituents of the YO proteome were proteins involved in energy metabolism and oxidative stress. Most of the metabolic proteins that showed significant changes were involved in shunting metabolites between glycolytic branch points and alternative metabolic pathways; this response was quite different from the broad metabolic shifts observed in other studies (Garland et al., 2015, Tomanek and Zuzow, 2010). However, we did uncover a correlation that suggests the possible involvement of a nutrient sensing pathway in the YO.

The primary hypothesis supported by this data involves a pathway whereby reactive oxygen species initiate atrophy in the postmolt YO through the secretion of a protein that is capable of directly and indirectly breaking down cytoskeletal and extracellular proteins. This hypothesis describes, for the first time, an explanation for the mechanism underlying YO atrophy during postmolt.

Materials and Methods

Animal Acquisition and Dissection

In March 2013, adult *Carcinus maenas* were captured from an invasive population inhabiting an estuary of Doran Regional Park, Bodega Bay, California, USA (38.314858,-123.037777). Species confirmation was based on physical characteristics unique to *C. maenas* such as size and coloration. The presence of an array of five spines located lateral to each eyestalk and the presence of three anterior bumps located between the eyes could be used if size and color were insufficient for positive identification. Once captured the animals were moved to holding tanks containing recirculating seawater at the Bodega Marine Laboratory (BML). They were fed a diet of locally caught squid every other day. The animals were housed under these conditions for no longer than a month pending dissection. During this time the carapace width of each animal was measured and recorded. We also regularly quantified hemolymph ecdysteroid titers using an ELISA assay, which allowed us to define the current molt stage of each animal. Based on the results of the ELISA analyses, when animals entered a molt stage of interest they were sacrificed and their YOs harvested.

Dissection of the Y-organs took place at the BML during the third week of March 2013. Each YO pair was rinsed following removal from the cephalothorax and immediately frozen in liquid nitrogen to prevent degradation. Hemolymph samples from each animal were also taken at the time of sacrifice so that ELISA assays could be performed for ecdysteroid content. The YO samples were stored at -80°C and later overnight shipped to California Polytechnic State University, San Luis Obispo on dry ice. Upon reception, samples were again stored at -80°C.

Homogenization and Protein Isolation

Animals were categorized by molt stage using the results of the aforementioned ELISA assay. These results provided quantitative data concerning hemolymph ecdysteroid titers, a proxy for identifying molt stage. Physical cues noted at the time of dissection, like endocuticle thickness and time since ecdysis, were crucial in differentiating between molt stages where ecdysteroid titers overlapped. The ecdysteroid concentrations used to make these determinations were as follows: 2-10 pg/µl (Intermolt, Stage C_4), 25-75 pg/µl (early premolt, stage D_0), and 0-8 pg/µl (postmolt, stage B and late postmolt stage C_{1-3}). Distinguishing between B and C_{1-3} animals depended entirely on the use of visual cues. These different molt stages were treated as the "treatment" groups for the remainder of the experiment.

Based on the small size of *C.* maenas YOs, it was decided that the tissue from multiple animals should be pooled before proceeding. Samples within each molt stage were pooled according to similarities in the content of hemolymph ecdysteroid. It was determined through a proof of concept trial that the YOs of three animals would provide sufficient protein to continue with the proteomic workflow. The sample size to be used in each molt stage group was determined by way of finding the lowest common denominator. Only twelve YOs, three of which were unsuitable for analysis, had been harvested from animals in the D_0 stage. Thus, the nine available YOs were pooled into groups of three giving a final treatment size of three. Subsequently, nine YOs were picked at random from stage B, C_{1-3}, and C_4 samples and pooled as described.

Samples were removed from -80°C and immediately pooled accordingly and placed on ice in 0.6ml, approximately 1:2 ratio, homogenization buffer (7 M urea, 2 M

thiourea, 1% ASB-14, 40 mM Tris-base, 0.001% bromophenol blue, 40 mM dithiothreitol (DTT), and 0.5% immobilize pH 3-10 gradient (IPG) buffer). The delicate nature of the YO allowed us to forgo the traditional method of homogenization, using a glass homogenizer. In doing so we avoided the inherent loss of tissue that comes with using such a method. Instead, homogenization was accomplished using a pipette tip to triturate the homogenate against the side of a standard 2 mL siliconized microcentrifuge tube until all tissue solids had dissolved. The tubes were then incubated at room temperature for one hour to ensure complete protein solubilization.

The samples were next centrifuged at room temperature for 30 minutes at 16,000 g allowing for separation of the solubilized proteins from other insoluble cellular components. The supernatant was transferred to fresh 2 mL siliconized tubes and the gelatinous pellets were discarded. Each sample was divided into two aliquots, each containing approximately 300 μL of the solubilized protein solution. To each of these aliquots was added 1.6 mL of -20°C 10% trichloroacetic acid (TCA) in acetone. Each sample was vortexed briefly and placed at -20°C overnight, allowing proteins to precipitate out of solution. Next, each sample was centrifuged at 4°C for 15 minutes at 18,000 g. The supernatant was poured off as waste and the pellet was rinsed using 1.6 mL of -20°C 100% acetone, vortexed, and again centrifuged at 4°C for 15 minutes at 18,000 g. The remaining acetone was decanted and to each dry pellet was added 0.2 mL of rehydration solution (7 M urea, 2 M thiourea, 2% 3-[(3-Cholamidopropyl)dimethylammonio]-1-propanesulfonate (CHAPS), 2% octylphenoxypolyethoxyethanol (Nonidet P-40), 0.002% bromophenol blue, 0.5% pH 3-10 IPG buffer, and 100 mM dithioerythritol (DTE). The aliquots were pooled, thus

reconstituting the original samples, and vortexed every 10 minutes at room temperature to precipitate the protein. A subset of each sample (volume?) was used to determine protein concentration following the protocol of GE Healthcare's 2D Quant kit.

Two-Dimensional Gel Electrophoresis

Isoelectric focusing was utilized to disperse a total of 400 µg of isolated protein from each sample across an immobilized pH 3-10 IPG strip (Berth et al., 2007; Magdeldin et al., 2014). The isoelectric focusing protocol used consisted of 6 steps carried out over a 24 hour period. As part of this protocol, proteins were initially allowed to passively rehydrate for 5 hours at 0 V, then actively rehydrated for 12 hours at 50 V. The remainder of the protocol consisted of a series of rapid voltage change steps followed by 500 V holding step. To prevent gel overheating, 1.6 mL of mineral oil was added to each lane prior to running the protocol. Once complete the gels were stored overnight at -80°C.

In the next step, the IPG strips were prepared for SDS-PAGE. They were removed from cold storage and incubated in equilibration buffer A (375 mM Tris-base, 6 M urea, 30% glycerol, 2% SDS and 0.002% bromophenol blue, and 65 mM DTT). After 15 minutes at room temperature the solution was replaced with equilibration buffer B (375 mM Tris-base, 6 M urea, 30% glycerol, 2% SDS and 0.002% bromophenol blue, and 135 mM Iodoacetamide) for the same period of time. Once complete, each strip was suspended within a 0.8% agarose layer laid across the top of a 12% polyacrylamide gel. Gels were run using Criterion™ Dodeca™ Cells at 200 V in actively cooled running buffer (25 mM Tris-base, 192 mM glycine, and 0.1% SDS) for 52 minutes. Once the run

was complete the gels were immediately removed and placed in a colloidal Coomassie Blue G-250 staining solution overnight. The next day the gels were de-stained through periodic rising with Milli-Q water until background Coomassie was no longer visible. Digital gel images were acquired by scanning each gel with an Epson 1280 transparency scanner.

Delta 2D

Each gel image was loaded into Delta 2D, a program designed to assist the user in making a composite gel image (Berth et al., 2007). The program allows for spots to be automatically warped, but as is often the case, it was found that this method was unreliable and resulted in many false matches. Thus, all spots were user-matched and then warped to obtain an optimized fused gel image. This fused gel image allowed for all proteins to be conveyed on a single image based on average relative spot intensity. The fused image was next annotated such that each protein whose visual intensity exceeded that of the background was assigned a number and spot boundary. Following identification these numbers would be replaced by the names of the proteins. Creation of heat maps and statistical analysis were both handled within Delta 2D.

Mass Spectrometry

In order to maximize the likelihood of identification the assigned spots were excised from the gels in which they were most intense. These gel plugs were next prepared using a modified version of a previously published protocol, in which spots were trypsinized and plated within a crystalize matrix, and rinsed of excess salts in

preparation for mass spectrometry. (Lovric, 2011; Tomanek and Zuzow, 2010). Porcine trypsin (Promega) was used as an internal calibration standard.

Initially, peptide mass fingerprints (PMF) were collected. Tandem MS of peptide fragment fingerprints (PFF) were then analyzed further to increase identification accuracy. At least 12 PFFs per protein were analyzed. Minimum peak intensity was set to 400-600 to eliminate background noise. These mass data were then used to search against an online database in order to make identifications.

Protein identification was conducted using Mascot (version 2.4; Matrix Science, Inc.; Boston, MA). The results were compared against the NCBI metazoan database, which contains entries compiled from GenBank CDS translations, PIR, SWISS-PROT, PRF, and PDB. Search results were deemed significant ($p<0.05$) if their molecular weight score was above the minimum threshold. Finalized positive identifications based on a significant MOWSE scores were only confirmed if they included two matched peptide sequences.

Statistical analysis

Multiple one-way ANOVA tests were performed to assess the significance of the data at different levels of stringency ($p<0.05$ and $p<0.1$). Treatment groups within these analyses were separated by molt stages C_4, D_0, B, and $C_{1\text{-}3}$. Because Delta 2D lacks the ability to run post-hoc Tukey analyses, these were carried out using Minitab v16.1. Expression profiles were generated from the graphs depicting the post-hoc results of the Tukey test run in Minitab. The PCA analysis and a t-test were both run using Delta 2D built in statistical software. The PCA utilized an identical method grouping as that used

in the ANOVA. In the t-test, groups were formed by combining intermolt/early-premolt into one group and the postmolt stages into another.

Results and Discussion

Results

YO samples were pooled and assigned to specific molt stages based on hemolymph ecdysteroid concentration, determined by ELISA (Table 1). Each pool consisted of three animals (6 YOs) and each group contained a total of three pooled samples. The intermolt molt-stage C_4 group contained animals with ecdysteroid titers ranging from 2.45 to 4.98 pg/μL. The premolt stage D_0 group contained animals with ecdysteroid titers ranging from 18.57 to 66.29 pg/μL. The postmolt stage B group contained animals with ecdysteroid titers ranging from 0.62 to 8.40 pg/μL. The late postmolt stage C_{1-3} group contained animals with ecdysteroid titers ranging from 0.7 to 2.98 pg/μL. Table 1 contains additional information on carapace width, as well as other details regarding the grouping of animals.

The results of our proteomic workflow were first visualized as a fused gel image generated within Delta 2D (Figure 17). Following careful editing of spot boundaries, we detected 279 unique spots, representing individual proteins or their isoforms. Of these, 91 (32.6%) were positively identified using MALDI-ToF/ToF tandem mass spectrometry (Table 4), a fairly decent identification rate given that neither a full genome or transcriptome exists for *C. meanas*. Using Pearson correlation coefficient values, we were able to organize proteins hierarchically to cluster proteins exhibiting similar trends together. The resulting heat maps provided us with qualitative insight into broad-scale changes in protein abundance over each molt stage (Figure 18).

Table 1. Organization of YO samples collected including results of ELISA analysis for hemolymph ecdysteroid titers. Color blocks (e.g. yellow, green, and blue) indicate samples that were pooled within each molt stage.

Stage C4

Animal #	Molt stage	Carapace width (cm)	Color Morph*	Date YO harvested	Hemolymph ecdyteroid (pg/ul)	Comments	Delta 2D labeling
13064	Intermolt (C	8.27	G (O)	3/20/13	2.45	Intact	C4 (Y)
13011	Intermolt (C	8.12	G (O)	3/15/13	2.57	Intact	C4 (Y)
13066	Intermolt (C	7.93	G (O)	3/20/13	2.89	Intact	C4 (Y)
13063	Intermolt (C	8.07	G (O)	3/20/13	4.36	Intact	C4 (G)
13015	Intermolt (C	6.92	G	3/15/13	4.37	Intact	C4 (G)
13016	Intermolt (C	8.46	G	3/15/13	4.42	Intact	C4 (G)
13023	Intermolt (C	7.70	G (O)	3/17/13	4.88	Intact	C4 (B)
13022	Intermolt (C	8.00	G (O)	3/17/13	4.97	Intact	C4 (B)
13042	Intermolt (C	7.41	G	3/17/13	4.98	Intact	C4 (B)

Stage B

Animal #	Molt stage	Carapace width (cm)	Color Morph*	Date YO harvested	Hemolymph ecdyteroid (pg/ul)	Comments	Delta 2D labeling
13082	Postmolt (B	9.15	G	3/20/13	0.62	Intact	B (Y)
13020	Postmolt (B	7.46	G	3/15/13	0.73	Intact	B (Y)
13062	Postmolt (B	9.03	G	3/19/13	0.77	Intact	B (Y)
13005	Postmolt (B	8.13	G	3/15/13	1.06	Intact	B (G)
13060	Postmolt (B	7.66	G	3/19/13	2.17	Intact	B (G)
13080	Postmolt (B	7.60	G	3/20/13	2.33	Intact	B (G)
13040	Postmolt (B	6.94	G	3/17/13	4.08	Intact	B (B)
13041	Postmolt (B	7.91	G	3/17/13	5.97	Intact	B (B)
13024	Postmolt (B	6.58	G	3/17/13	8.40	Intact	B (B)

Stage D0

Animal #	Molt stage	Carapace width (cm)	Color Morph*	Date YO harvested	Hemolymph ecdyteroid (pg/ul)	Comments	Delta 2D labeling
13043	Premolt (D0	7.14	G (O)	3/18/13	18.57	Intact	D0 (Y)
13014	Premolt (D0	7.51	R	3/15/13	21.84	Intact; early	D0 (Y)
13077	Premolt (D0	6.56	G	3/20/13	23.18	Intact	D0 (Y)
13030	Premolt (D0	7.24	R	3/17/13	24.99	Intact	D0 (G)
13033	Premolt (D0	6.42	G	3/17/13	33.05	Intact	D0 (G)
13035	Premolt (D0	6.30	G	3/17/13	38.04	Intact	D0 (G)
13036	Premolt (D0	6.32	G	3/17/13	39.81	Intact	D0 (B)
13093	Premolt (D0	7.86	G (O)	3/22/13	62.77	Intact	D0 (B)
13034	Premolt (D0	5.57	R	3/17/13	66.29	Intact	D0 (B)

Stage C1-3

Animal #	Molt stage	Carapace width (cm)	Color Morph*	Date YO harvested	Hemolymph ecdyteroid (pg/ul)	Comments	Delta 2D labeling
13079	Postmolt (C	8.25	G	3/20/13	0.70	Intact	C1-3 (Y)
13078	Postmolt (C	8.56	G	3/20/13	0.76	Intact	C1-3 (Y)
13056	Postmolt (C	8.27	G	3/19/13	0.79	Intact	C1-3 (Y)
13010	Postmolt (C	8.28	G	3/15/13	1.32	Intact	C1-3 (G)
13007	Postmolt (C	7.36	G	3/15/13	1.44	Intact	C1-3 (G)
13009	Postmolt (C	7.29	G	3/15/13	1.51	Intact	C1-3 (G)
13053	Postmolt (C	8.32	G	3/19/13	1.82	Intact	C1-3 (B)
13055	Postmolt (C	7.20	G	3/19/13	2.69	Intact	C1-3 (B)
13004	Postmolt (C	8.34	G	3/15/13	2.98	Intact	C1-3 (B)

Figure 17. Results of a custom warping strategy employed within Delta 2D (DECODON) are displayed here as a "proteome map", which displays all proteins successfully separated from *C. maenas* Y-organs. Pixel density in the fused gel image has been normalized using the average pixel density across all gels. The x-axis represents proteins separated by isoelectric point (pI), while the y-axis represents separation via molecular weight (MW). All proteins were selected for tandem mass spectrometry, of which 91 of the 279 (32.6%) were positively identified.

Table 2. Complete list of proteins identified via MS/MS mass spectrometry that were present in the YO of *C. maenas* during at least one molt stage.

Spot ID	Protein ID	Estimated MW (kDa)	Estimated pI	Predicted MW (kDa)	Predicted pI	GenBank ID	Mascot Score	Peptide Matches	Sequence Coverage (%)	Functional Category
017	Arginine kinase	49	7.32	40.2	6.39	gi|25453075	64	3	15	Energy metabolism
018	Aspartate aminotransferase	46	7.46	46.2	6.68	gi|871422	106	2	5	Amino acid metabolism
021	Proteasome subunit alpha type-5	26	4.8	25.71	4.83	gi|170204594	56	2	11	Protein degradation
022	Arginine kinase	42	7.52	40	6.05	gi|585342	107	6	24	Energy metabolism
029	Heat shock protein 70	37	5.37	69.7	5.4	gi|170208924	157	3	15	Molecular chaperone
032	Triosephosphate isomerase	35	6.87	27	5.86	gi|307564155	89	4	9	Energy metabolism
037	Mitochondrial SOD	31	6.75	23.8	7.13	gi|317415923	64	2	7	Oxidative stress
038	Cryptocyanin	28	5.41	75.7	5.49	gi|4191390	84	2	3	Blood Species
039	Cryptocyanin 2	28	5.66	78.21	5.71	gi|81230850	77	2	2	Blood Species
041	Cryptocyanin	27	5.28	75.72	5.49	gi|4191390	91	2	3	Blood Species
042	Cdc42	27	6.69	15.21	8.64	gi|1644283	76	2	17	Intracellular transport
043	Cryptocyanin	27	5.48	75.72	5.49	gi|4191390	72	2	3	Blood Species
054	Collagen	48	8.91	160.83	9.21	gi|504157543	73	2	1	Cytoskeleton
057	Cyclophilin A (CypA)	18	9.14	17.35	8.75	gi|294718609	153	3	14	Oxidative Stress
058	Cyclophilin A (CypA)	18	9.3	17.35	8.75	gi|294718609	157	3	14	Oxidative Stress
068	Receptor for activated protein kinase c1 (RACK1)	35	8.91	35.62	8.07	gi|170189770	60	3	10	Signal transduction
070	Cyclophilin A (CypA)	18	8.64	17.35	8.75	gi|294718609	115	3	14	Oxidative Stress
071	Cyclophilin A (CypA)	18	8.66	17.35	8.75	gi|294718610	194	3	14	Oxidative Stress
074	Mitochondrial malate dehydrogenase	44	7.67	35.55	8.92	gi|170204397	113	2	9	Energy metabolism
075	Cytosolic SOD	39	7.4	31.37	6.31	gi|8347760	102	4	15	Oxidative stress
104	Cryptocyanin 2	89	6.19	78.21	5.71	gi|81230850	206	4	6	Blood Species
108	Hemocyanin subunit	88	5.9	77.05	5.26	gi|7582388	233	6	10	Blood Species
115	Cryptocyanin 2	95	4.21	78.21	5.71	gi|81230850	96	4	6	Blood Species
119	Cryptocyanin 2	89	6	78.21	5.71	gi|81230851	156	5	7	Blood Species
127	Serum albumin	85	6.37	69.25	5.82	gi|1351907	134	4	8	Blood Species
128	Serum albumin	85	6.33	69.25	5.82	gi|1351908	190	5	9	Blood Species
134	β-actin	74	5.83	34.67	6.1	gi|170198993	83	3	15	Cytoskeleton
138	Cryptocyanin	74	6.16	75.72	5.49	gi|4191390	90	3	4	Blood Species
140	β-tubulin	73	5.53	29.67	8.24	gi|170185119	99	3	12	Cytoskeleton
141	Cryptocyanin	73	6.3	75.72	5.49	gi|4191390	120	5	7	Blood Species
142	Cryptocyanin 2	73	6.56	78.21	5.71	gi|81230850	155	3	4	Blood Species
143	Catalase	71	7.46	58.58	6.58	isotig00080	46	2	3	Oxidative stress
144	Hemocyanin	73	4.89	77.05	5.26	gi|7582388	70	2	3	Blood Species
145	Hemocyanin subunit	74	6.9	77.05	5.26	gi|7582388	84	2	3	Blood Species
147	Cryptocyanin 2	74	6.4	78.21	5.71	gi|81230850	134	4	7	Blood Species
149	β-tubulin	71	5.4	50.9	4.83	gi|170204596	142	3	16	Cytoskeleton
150	Cryptocyanin 2	73	6.49	78.21	5.71	gi|81230850	85	4	7	Blood Species
151	Cryptocyanin	73	6.25	75.72	5.49	gi|4191390	141	5	7	Blood Species
153	Peroxiredoxin 3	73	5.69	26.82	8.73	gi|193627312	53	2	8	Oxidative stress
160	Cryptocyanin 2	73	6.39	78.21	5.71	gi|81230850	171	5	8	Blood Species
161	Catalase	71	7.34	58.58	6.58	gi|260586476	65	2	3	Oxidative stress
162	Mitochondrial glutamate dehydrogenase	71	6.69	11.39	9.39	gi|338224490	72	2	28	Amino acid metabolism
163	F1F0-ATP synthase β-subunit	69	5.29	55.77	5.07	gi|170245256	314	6	36	Energy metabolism
165	β-tubulin	70	5.49	50.71	4.88	gi|170204596	181	3	16	Cytoskeleton
166	Cryptocyanin 2	71	6.22	78.21	5.71	gi|81230850	146	3	4	Blood Species
168	Cryptocyanin 2	70	6.29	78.21	5.71	gi|81230850	172	3	4	Blood Species
169	Cryptocyanin 2	71	6.49	78.21	5.71	gi|81230850	176	4	7	Blood Species
174	β-tubulin	67	5.42	50.9	4.83	gi|3915093	70	4	8	Cytoskeleton
176	β-actin	60	5.81	28.58	4.98	gi|170185032	190	4	24	Cytoskeleton
183	Enolase	63	6.98	39.85	5.45	gi|41394399	140	4	17	Energy metabolism
186	Rab gdp-dissociation inhibitor (Rab-GDI)	64	6.17	49.95	5.28	isotig00151	72	2	2	Intracellular transport
188	Phosphoglycerate kinase	63	7.04	44.08	6.22	gi|357610086	66	2	6	Energy metabolism
190	78 kDa glucose regulated protein (BiP)	62	4.86	72.54	4.98	gi|402536580	59	3	5	Molecular chaperone
191	Phosphoglycerate kinase	65	6.86	44.08	6.22	gi|357610086	65	2	6	Energy metabolism
192	β-actin	61	5.7	41.91	5.16	gi|170190957	251	5	12	Cytoskeleton
194	Isocitrate dehydrogenase	61	7.17	50.23	7.56	gi|170207260	98	3	13	Energy metabolism
196	β-actin	66	5.5	41.91	5.16	gi|170190957	134	5	12	Cytoskeleton
197	78 kDa glucose regulated protein (BiP)	61	4.77	39.77	4.56	gi|170205314	254	6	24	Molecular chaperone
204	4-hydroxyphenylpyruvate dioxygenase	57	6.63	32.92	5.48	isotig00955	42	2	5	Amino acid metabolism
206	Fructose 1,6-bisphosphate aldolase	56	7.62	39.68	7.67	gi|170182278	131	2	15	Energy metabolism
207	β-actin	56	5.63	41.91	5.16	gi|170190957	77	2	5	Cytoskeleton
208	α-tubulin	55	6.2	49.91	5	gi|170244245	167	5	28	Cytoskeleton
209	Arginine kinase	54	7.14	40.27	6.19	gi|170186144	278	7	24	Energy metabolism
210	Catalase	56	7.3	58.58	6.58	gi|260586476	59	2	2	Oxidative stress
213	β-actin	55	5.63	33.07	5.01	gi|40217868	72	4	15	Cytoskeleton
214	β-tubulin	52	5.95	50.9	4.83	gi|170204596	111	3	16	Cytoskeleton
217	β-tubulin	50	5.89	50.71	4.88	gi|170204596	140	4	16	Cytoskeleton
218	β-tubulin	49	5.74	50.71	4.88	gi|170192063	123	3	12	Cytoskeleton
219	β-tubulin	48	5.87	50.71	4.88	gi|170204596	180	5	21	Cytoskeleton
220	Glyceraldehyde-3-phosphate dehydrogenase	45	6.73	35.7	6.6	gi|300518909	109	2	7	Energy metabolism
223	Glyceraldehyde-3-phosphate dehydrogenase	46	6.91	35.7	6.6	gi|300518910	185	3	11	Energy metabolism
224	G protein β-1 subunit	46	5.96	37.43	5.83	gi|3913720	72	4	10	Signal transduction
229	Cytoplasmic carbonic anhydrase	41	6.94	21.12	6.2	gi|161367857	127	4	26	Oxidative stress
231	Heat shock protein 70	39	6.74	69.7	5.4	gi|170208924	123	3	15	Molecular chaperone
232	F1F0-ATP synthase β-subunit	62	5.29	55.77	5.07	gi|170245256	211	6	27	Energy metabolism
233	F1F0-ATP synthase β-subunit	63	5.19	55.77	5.07	gi|170245256	198	6	34	Energy metabolism
234	Heat shock protein 70	59	5.28	71.87	5.28	gi|170221797	91	2	19	Molecular chaperone
235	β-actin	55	5.39	28.58	4.98	gi|170185032	338	5	37	Cytoskeleton
236	β-actin	54	5.28	28.58	4.98	gi|170185032	209	4	24	Cytoskeleton
237	β-tubulin	47	5.58	50.2	4.74	gi|501290333	70	3	6	Cytoskeleton
238	β-tubulin	46	5.73	50.9	4.83	gi|170204596	223	5	21	Cytoskeleton
239	β-tubulin	46	5.84	50.71	4.88	gi|3915087	147	4	21	Cytoskeleton
240	G protein β-1 subunit	45	5.96	37.39	5.98	gi|3913720	98	4	10	Signal transduction
242	β-tubulin	42	5.27	50.9	4.83	gi|170204596	102	3	13	Cytoskeleton
243	Farnesoic acid O-methyltransferase (FaMet)	49	4.95	31.45	4.71	gi|300693007	154	3	14	Hormone synthesis
248	Cytoplasmic SOD	39	7.19	31.28	6.87	gi|8347760	136	4	16	Oxidative stress
250	Heat shock protein 70	38	7.01	69.7	5.4	gi|170208924	139	3	15	Molecular chaperone
251	Cryptocyanin	38	6.25	75.72	5.49	gi|4191390	72	2	3	Blood Species
259	Transketolase	129	5.54	68	8.33	gi|91076192	96	2	12	Energy metabolism
273	α-tubulin	65	6.33	50.31	5.11	gi|170183096	63	2	8	Cytoskeleton
274	α-tubulin	54	6.45	49.91	5	gi|170244245	51	2	11	Cytoskeleton

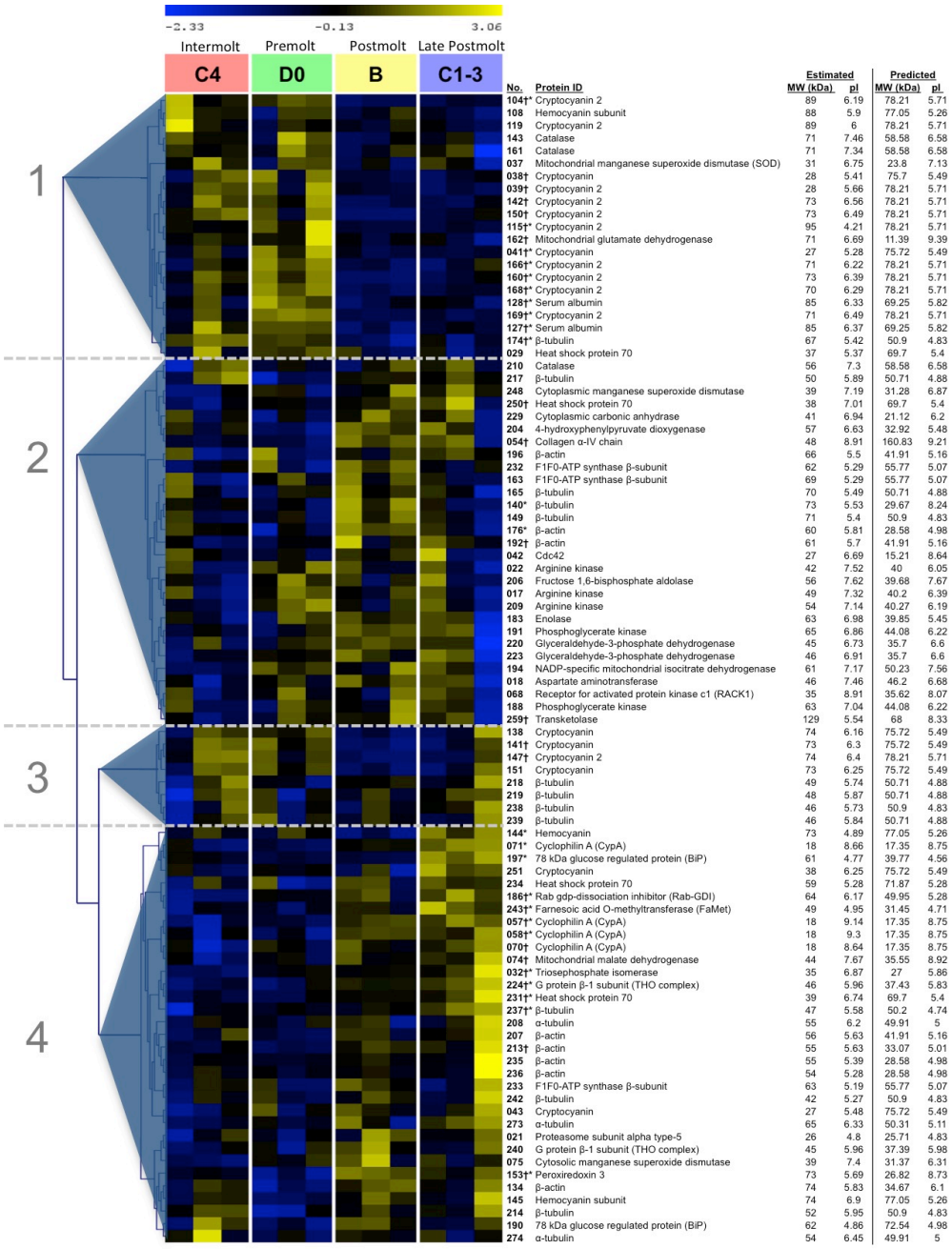

No.	Protein ID	Estimated MW (kDa)	Estimated pI	Predicted MW (kDa)	Predicted pI
104†*	Cryptocyanin 2	89	6.19	78.21	5.71
108	Hemocyanin subunit	88	5.9	77.05	5.26
119	Cryptocyanin 2	89	6	78.21	5.71
143	Catalase	71	7.46	58.58	6.58
161	Catalase	71	7.34	58.58	6.58
037	Mitochondrial manganese superoxide dismutase (SOD)	31	6.75	23.8	7.13
038†	Cryptocyanin	28	5.41	75.7	5.49
039†	Cryptocyanin 2	28	5.66	78.21	5.71
142†	Cryptocyanin 2	73	6.56	78.21	5.71
150†	Cryptocyanin 2	73	6.49	78.21	5.71
115†*	Cryptocyanin 2	95	4.21	78.21	5.71
162†	Mitochondrial glutamate dehydrogenase	71	6.69	11.39	9.39
041†*	Cryptocyanin	27	5.28	75.72	5.49
166†*	Cryptocyanin 2	71	6.22	78.21	5.71
160†*	Cryptocyanin 2	73	6.39	78.21	5.71
168†*	Cryptocyanin 2	70	6.29	78.21	5.71
128†*	Serum albumin	85	6.33	69.25	5.82
169†*	Cryptocyanin 2	71	6.49	78.21	5.71
127†*	Serum albumin	85	6.37	69.25	5.82
174†*	β-tubulin	67	5.42	50.9	4.83
029	Heat shock protein 70	37	5.37	69.7	5.4
210	Catalase	56	7.3	58.58	6.58
217	β-tubulin	50	5.89	50.71	4.88
248	Cytoplasmic manganese superoxide dismutase	39	7.19	31.28	6.87
250†	Heat shock protein 70	38	7.01	69.7	5.4
229	Cytoplasmic carbonic anhydrase	41	6.94	21.12	6.2
204	4-hydroxyphenylpyruvate dioxygenase	57	6.63	32.92	5.48
054†	Collagen α-IV chain	48	8.91	160.83	9.21
196	β-actin	66	5.5	41.91	5.16
232	F1F0-ATP synthase β-subunit	62	5.29	55.77	5.07
163	F1F0-ATP synthase β-subunit	69	5.29	55.77	5.07
165	β-tubulin	70	5.49	50.71	4.88
140*	β-tubulin	73	5.53	29.67	8.24
149	β-tubulin	71	5.4	50.9	4.83
176*	β-actin	60	5.81	28.58	4.98
192†	β-actin	61	5.7	41.91	5.16
042	Cdc42	27	6.69	15.21	8.64
022	Arginine kinase	42	7.52	40	6.05
206	Fructose 1,6-bisphosphate aldolase	56	7.62	39.68	7.67
017	Arginine kinase	49	7.32	40.2	6.39
209	Arginine kinase	54	7.14	40.27	6.19
183	Enolase	63	6.98	39.85	5.45
191	Phosphoglycerate kinase	65	6.86	44.08	6.22
220	Glyceraldehyde-3-phosphate dehydrogenase	45	6.73	35.7	6.6
223	Glyceraldehyde-3-phosphate dehydrogenase	46	6.91	35.7	6.6
194	NADP-specific mitochondrial isocitrate dehydrogenase	61	7.17	50.23	7.56
018	Aspartate aminotransferase	46	7.46	46.2	6.68
068	Receptor for activated protein kinase c1 (RACK1)	35	8.91	35.62	8.07
188	Phosphoglycerate kinase	63	7.04	44.08	6.22
259†	Transketolase	129	5.54	68	8.33
138	Cryptocyanin	74	6.16	75.72	5.49
141†	Cryptocyanin	73	6.3	75.72	5.49
147†	Cryptocyanin 2	74	6.4	78.21	5.71
151	Cryptocyanin	73	6.25	75.72	5.49
218	β-tubulin	49	5.74	50.71	4.88
219	β-tubulin	48	5.87	50.71	4.88
238	β-tubulin	46	5.73	50.9	4.83
239	β-tubulin	46	5.84	50.71	4.88
144*	Hemocyanin	73	4.89	77.05	5.26
071*	Cyclophilin A (CypA)	18	8.66	17.35	8.75
197*	78 kDa glucose regulated protein (BiP)	61	4.77	39.77	4.56
251	Cryptocyanin	38	6.25	75.72	5.49
234	Heat shock protein 70	59	5.28	71.87	5.28
186†*	Rab gdp-dissociation inhibitor (Rab-GDI)	64	6.17	49.95	5.28
243†*	Farnesoic acid O-methyltransferase (FaMet)	49	4.95	31.45	4.71
057†*	Cyclophilin A (CypA)	18	9.14	17.35	8.75
058†*	Cyclophilin A (CypA)	18	9.3	17.35	8.75
070†	Cyclophilin A (CypA)	18	8.64	17.35	8.75
074†	Mitochondrial malate dehydrogenase	44	7.67	35.55	8.92
032†*	Triosephosphate isomerase	35	6.87	27	5.86
224†*	G protein β-1 subunit (THO complex)	46	5.96	37.43	5.83
231†*	Heat shock protein 70	39	6.74	69.7	5.4
237†*	β-tubulin	47	5.58	50.2	4.74
208	α-tubulin	55	6.2	49.91	5
207	β-actin	56	5.63	41.91	5.16
213†	β-actin	55	5.63	33.07	5.01
235	β-actin	55	5.39	28.58	4.98
236	β-actin	54	5.28	28.58	4.98
233	F1F0-ATP synthase β-subunit	63	5.19	55.77	5.07
242	β-tubulin	42	5.27	50.9	4.83
043	Cryptocyanin	27	5.48	75.72	5.49
273	α-tubulin	65	6.33	50.31	5.11
021	Proteasome subunit alpha type-5	26	4.8	25.71	4.83
240	G protein β-1 subunit (THO complex)	45	5.96	37.39	5.98
075	Cytosolic manganese superoxide dismutase	39	7.4	31.37	6.31
153†*	Peroxiredoxin 3	73	5.69	26.82	8.73
134	β-actin	74	5.83	34.67	6.1
145	Hemocyanin subunit	74	6.9	77.05	5.26
214	β-tubulin	52	5.95	50.9	4.83
190	78 kDa glucose regulated protein (BiP)	62	4.86	72.54	4.98
274	α-tubulin	54	6.45	49.91	5

Figure 18. Heat map displaying all proteins successfully identified from the Y-organ of *C. maenas* using tandem mass spectrometry. Each labeled/colored group represents a molt stage. Each molt stage is represented by the YOs of 9 individual crabs, which were pooled such that each vertical column of the heat map represents the averaged protein abundances of 3 crabs. A dagger (†) next the protein ID number represents significance at a p-value of 0.05 within a t-test. An asterisk (*) represents significance at a p-value of 0.05 within an ANOVA. Results of the ANOVA using a p-value of 0.1 not shown. The dashed white line represents the bounds of each cluster determined using Pearson correlation coefficients. Yellow indicates increased abundance. Black represents no change form the mean. Blue represents a relative decrease in abundance. Numbering along left side represent clusters of proteins exhibiting similar abundance patterns.

At a p-value ≤ 0.05, 24 of the 91 (26.4%) successfully identified proteins significantly changed in abundance in at least one molt stage relative to the others. From these results, additional significant-only hierarchically clustered heat maps were created (Figure 19). We also compared combined treatments as intermolt/early-premolt (C_4 and D_0) and postmolt (B and C_{1-3}) using a t-test ($p<0.05$) and found that 34 of the 91 (37.4%) successfully identified proteins changed in abundance between these two groups. The results of the t-test provide a statistical "middle ground" between the results of the two ANOVA analyses and allowed us to make alternative hypotheses focused on the difference in the pre-ecdysial and post-ecdysial animals. Support for utilizing the results of this approach will be discussed.

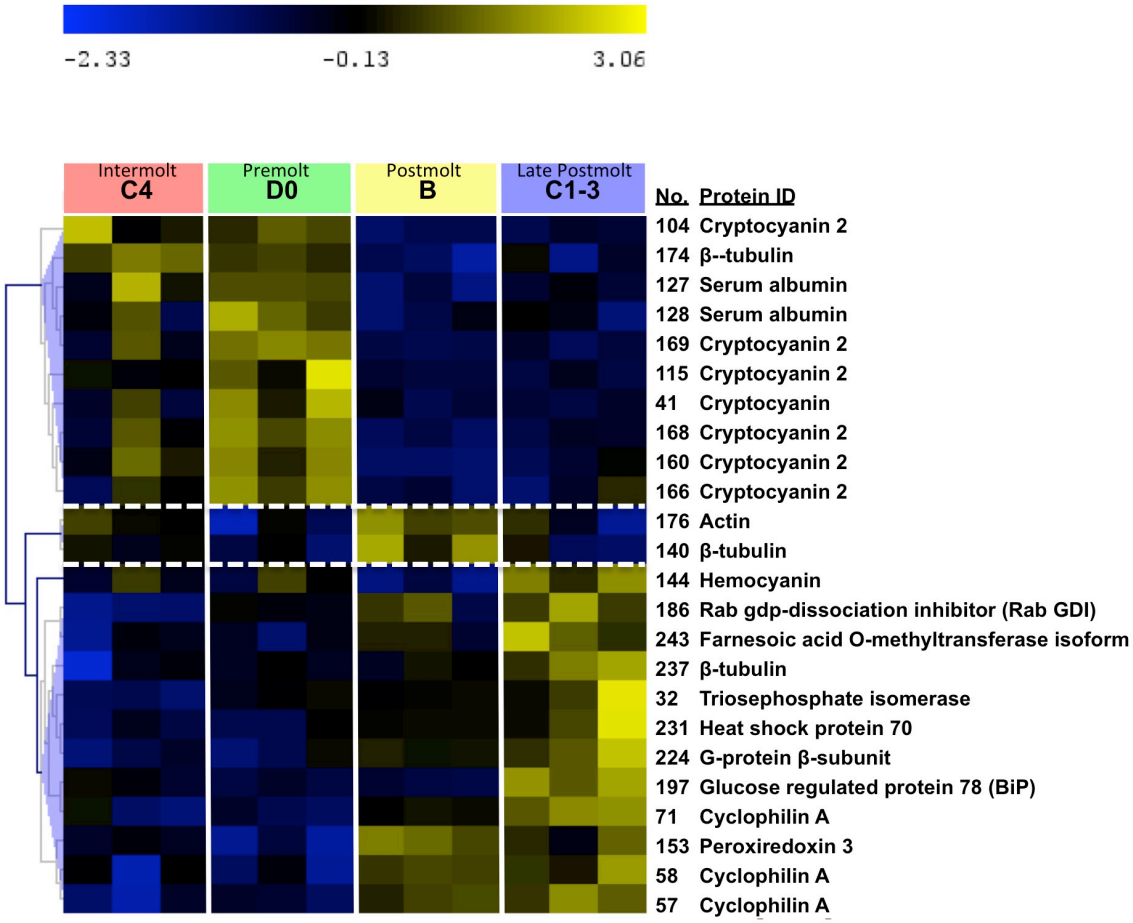

Figure 19. Heat map showing relative abundances of proteins that significantly changed over the course of the molt cycle in at least one molt stage of *C. maenas* YOs (ANOVA $p<0.05$). Brighter yellow indicates increased abundance. Black represents no change form the mean. Blue represents a relative decrease in abundance.

Principle component analysis of the ANOVA results ($p<0.05$) visualized patterns and differences in protein abundances between each of the molt stages (Figure 20). The differences were quantified by evaluating their respective loading values (Table 3). The top 10 significant positive and negative loadings for both PC1 and PC2 are listed in Table 1. These proteins represent those that exhibited the greatest contribution to the clustering observed within the PCA. Separation between molt stages was most striking along the x-axis (PC1) where changes in cytoskeletal, oxidative stress (cyclophilin A, heat shock

protein 70, and peroxiredoxin 3), (tubulin, actin, Rab-GDI), and blood (crytptocyanin, hemocyanin, serum albumin) proteins predominated. The separation observed along PC1 existed, almost exclusively, between intermolt/early-premolt (C_4 and D_0) and postmolt (B and $C_{1\text{-}3}$) stages (Figure 20). Molt stages C_4 and D_0 showed a substantial amount of overlap indicating similar patterns of protein abundance. Molt stages B and $C_{1\text{-}3}$ were marginally separated from each other along PC2, but not PC1.

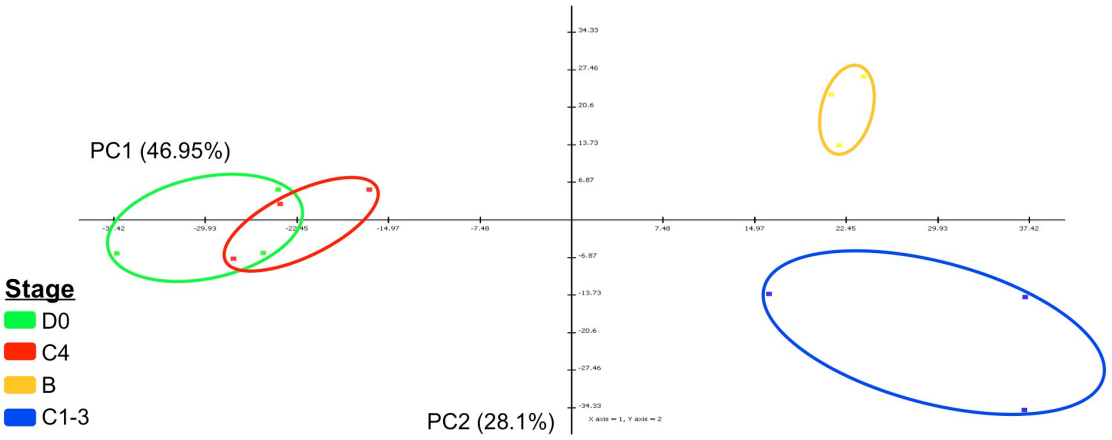

Figure 20. Results of the principal component analysis run on proteins that significantly changed according to the results of ANOVA ($p<0.05$). The axes displayed represent the two primary dimensions along which differences in the protein abundances of each molt stage can be compared.

Table 3. Loading values for PC1 and PC2 separating molt stages according to significant changes of protein abundances.

	Principle Component 1		Principle Component 2	
Component Loading Rank	Protein (Spot ID)	Loading Value	Protein (Spot ID)	Loading Value
	Positive Loadings for Molt Stage			
1	71 Cyclophilin A	1.71853	41 Cryptocyanin	1.64384
2	104 Cryptocyanin 2	1.52093	127 Serum albumin	1.36359
3	144 Hemocyanin subunit	1.45552	243 Farnesoic acid O-methyltransferase isoform	1.30315
4	197 Heat shock protein 70 kDa	1.4069	57 Cyclophilin A	1.24516
5	153 Thioredoxin-dependent peroxide reductase	1.2105	176 Actin	1.10789
6	57 Cyclophilin A	1.04123	160 Cryptocyanin 2	1.03442
7	174 Beta-2-tubulin	0.97158	166 Cryptocyanin 2	1.00695
8	237 Tubulin beta chain	0.73144	237 Tubulin beta chain	0.71189
9	115 Cryptocyanin 2	0.61136	128 Serum albumin	0.63429
10	140 Beta-tubulin	0.54234	174 Beta-2-tubulin	0.36553
	Negative Loadings for Molt Stage			
1	186 Rab gdp-dissociation inhibitor	-1.35346	58 Cyclophilin A	-1.82022
2	176 Actin	-1.22992	169 Cryptocyanin 2	-1.78554
3	32 Triosephosphate isomerase	-1.19317	231 Heat shock protein 40	-1.64209
4	128 Serum albumin	-1.06227	168 Cryptocyanin 2	-1.08615
5	160 Cryptocyanin 2	-0.75825	153 Thioredoxin-dependent peroxide reductase	-0.64259
6	168 Cryptocyanin 2	-0.59624	144 Hemocyanin subunit	-0.57576
7	127 Serum albumin	-0.53733	104 Cryptocyanin 2	-0.49619
8	169 Cryptocyanin 2	-0.40714	115 Cryptocyanin 2	-0.42366
9	243 Farnesoic acid O-methyltransferase isoform	-0.33215	197 Heat shock protein 70 kDa	-0.30779
10	41 Cryptocyanin	-0.07735	224 G-protein beta-1-subunit	-0.23807

We also assessed the results of a PCA analysis run on our entire set of positively identified proteins (Figure 21). We were unable to make any specific claims from this analysis because it included "non-significant" proteins. However, we found that the pattern of separation between intermolt/early-premolt and postmolt stages was preserved. In fact, there was a degree of homogeneity within the proteins whose loading values contributed to the clustering in both of these analyses (Table 4).

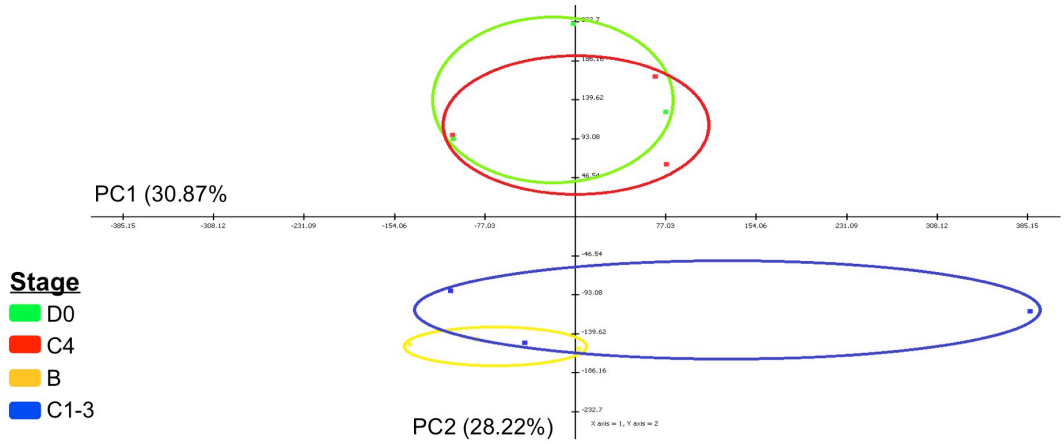

Figure 21. Results of the principal component analysis on all identified proteins regardless of significance. The axes displayed represent the two primary dimensions along which differences in the protein abundances of each molt stage were separated.

Table 4. Loading values for significant and non-significant proteins according to molt stage.

	Principle Component 1		Principle Component 2	
Component Loading Rank	Protein (Spot ID)	Loading Value	Protein (Spot ID)	Loading Value
	Positive Loadings for Molt Stage			
1	071 Cyclophilin A	1.71853	041 Cryptocyanin	1.64384
2	042 GTP binding protein	1.63238	248 Cytoplasmic manganese superoxide dismutase	1.55522
3	149 Beta 2-tubulin	1.59546	150 Cryptocyanin 2	1.48954
4	142 Cryptocyanin 2	1.59045	240 Transducin beta chain 1	1.47163
5	220 Glyceraldehyde-3-phosphate dehydrogenase	1.57218	191 Phosphoglycerate kinase	1.37796
6	018 Aspartate aminotransferase	1.5704	127 Serum albumin	1.36359
7	208 Alpha-actin	1.54319	219 Beta 1-tubulin	1.33893
8	104 Cryptocyanin 2	1.52093	243 Farnesoic acid O-methyl transferase	1.30315
9	039 Cryptocyanin 2	1.50129	068 Receptor for activated protein kinase c1	1.30027
10	144 Hemocyanin subunit	1.45552	165 Beta 1-tubulin	1.27208
	Negative Loadings for Molt Stage			
1	194 Mitochondrial isocitrate dehydrogenase [NADP]	-1.51647	058 Cyclophilin A	-1.82022
2	210 Catalase	-1.44168	169 Cryptocyanin 2	-1.78554
3	186 Rab GDP-dissociation inhibitor	-1.35346	238 Tubulin beta-2 chain	-1.75879
4	108 Hemocyanin subunit	-1.23877	183 2-phospho-D-glycerate hydrolase	-1.75519
5	176 Actin	-1.22992	207 Alpha-actin	-1.72908
6	229 Cytoplasmic carbonic anhydrase	-1.22291	259 Transkelotase-like protein	-1.71899
7	259 Transkelotase-like protein	-1.21346	231 Heat shock protein 70	-1.64209
8	054 Collagen	-1.2004	188 Phosphoglycerate kinase	-1.62051
9	032 Triosephosphate isomerase	-1.19317	162 Glutamate dehydrogenase	-1.58487
10	213 Actin D	-1.15462	217 Beta 1-tubulin	-1.56479

The grouping of molt stages observed within both the heat maps and PCA analyses caught our attention. These visual trends were the basis for our decision to include the results of a t-test within the data set (Figure 22). Doing so allowed us to consider significant differences in protein abundance observed between the

intermolt/early-premolt and postmolt without being excessively stringent – a problem given our small sample size. The pooling of molt stages provided a more powerful statistical approach as it increased our sample number and therefore our degrees of freedom. We felt both analyses, the t-test and ANOVA, provided a more comprehensive approach to detecting biological important changes in the Y-organ proteome.

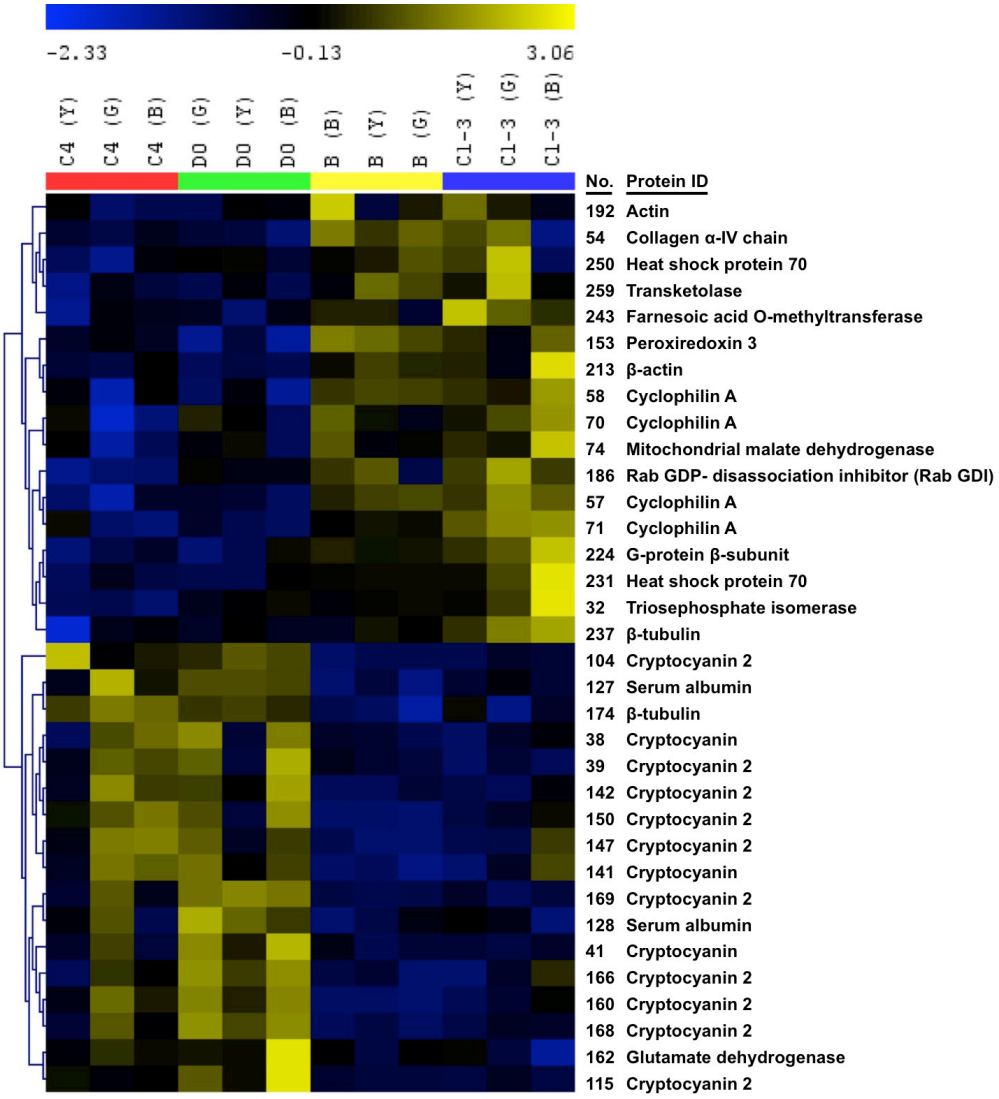

Figure 22. Heat map displaying the hierarchical clustering of proteins that changed in abundance between pre- (C_4 and D_0) and postmolt (B and $C_{1\text{-}3}$) stages using a student's t-test (p-value≤0.05).

We organized our discussion according to protein function and involvement in distinct cellular processes. Thus, we will discuss *energy metabolism, the stress response, downstream effects of ROS, and hemolymph species*. These functional categories provide the framework through which we will interpret the relevance of particular intracellular processes to molting, and ultimately to general YO physiology.

Within each functional category we will discuss the results of our t-test, which represents broad premolt/postmolt changes in the YO proteome. We will also make claims specific to individual molt stages by utilizing the results of our ANOVA and corresponding post-hoc analyses (Tukey-HSD). While a number of identified proteins did not change significantly, their abundances often changed in similar patterns to those proteins whose abundances changed significantly. In some cases, it appears that the changes were not significant due to our limited sample size. Where we think it is justified, we will include these proteins in our discussion while being mindful of their statistical non-significance. We feel that this is important because this is the first characterization of a whole proteome specific to the YO.

Energy metabolism

We identified proteins belonging to a number of metabolic pathways, including glycolysis, tricarboxylic acid cycle and pentose phosphate pathways. As these pathways are interconnected, we will relate the changes in abundances of proteins representing these pathways to each other.

Glycolysis

Triosephosphate isomerase (TPI; spot 32) was the only identified glycolytic enzyme that showed significance by increasing in abundance in the postmolt YO (t-test $p<0.05$, ANOVA $p<0.05$). Fructose 1,6-bisphosphate aldolase (FBP), glyceraldehyde-3-phosphate dehydrogenase (GAPDH), $NADP^+$-dependent isocitrate dehydrogenase (NADP-ICDH), phosphoglycerate kinase (PGK), and enolase were all identified but none showed significant changes in abundance across molt stages. However, it should be noted that when clustered together many of these proteins showed trends in their abundance patterns. For the most part, their abundance patterns appeared random. However there is a general trend toward being at the lowest abundance during the intermolt stage. We can only make inference regarding this non-significant data but the idea of lower abundance during intermolt is logical since the YO is in a basal state during this stage.

Glycolysis forks forming two products following the enzymatic reaction carried out by aldolase. These products are then interconverted by the enzyme TPI. Thus, increased activity of TPI is associated with enhanced glycolytic rates by increasing the abundance of glyceraldehyde-3-phosphate (G3P) available to GAPDH. Inhibiting TPI activity reduces the rate of interconversion between dihydroxyacetone phosphate (DHAP) and glyceraldehyde-3-phosphate (GAP). Ultimately, this has the potential to limit the input of substrate for GAPDH, the subsequent enzyme in glycolysis, and increases intracellular DHAP concentrations, leading to increasing synthesis of glycerol 3-phosphate and triacylglycerides. Additionally, as normal glycolysis is slowed by this process, an increase in the metabolites of the pentose phosphate pathway (PPP) are observed (Grüning et al., 2014). It is reasonable to assume that a similar increase in

DHAP would be observed if overall TPI protein abundances were decreased like is the case in the intermolt/early premolt YO. A possible explanation for this observed pattern involves the downstream conversion of DHAP to triglycerides as a form of energy storage, especially during intermolt when TPI abundance is lowest.

Transketolase (TK; spot 259) is an enzyme involved in multiple steps of the PPP and is significantly increased in abundance during postmolt (t-test $p<0.05$). Transketolase plays a crucial role in connecting the PPP and glycolytic pathways by catalyzing two important interconversions, both of which involve transformation of PPP specific metabolites into metabolites that can be fed back into glycolysis. The first reaction involves rearrangement of carbons from xylulose-5-P and ribose-5-P to form sedoheptulose-7-P and glyceraldehyde-3-P, the latter of which can be fed directly back into glycolysis. The second reaction involves a similar carbon transfer that utilizes xylulose-5-P and erythrose-4-phosphate to form fructose 6-phosphate and glyceraldehyde-3-P, both of which can be fed directly back into glycolysis. In addition to its important role as a generator of NADPH, the PPP functions to create and recycle pentose sugars. Again, TK plays a central role in this process. We believe that the increase in TPI and TK abundances during postmolt is established to aid in the recycling of excess pentose sugars that were previously synthesized for mRNA construction during the activated YO stages of premolt.

The last metabolic enzyme that changed abundance during the molt-cycle was the TCA cycle enzyme mitochondrial malate dehydrogenase (mMDH; spot 74). The abundance of mMDH increased in postmolt stages (t-test $p<0.05$), but not significantly based on our ANOVA analysis. Malate dehydrogenase is responsible for the oxidation of

malate into oxaloacetate via the reduction of a NAD^+ cofactor to NADH. The NADH formed is in turn fed into the oxidative phosphorylation pathway, helping to establish the proton gradient across the inner mitochondrial membrane. During gluconeogenesis, the reaction is favored to proceed in reverse order. Regardless of direction, this reaction is generally thought of as a non-regulatory step - that is, directionality depends on the concentration of substrate. One possible explanation for the observation of increased mMDH in the postmolt YO is that of increased demand for NADH in the mitochondria.

With the exception of TPI in glycolysis, TK in the PPP, and MDH in the TCA cycle, there was very little change in the primary metabolic pathways of the YO. This suggests that the YO in the molt stages observed is metabolically stable and geared toward glycolysis rather than gluconeogenesis. This hypothesis is supported by the finding that arginine kinase (AK; spots 17, 22, and 209), a phosphotransferase enzyme involved in maintaining energy homeostasis through the transfer of phosphate groups from arginine-phosphate to adenosine diphosphate (ADP), remained unchanged across molt stages. Previous studies showed that when crustaceans undergo periods of metabolic stress, AK concentrations fluctuate dramatically to meet the cellular demand for ATP (Garland et al., 2015). The lack of significant changes in this and the other metabolic proteins mentioned supports the idea that there is limited change in energy metabolism in the YO during intermolt, early premolt, and postmolt. Instead, changes in abundances may be related to discreet shifts favoring the production of NADPH and catabolism, specifically the recycling of pentose sugars, during postmolt. The activated YO hypertrophies in response to increased biosynthetic requirements. Future studies should test the idea that the YO only increases energy metabolism during mid and late premolt,

where demand for energy would be expected to increase in response to increase in cell size and biosynthetic output.

YO activation through metabolites

Despite a lack of change in most metabolic enzymes, the data suggest that the YO participates in nutrient sensing in a manner not previously described in this tissue. The rational leading to our investigation of such a process is that the YO only becomes activated when the animal has acquired enough nutrients to support a new round of growth. Furthermore, acute metabolic stress during early premolt will send the animal back to intermolt until such a stress is removed. Thus, the YO may utilize nutrient sensing as a way of dictating the progression through the premolt stages.

Specifically, we believe that the changes in the abundance of glutamate dehydrogenase (GLDH; spot 162) may hold the key to a major nutrient sensing pathway within the YO. We found that GLDH significantly increased in abundance in the intermolt/early premolt YO (t-test $p<0.05$). Importantly, increased GLDH abundance correlated with an increase in hemolymph ecdysteroid (Figure 23). To support this we draw attention to the fact that third cell in the heat map (Figure 2, Spot 162) contained YOs from crabs with significantly higher hemolymph ecdysteroid concentrations than the two other sample pools within this molt stage ($p<0.05$). The high ecdysteroid content indicates that these animals are further along in D_0 than others in this group. The significance of this finding should not distract from the fact that ecdysteroid titer is still within the range constituting the D_0 stage. Rather, it is an example of the degree of change that occurs as the animal enters early premolt. Here, we hypothesize that this

increase in hemolymph ecdysteroid content may, in part, be the result of the increased intracellular α-ketoglutarate concentrations.

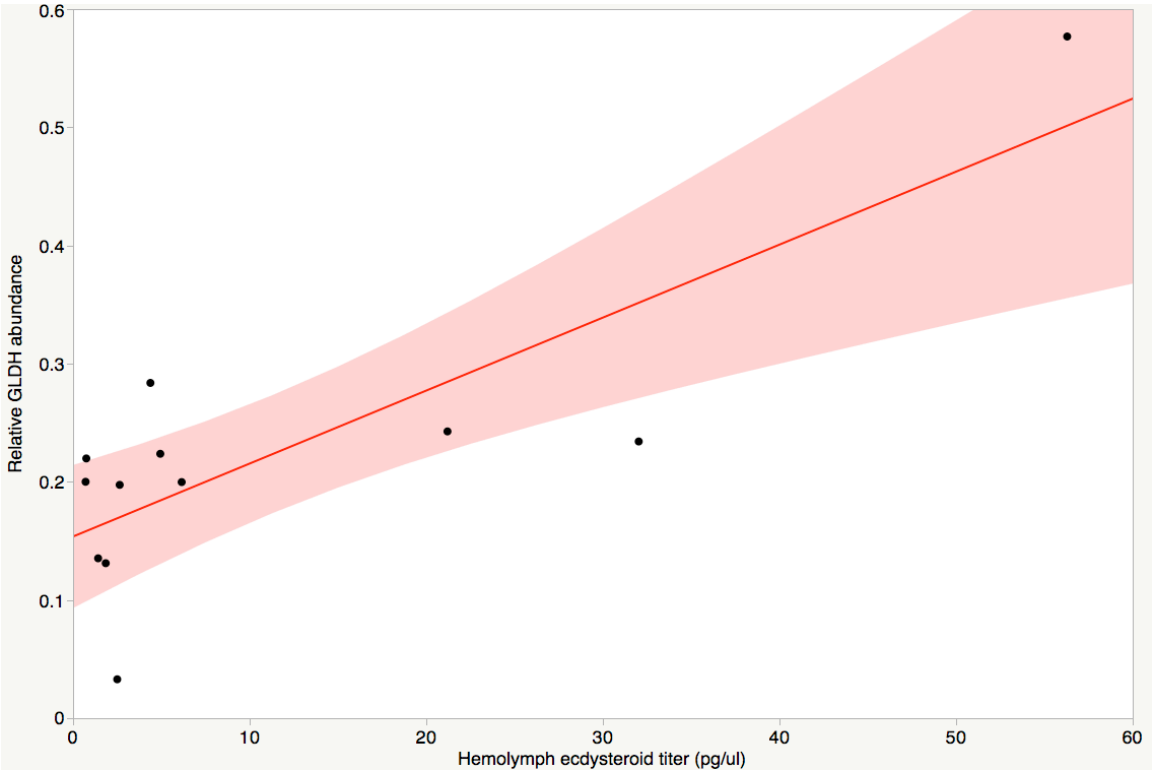

Figure 23. Relationship between ecdysteroid titers and abundance of GLDH. A correlation analysis indicated a significant positive relationship between these two factors (R2 = 0.672; Prob(F)>0.001)

Enzymatically GLDH is involved in a process known as glutaminolysis, which involves the double deamination of glutamine into glutamate, then α-ketoglutarate (αKG). Glutaminolysis primarily occurs under conditions when nutrient availability is high. An increase in GLDH supports the hypothesis that the YO is undergoing an increase in glutaminolysis during early premolt, which as stated indicated high amino-acid availability. Glutamate is a particularly important amino acid because it is required

for the synthesis of nearly a dozen other amino acids. The synthesis of these amino acids is carried out through transamination reactions where the amine group of glutamate is transferred to the newly synthesized amino acid. A byproduct of the deamination of glutamate is αKG. Occurring in parallel, glutaminolysis and increased amino acid synthesis would result in a drastic increase in intracellular αKG concentrations.

Recent studies have linked a family of αKG-dependent dioxygenases (prolyl hydroxylases) with the activation state of mTOR (Durán and Hall, 2012). Since that time, direct links have been established between increased αKG concentrations and mTOR activity (Durán and Hall, 2012). Because mTOR has been implicated in the activation state of the YO, we suggest that glutaminolysis and the subsequent increase in αKG concentration may represent a potential regulatory checkpoint within YO and molting itself.

The possibility of early-stage YO activation through nutrient sensing has been proposed in the past (Chang and Mykles, 2011). However, the possibility of initial mTOR activation through a αKG-mediated pathway has not yet been suggested. The D_0 YO is in an activated, non-committed state that can easily return to intermolt if the animal is subjected to stress. Regulation of molting through metabolites provides the sensitivity and plasticity required for proper functioning of such a mechanism. It also provides a direct link between availability of amino acids and the animal's decision to molt. It is worth noting that studies addressing the biosynthetic potential of pancreatic islet cells in response to increased αKG levels, and consequently mTOR activation, have detected decreased autophagy and hypertrophy, both of which are also observed in cells of the activated YO (Duran and Hall, 2012; Zoncu et al., 2011).

Stress response proteins in the YO

All of cellular life is under a constant pressure to maintain intracellular redox homeostasis. Regardless of the source, we discuss deviation from this homeostasis in terms of oxidative stress, where a build-up in reactive oxygen species (ROS) results from overcoming the cell's internal mechanisms that have evolved to control their production. ROS are mainly associated with negative consequences for the cell because of their propensity to alter the functions of proteins, damage DNA and lipids, and ultimately lead to various pathologies. However, one of the most common ROS, H_2O_2, has been implicated as a signaling molecule controlling a number of cellular processes (Giorgio et al., 2007).

Evidence for ROS production in the YO

We identified a number of proteins associated with the production of ROS. Hydrogen peroxide is produced as a byproduct of many intracellular processes carried out in the mitochondria and cytoplasm, including those of metabolism and steroid hormone biosynthesis (Chae et al., 1999). Cellular life has evolved numerous mechanisms to cope with the production of ROS. The existence of the peroxisome is testament to both the pervasiveness of ROS and the cell's ability to neutralize and manage these potentially destructive molecules. Superoxide dismutase can be found in both the mitochondria and cytosol, indicating a need to reduce hydrogen peroxide in a number of cellular environments. We identified multiple superoxide dismutase and catalase isoforms in the YO but neither the peroxisome-associated proteins or their cytosolic isoforms showed

any significant change in abundance across molt stages ($p<0.05$). We therefore turned our attention to alternative ROS systems, particularly those existing within the mitochondria.

The mitochondria are a major source of ROS due to numerous redox reactions catalyzed within them. Components of the electron transport chain, especially complexes I and III, are well recognized as major sources of mitochondrial ROS (Andreyev et al., 2005). In addition, ecdysteroidogenesis within the mitochondria is carried out by a number of cytochrome p450 mono-oxygenases encoded by the *Halloween* gene family. Cytochrome p450 monooxygenase enzymes generate ROS - a result of inefficient reactions characterized by incomplete product formation. Currently there is no literature describing the amount of hydrogen peroxide produced by the *Halloween* genes specifically, nor their rate of degradation following YO activation. Likewise, it is unclear what happens to the *Halloween* gene products themselves during the postmolt stages. Regardless, the abundance of YO mitochondria, which exist to support ecdysteroid synthesis, should be considered a significant contributor to ROS production within this cell type.

We identified a number of proteins implicated in oxidative stress pathways that support the idea of ROS, especially H_2O_2, being produced in increasing concentrations by the mitochondria of the YO. Besides the identification of the common peroxisomal proteins already mentioned, we also identified other proteins associated with the oxidative stress response. Peroxiredoxin 3 (Prx3, spot 153), a ubiquitous mitochondrial antioxidant enzyme capable of reducing hydrogen peroxide, increased in abundance during postmolt (t-test $p<0.05$). Prx3 relies on the reducing power of the disulfide reductase thioredoxin to remain in a reduced and active state. Thioredoxin itself is

reduced by thioredoxin reductase, which requires NADPH as a reducing equivalent to maintain intracellular protein thiols in their reduced state (Tovar-Méndez et al., 2011).

The identification of a mitochondria-specific antioxidant enzyme at this stage supports the idea that the mitochondria are responding to an increase in ROS production, and in particular, an increase in hydrogen peroxide. Past studies have shown a significant relationship between oxidative stress in mitochondria and the abundance of Prx enzymes (Arnér and Holmgren, 2000). Furthermore, Prx3 is found to be highly expressed in the adrenal glands of mammals (Chae et al., 1999). Like the YO, the adrenal glands primary function is the biosynthesis of steroid-derived hormones through cytochrome p450 monooxygenase activity (Chae et al., 1999; Leyens et al., 2003). These studies suggest links between these ROS-producing enzymes and the induction of amplified Prx3 abundance (Chae et al., 1999). Even if a significant fraction of the hydrogen peroxide is being generated by the electron transport chain, it is likely that the existence of cytochrome p450 monooxygenases also contributes significantly to the production of ROS. The implications of an increase in hydrogen peroxide at this stage will be elucidated upon in the coming sections.

Other stress-related proteins

We also identified four heat shock protein 70 (Hsp70) isoforms, of which two significantly increased in abundance during postmolt (t-test $p<0.05$; spots 231 and 250). The Hsp70 isoform represented in spot 231 was more specifically identified as increasing in abundance in $C_{1\text{-}3}$ (ANOVA $p<0.05$). Heat shock proteins are chaperones involved in maintaining other proteins in the properly folded conformations during periods of acute

or sustained cellular stress. In addition to the potential oxidative stress just described, the inherent osmotic and ionic stress that accompanies the process of ecdysis provides ample explanation for the observation of these proteins in the YO. It seems unlikely that they would play any role in YO-specific function but are instead participating in regular housekeeping functions. One should note that even though non-significant, the pattern in abundance of another Hsp70 isoform (spot 29) was opposite of that observed in the other isoforms. Differential expression patterns of Hsp family isoforms have been well documented in other species (Daugaard et al., 2007). That said, our results generally agree with those of previous studies, which concluded that Hsp abundances in other crustacean tissues were lowest during intermolt (Spees et al., 2003).

Two glucose regulated protein 78 (GRP78) isoforms - chaperone proteins localized to the endoplasmic reticulum (ER) - were also identified (spots 190 and 197). The GRP78 isoform represented in spot 197 significantly increased in abundance in $C_{1\text{-}3}$ (ANOVA $p<0.05$). Being a member of the Hsp70 family of molecular chaperones, GRP78 plays a role in maintaining cellular function during periods of stress. It is especially important within the ER-localized unfolded protein response (UPR), where it acts to rearrange disulfide bonds that have been erroneously established and consequently lead to improper folding patterns. If this step fails, further steps in the UPR are initiated, which can eventually lead to cell death through apoptosis. In the stage $C_{1\text{-}3}$ YO, an increase in GRP78 may be the result of an increase in protein turnover as the YO returns to its basal state.

Cyclophilin A and the ROS-induced response in the YO

Cyclophilin A (CypA) is a ubiquitous 17 kDa protein whose primary intracellular functions are most commonly associated with its peptidylprolyl isomerase (PPIase) activity. This highly specific enzymatic activity effectively allows CypA to accelerate the folding of certain proteins otherwise hindered by the distinct cyclic nature of their proline residues (Obchoei et al., 2009). CypA has also been implicated in a variety of other functions, including non-enzymatic scaffolding, intercellular inflammatory signaling, oxidative stress, and metalloproteinase activation (Satoh et al., 2014; Satoh et al., 2009)

Cyclophilin A exocytic mechanism

Though secretion of ecdysteroid is the primary function of the YO, it is generally not thought of as an exocytic organ. The amphiphilic nature of ecdysteroid allows it to freely diffuse across the membrane and into the hemolymph immediately following completion of its synthesis (Mykles, 2011). However, the identification of several proteins involved in exocytosis and inter-membrane transport suggest a role for this cellular process. In this section we will describe these proteins and our hypothesis involving the exocytosis of the CypA from the YO during postmolt. Ultimately, we believe this exocytic mechanism to be at least partially responsible for the ultrastructural changes observed in the postmolt YO.

We have previously described in detail how increased hydrogen peroxide concentrations within the mitochondria of the postmolt YO is a likely outcome of metabolic processes compounded by a decrease in the efficiency of ecdysteroidogenic cytochrome p450 monooxygenases. In that section we eluded to the idea of hydrogen

peroxide acting as a critical messaging molecule within the YO. By studying mammalian vascular pathogenesis, Suzuki *et al.* (2006) has described a mechanism by which ROS induces the secretion of CypA through a highly regulated exocytic mechanism involving a number of requisite transport proteins. Here, we will provide support for the hypothesis that hydrogen peroxide functions to activate the exocytosis of CypA in the postmolt YO through a mechanism similar to that previously defined in a number of mammalian cell types (Suzuki et al., 2006) (Nishioku et al., 2012; Satoh et al., 2009). We will then discuss some of the potential outcomes of CypA secretion on the tissues surrounding the YO as well as the intracellular effects this protein may be invoking.

Our results show a trend whereby all four of the identified CypA isoforms increased in abundance following ecdysis (t-test $p<0.05$). Soe *et al.* (2014) previously showed that "ROS-dependent acetylation of CypA is required for the generation of extracellular CypA." Thus, when hydrogen peroxide originating from either the mitochondria or the cytosol comes into contact with CypA, there is an increased chance of induced CypA acetylation, though the mechanism through which this occurs is at the moment unclear. We surveyed our mass spectrometry results of the four isoforms for any signs indicating acetylation but were unsuccessful, possibly because the acetylated peptide was not ionized. However, as acetylation shifts the pI of proteins by approximately 0.5 pH units (ProMoST, Medical College of Wisconsin, v2014) and the four isoforms (all ~18kDa) differed in pI, ranging from 8.64 to 9.30, thus indicating the presence of an acetylation on two of the four CypA isoforms.

Exocytosis is regulated by a number of proteins, most notably those of the Ras family of GTPases and the SNARE complex proteins (Savigny et al., 2007). One of the

proteins indispensible to the exocytosis of CypA is the small Rho GTPase cell division control protein 42 (Cdc42; spot 42) (Suzuki et al., 2006). Cdc42 is commonly associated with a role in establishing cell polarity, a task vital to processes ranging from mitosis to exocytosis (Johnson, 1999). Cdc42 has been explicitly linked to CypA exocytosis through studies where Cdc42 dominant-negative mutants showed a 63% reduction in CypA exocytosis (Suzuki et al., 2006). We identified Cdc42 within our YO samples but found that abundances of this protein remained unexpectedly static over the molt cycle. However, because the GTP-bound state of Cdc42 is likely more important to its activity than overall abundance, changes in protein concentration may not be required to modify its activity.

We did not identify any of the potential guanine nucleotide exchange factors (GEF) by which Cdc42 is activated. However there were significant changes in the abundances of cytoskeletal actin and tubulin isoforms over the molt cycle. Some increased in abundance during postmolt (actin and tubulin, spots 176 and 140, respectively; t-test and ANOVA $p<0.05$), while a tubulin isoform increased in abundance during intermolt/early premolt stages (spot 174, t-test $p<0.05$). We also observed an increase in the abundance of Rab GTP-disassociation inhibitor (Rab GDI) during postmolt. Rab GDI functions to inhibit the exchange of GDP for GTP on Rab, thereby increasing the cells ability to recycle membrane trafficking proteins. It is therefore crucial to maintaining the functional capacity of these transport systems. At the very least, the identification of Cdc42 and changes in cytoskeletal proteins provides evidence that maintaining polarity within YO cells is important. Increased postmolt Rab GDI

abundances indicate that the cell is increasing its capacity to recycle membrane transport proteins, which may aid in processes involving exocytosis of CypA.

Downstream evidence for ROS-induced secretion of CypA can be found in the well-established ultrastructural changes observed in the postmolt YO (Birkenbeil, 1983. As mentioned previously, the postmolt YO undergoes rapid atrophy associated with a precipitous drop in ecdysteroidogenic capacity. Under conditions of oxidative stress the secreted form of CypA plays a role in vascular inflammation and restructuring (Satoh et al., 2009). Over time this CypA-specific mechanism can lead to severe pathologies such as atherosclerosis (Satoh et al., 2014). The YO is highly vascularized to support its role in distributing ecdysteroid into the hemolymph. However, once the animal has molted and ecdysteroid is no longer needed, YO activity must be arrested. Because the vasculature of crustaceans differs from that of mammals - exemplified by the lack of an endothelial cell layer - it is unclear what the exact effect of CypA might be on the vasculature in this tissue. However, the basis upon which CypA has been shown to affect the structure of the vasculature and extracellular matrix in mammals may hold true in the extracellular structure of the YO. One possibility is through restructuring of proline-rich collagen fibers (Steinmann et al., 1991). Another is through the activation of matrix metalloproteinases (Nishioku et al., 2012). Ultimately, the release of CypA from YO cells may help to reduce blood flow through the YO by reorganizing the extracellular matrix (ECM) and the surrounding vasculature. It may also act to directly induce atrophy in the postmolt YO. We will provide additional downstream evidence for this point in our discussion on hemolymph-specific proteins.

CypA as a mediator of Prx activity

The findings presented so far suggests that CypA secretion from the YO is feasible and would explain the physiological effect of atrophy observed in the postmolt YO. That said, we propose that CypA may also be involved in one of the intracellular oxidative stress mechanisms already described, specifically through an interaction with the antioxidant enzyme Prx3. Owing to its antioxidant activity, Prx3 relies on reducing equivalents (NADPH), primarily by the protein thioredoxin, to maintain functional activity. In this sense thioredoxin's primary purpose is to act as an electron donor, helping to maintain Prx's conserved cysteine residues in reduced states. This reducing power can, in turn, be used to reduce hydrogen peroxide to water.

When challenged by oxidative stress, or when NADPH concentrations are non-optimal, CypA can act to supplement this ROS scavenging system. By reducing hydrogen peroxide, Prx plays a vital role in maintaining the function of various proteins. Traditionally, glutamine synthetase (GS), a protein highly susceptible to the oxidative effects of hydrogen peroxide, has been used as a proxy for determining the activity and efficiency of Prx. Thus, a functionally active Prx allows GS to remain active. CypA significantly contributes to maintaining GS activity in a Prx-dependent fashion (Lee et al., 2001). The implication of this allows us to predict that CypA is acting as a as a mediator of oxidative stress in the postmolt YO.

We have provided indirect support of hydrogen peroxide production within the postmolt YO. The connection between Prx3 and CypA, along with similar abundance patterns observed in these proteins, is proposed to provide a valuable negative feedback

mechanism through which hydrogen peroxide levels can be maintained at safe levels within the cell, but still act as an intracellular second messenger (Giorgio et al., 2007). The result is a self-regulating system through which acetylated CypA is secreted, while intracellular CypA ensures the prevention of toxic hydrogen peroxide accumulation (Figure 24).

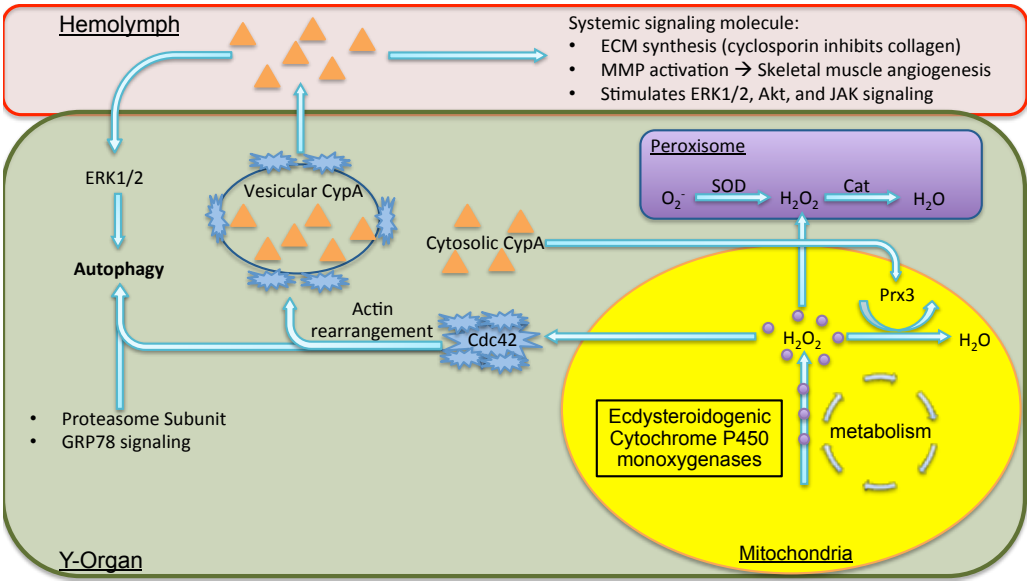

Figure 24. Hypothesized Cyclophilin A (CypA) exocytosis mechanism. Our results indicate that a secreted form of CypA may be present in the YO during postmolt. The presence of acetylated CypA is more likely in a highly oxidative environment like the one being proposed. Proteins like Cdc42 help maintain cell polarity, which is crucial for exocytic mechanisms. CypA may be acting both intracellularly and intracellularly to restructure the YO. The most obvious mechanism of action would be through collagen reorganization. CypA also has the potential to initiate changes through cell signaling as well as through the activation proteins such as matrix metalloproteinases (MMP). The ERK1/2 pathway is merely one downstream intracellular signaling pathway that has been shown to be initiated by CypA signaling.

Blood species

Up until this point we have made passing indications that our proteomic findings support the historical physiological observations of ultrastructural changes in the postmolt YO. More specifically we have presented evidence that the exocytosis of CypA into the extracellular space of the YO has the potential to cause vascular and ECM restructuring. Another compelling piece of evidence that supports our claim of CypA-induced YO restructuring is the sharp contrast observed in the abundance of blood species proteins between premolt and postmolt. In this section we will describe these blood species and why the patterns observed in their abundance might be explained by our other data.

The primary constituent of hemolymph during the majority of the crustacean molt cycle is the copper-containing, oxygen-binding protein hemocyanin (Terwilliger et al., 1999). Oxygen transport, though an obvious task for this protein, is not its only one. The alternative functions of hemocyanin have been well studied and show noteworthy roles in other aspects of crustacean physiology, particularly in molting and immunity.

Hemocyanin's relationship to other phenoloxidase enzymes supports its involvement in melanization and sclerotization of the cuticle following ecdysis (Terwilliger and Ryan, 2006). In fact, it may be more effective in its functional role as a phenoloxidase than other members of this enzyme family. Unlike other phenoloxidase enzymes, hemocyanin-derived phenoloxidases show tyrosinase activity and are capable of converting monophenols directly to o-diphenols (Rodríguez-López et al., 2001; Terwilliger and Ryan, 2006). All phenoloxidases convert diphenols to o-quinones, a crucial step early in the melanization reaction pathway (Terwilliger and Ryan, 2006).

Sclerotization and melanization utilize the tyrosine-derived precursors N-acetyldopamine (NADA) and dopamine (DOPA), respectively. These precursors are substrates for a complex series of enzymatic and non-enzymatic reactions specific to each pathway (Sugumaran, 1991). Phenoloxidases play crucial roles in both of these processes but it is important to recognize that these pathways can and do occur independently of each other.

Traditionally, it was believed that the presence of microbes in the hemolymph initiated the activation of phenoloxidases from pro-phenoloxidase (e.g. hemocyanin). However, recent work has shown that the melanization pathway can be activated through wounding itself, independently of microbial invasion (Clark and Strand, 2013). This idea is supported by i) a study assessing molt-cycle related expression patterns of hemocyanin, where results showed that expression of this hemolymph protein increased immediately following ecdysis (Terwilliger et al., 2005), and ii) our own proteomic observations where a significant increase in hemocyanin abundance was detected in post-ecdysal YOs, specifically in stage C1-3 where the animal's endocuticle is undergoing the final stages of hardening but can still be easily damaged or invaded (Skinner, 1985a).

Hemocyanin also plays a direct role in the sclerotization of new cuticle following ecdysis. Quinone tanning reactions, in which phenoloxidases play a crucial role, result in the production of quinone products capable of non-enzymatically crosslinking nucleophilic cuticular proteins through β-sclerotization (Sugumaran, 1991). This crosslinking is not the only process through which cuticle hardening occurs, but does help to explain the expression patterns observed in our results.

Though the presence of hemolymph proteins in our YO samples is likely an artifact – that is, due entirely to presence of vasculature within and surrounding this organ

- the possibility that hemocyanin is playing a unique role in the YO should not be discounted. It is a protein that has already been proven to have diverse function in numerous tissues (Glazer et al., 2013), one of which might be the YO itself. What exactly that function is requires further investigation, but would likely be immunoprotective in nature. Another possibility, supported by evidence of ecdysone-hemocyanin binding in spiders, might be that that hemocyanin acts as a transporter protein for ecdysteroid secreted from the YO (Jaenicke et al., 1999). Finally, it is worth noting that phenoloxidases like hemocyanin produce hydrogen peroxide as a byproduct (Komarov et al., 2005). The reactions catalyzed by this enzyme could result in yet another source of hydrogen peroxide.

Generally, hemocyanin constitutes the majority of dissolved proteins within the hemolymph, but there is another protein often found in relatively high concentrations within the blood of crustaceans. In fact, during peak premolt stages, cryptocyanin can be found at levels greater than 200% that of hemocyanin. Cryptocyanin, like hemocyanin, is produced in resorptive cells of the hepatopancreas (Terwilliger et al., 2005). Unlike hemocyanin, it has lost its oxygen-carrying capacity along with three of its copper binding sites (Terwilliger et al., 2005). Nonetheless, it remains a significant component of the hemolymph. Studies assessing mRNA and hemolymph protein concentrations of both hemocyanin and cryptocyanin suggest differential expression patterns related to distinct physiological functions (Terwilliger et al., 2005).

Hemolymph concentrations of cryptocyanin over consecutive molt cycles show low expression during intermolt followed by a rapid increases during premolt and a marked drop of immediately following ecdysis (Terwilliger et al., 2005). Cryptocyanin is

believed to physically reconstitute the extracellular matrix following ecdysis. Immunohistochemical analysis in past studies have probed for cryptocyanin and shown that incorporation of this protein occurs throughout the extracellular matrix surrounding internal organs and in the new exoskeleton itself (Terwilliger et al., 2005). Once incorporated, the protein is essentially locked away in the extracellular matrix through crosslinking and proteolytic cleavage (Terwilliger et al., 2005).

Our data mostly support the observations of Terwilliger *et al.* (2005) We found that the abundances of multiple cryptocyanin isoforms was highest in stage D_0 animals. As expected, cryptocyanin abundance declined significantly immediately following ecdysis. As with hemocyanin, a specific functional role for cryptocyanin within the YO has not been demonstrated. However, we believe that the changes in abundance of these two hemolymph proteins provide further evidence for CypA-induced changes in the vasculature of the postmolt YO. Specifically, the postmolt decrease in abundance of thirteen cryptocyanin isoforms (t-test $p<0.05$) suggests that the hemolymph content within the YO is being drastically reduced. However, although ROS-induced changes in the vasculature and ECM may be partially responsible, it is important to remember that cryptocyanin integration into the exoskeleton during these stages has already been strongly supported and may be the primary reason for these observations. (Figures 24 and 25).

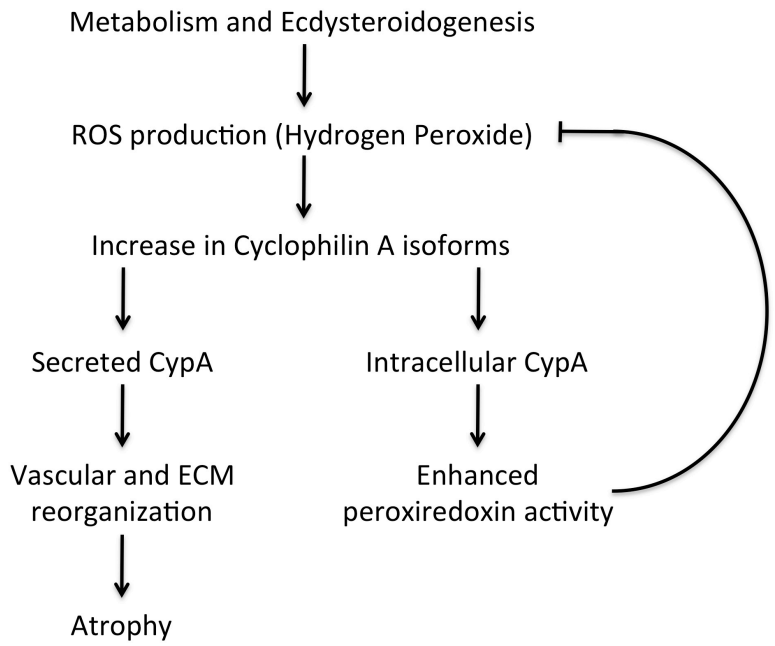

Figure 25. A simplified diagram proposing a ROS-induced mechanism by which both intracellular and exocytic cyclophilin A abundances increase.

Farnesoic acid O-methyltransferase (FaMet)

We have reserved discussion of this last protein because of the seemingly enigmatic role it plays in crustacean physiology. Farnesoic acid O-methyltransferase (FaMet; spot 243) is a protein that is widely expressed in a number of tissues in crustaceans (?) (Gunawardene et al., 2002). We identified a significant increase in the abundance of this protein during postmolt (t-test $p<0.05$). FaMet's primary role is the catalysis of farnesoic acid (FA) into methyl farnesoate (MF) through addition of a methyl group (Gunawardene et al., 2002). Because MF is insoluble in the hemolymph, FaMet acts to convert soluble FA into MF. Thus, FA released from the mandibular organ into the hemolymph is allowed to circulate until it reaches its target tissue, where it can then be converted to active MF. Historically, MF has gained attention because of its similarity

to the insect growth-regulating hormone (JH) (Chang, 1995). Strangely, the effects of this hormone seem to depend on which organism being observed. In some, MF regulates molting of juvenile larvae, while in other species MF seems to play a key role in ovarian development (Gunawardene et al., 2002).

Though various, sometimes conflicting, hypothesis have been developed surrounding the functional role of MF in crustaceans, most focus on a potential role in regulation of the molt cycle. It has been proposed that although MIH is the primary inhibitor of ecdysteroidogenesis, MF may contribute synergistically to its inhibitory effect through down regulation of specific ecdysteroidogenic cytochrome p450 transcripts (Asazuma et al., 2009). However, contradictory reports have suggested that MF actually increases the steroidogenic potential of the YO (Chang, 1995). Our results, where FaMet abundances increased significantly during postmolt, seem to support the former hypothesis, or may point to an alternative function role not yet elucidated.

Concluding remarks

To date, no study has described a molecular basis for the postmolt restructuring of the crustacean YO. Additionally, and for the first time, this study provides a comprehensive proteomic analysis of a decapod crustacean YO. Our initial goal was to provide evidence for ecdysteroidogenic signaling mechanisms proposed in the past work of others. Though we were unable to identify proteins from these specific pathways, the interpretations afforded us by our proteomic workflow have allowed us to predict novel mechanisms related to YO function.

The generation of hydrogen peroxide as a second messenger has become a highly validated mechanism by which organisms can respond to a variety of physiological events and stresses. In the YO, hydrogen peroxide sources include normal metabolic processes, ecdysteroidogenic cytochrome p450 monooxygenase enzymes, and possibly even hemolymph proteins like hemocyanin-derived phenoloxidases. We have established a hypothesis, which proposes that the generation of hydrogen peroxide in the postmolt YO is responsible for the physiological changes observed in the tissue during this time. Our primary piece of evidence to support this is the finding that the mitochondria-specific peroxiredoxin (Prx3) increased in abundance in the postmolt YO. Prx3, augmented by an intracellular interaction with CypA, combats the generation of high concentrations of hydrogen peroxide. Changes in the abundance of the triosephosphate isomerase and transketolase provide evidence of a system capable of supporting the increased demand for intracellular NADPH, an upstream reducing agent required for Prx3 activity. With this regulatory mechanism in place it is possible for hydrogen peroxide to also act as a second messenger for the exocytosis of CypA.

Differences in the pI's of the four CypA isoforms identified in the postmolt YO suggest that an acetylated and therefore secreted isoform is likely present. We also identified proteins key to the establishment of cellular polarity, a process mandatory for intracellular transport and exocytosis. Once released from the cell into the extracellular space, CypA may function to remodel the vasculature and ECM of the YO. We provide further support for this idea by pointing out that hemolymph protein abundances were consistently reduced in the postmolt YO. Whether these changes are the result of an induced inflammatory response or due to the specific enzymatic activity of CypA could be tested in the future using the CypA inhibitor cyclosporin A.

Function of the YO during the premolt stages $D_{0\text{-}4}$ has been thoroughly researched for decades, but has left the topic of postmolt cellular processes of the tissue largely overlooked. Understanding the inactive stage of the YO may help to expose what remains unknown about its active state in the future. Here we have described a system by which intracellular hydrogen peroxide signals for extracellular changes that result in physiological atrophy of the YO. Though less well supported, we have also suggested a possible glutamine nutrient sensing pathway whereby α-ketoglutarate concentrations activate the YO. Future studies on the YO of crustaceans should attempt to include a broader range of molt stages to further the understanding of this organ, its functions, and its importance to the whole organism.

References

Abuhagr, A. M., Blindert, J. L., Nimitkul, S., Zander, I. A., LaBere, S. M., Chang, S. A., MacLea, K. S., Chang, E. S. and Mykles, D. L. (2014). Molt regulation in green and red color morphs of the crab Carcinus maenas: gene expression of molt-inhibiting hormone signaling components. *Journal of Experimental Biology* 217, 1830–1830.

Andreyev, A. Y., Kushnareva, Y. E. and Starkov, A. A. (2005). Mitochondrial metabolism of reactive oxygen species. *Biochemistry Mosc.* 70, 200–214.

Arnér, E. S. E. and Holmgren, A. A. (2000). Physiological functions of thioredoxin and thioredoxin reductase. *FEBS J* 267, 6102–6109.

Asazuma, H., Nagata, S. and Nagasawa, H. (2009). Inhibitory effect of molt-inhibiting hormone on phantomexpression in the Y-organ of the kuruma prawn, Marsupenaeus japonicus. *Arch. Insect Biochem. Physiol.* 72, 220–233.

Baeta, A., Cabral, H. N., Neto, J. M., Marques, J. C. and Pardal, M. A. (2005). Biology, population dynamics and secondary production of the green crab Carcinus maenas (L.) in a temperate estuary. *Estuarine, Coastal and Shelf Science* 65, 43–52.

Berrill, M. (1982). The Life Cycle of the Green Crab Carcinus maenas at the Northern End of Its Range. *Journal of Crustacean Biology* 2, 31–39.

Berrill, M. and Arsenault, M. (1982). *Mating behavior of the green shore crab Carcinus maenas*. Bulletin of marine science.

Berth, M., Moser, F. M., Kolbe, M. and Bernhardt, J. (2007). The state of the art in the analysis of two-dimensional gel electrophoresis images. *Appl Microbiol Biotechnol* 76, 1223–1243.

Birkenbeil, D. H. (1983). Ultrastructural and immunocytochemical investigation of ecdysteroid secretion by the prothoracic gland of the waxmoth Galleria mellonella. *Cell Tissue Res* 229, 433–441.

Blais, C., Dauphin-Villemant, C., Kovganko, N., Girault, J. P., Descoins, C. and Lafont, R. (1996). Evidence for the involvement of 3-oxo-delta 4 intermediates in ecdysteroid biosynthesis. *Biochem. J.* 320 (Pt 2), 413–419.

Bradford, M. M. (1976). A rapid and sensitive method for the quantitation of microgram quantities of protein utilizing the principle of protein-dye binding. *Anal. Biochem.* 72, 248–254.

Chae, H. Z., Kim, H. J., Kang, S. W. and Rhee, S. G. (1999). Characterization of three isoforms of mammalian peroxiredoxin that reduce peroxides in the presence of thioredoxin. *Diabetes Res. Clin. Pract.* 45, 101–112.

Chang, E. S. (1995). Physiological and biochemical changes during the molt cycle in decapod crustaceans: an overview. *Journal of Experimental Marine Biology and Ecology* 193, 1–14.

Chang, E. S. and Mykles, D. L. (2011). General and Comparative Endocrinology. *General and Comparative Endocrinology* 172, 323–330.

Clark, K. D. and Strand, M. R. (2013). Hemolymph melanization in the silkmoth Bombyx mori involves formation of a high molecular mass complex that metabolizes tyrosine. *J. Biol. Chem.* 288, 14476–14487.

Cohen, A. N. and Carlton, J. T. (1995). *Nonindigenous aquatic species in a United States estuary*. UNITED STATES FISH AND WILDLIFE SERVICE.

Collins, F. S., Morgan, M. and Patrinos, A. (2003). The Human Genome Project: Lessons from Large-Scale Biology. *Science* 300, 286–290.

Cotter, R. J., Griffith, W. and Jelinek, C. (2007). Tandem time-of-flight (TOF/TOF) mass spectrometry and the curved-field reflectron. *J Chromatogr B Analyt Technol Biomed Life Sci* 855, 2–13.

Covi, J. A., Chang, E. S. and Mykles, D. L. (2009). Comparative Biochemistry and Physiology, Part A. *Comparative Biochemistry and Physiology, Part A* 152, 470–477.

Covi, J., Gomez, A., Chang, S. and Lee, K. (2008). Repression of Y-organ ecdysteroidogenesis by cyclic nucleotides and agonists of NO-sensitive guanylyl cyclase. *Fourth Meeting of ….*

Crothers, J. H. (1967). The biology of the shore crab Carcinus maenas (L.) 1. The Background - Anatomy, Growth and Life History. *Field Studies* 2, 407–434.

Crothers, J. H. (1968). The biology of the shore crab *Carcinus maenas* (L.) 2. The life of the adult crab. *Field Studies* 2, 579–614.

Darling, J. A., Bagley, M. J., Roman, J., Tepolt, C. K. and Geller, J. B. (2008). Genetic patterns across multiple introductions of the globally invasive crab genus Carcinus. *Mol Ecol* 17, 4992–5007.

Daugaard, M., Rohde, M. and Jäättelä, M. (2007). The heat shock protein 70 family: Highly homologous proteins with overlapping and distinct functions. *FEBS Letters* 581, 3702–3710.

Dauphin-Villemant, C., Böcking, D. and Blais, C. (1997). Involvement of a 3 β-hydroxysteroid dehydrogenase activity in ecdysteroid biosynthesis. *Molecular and Cellular Endocrinology* 128 (1997) 139–149

Dawirs, R. R., Püschel, C. and Schorn, F. (1986). Temperature and growth in Carcinus maenas L. (Decapoda: Portunidae) larvae reared in the laboratory from hatching through metamorphosis. *Journal of Experimental Marine Biology and Ecology* 100, 47–74.

Domingues, C. P., Creer, S., Taylor, M. I., Queiroga, H. and Carvalho, G. R. (2011). Temporal genetic homogeneity among shore crab (Carcinus maenas) larval events supplied to an estuarine system on the Portuguese northwest coast. *Heredity (Edinb)* 106, 832–840.

Drach, P. and Tchernigovtzeff, C. (1967). Sur la méthode de détermination des stades d'intermue et son application générale aux crustacés. *Vie et Milieu* 18 (3A), 595–610.

Durán, R. and Hall, M. (2012). Glutaminolysis feeds mTORC1. *Cell Cycle* 11, 4107–4108.

Garfin, D. and Heerdt, L. (2002). *2-D Electrophoresis for Proteomics*. (eds. Garfin, D. and Heerdt, L.

Gillespie, G. E. and Station, P. B. (2007). *Status of the European Green Crab, Carcinus Maenas, in British Columbia, 2006*.

Giorgio, M., Trinei, M., Migliaccio, E. and Pelicci, P. G. (2007). Hydrogen peroxide: a metabolic by-product or a common mediator of ageing signals? *Nat Rev Mol Cell Biol* 8, 722–728.

Glazer, L., Tom, M., Weil, S., Roth, Z., Khalaila, I., Mittelman, B. and Sagi, A. (2013). Hemocyanin with phenoloxidase activity in the chitin matrix of the crayfish gastrolith. *J. Exp. Biol.* 216, 1898–1904.

Grosholz, E. D. and Ruiz, G. M. (1995). Spread and potential impact of the recently introduced European green crab, Carcinus maenas, in central California. *Marine Biology* 122, 239–247.

Grosholz, E. D. and Ruiz, G. M. (1996). Predicting the impact of introduced marine species: Lessons from the multiple invasions of the European green crab< i> Carcinus maenas</i>. *Biological Conservation* 78, 59–66.

Grüning, N.-M., Du, D., Keller, M. A., Ben F Luisi and Ralser, M. (2014). Inhibition of triosephosphate isomerase by phosphoenolpyruvate in the feedback-regulation of glycolysis. *Open Biol* 4, 130232–130232.

Gunawardene, Y. I. N. S., Tobe, S. S., Bendena, W. G., Chow, B. K. C., Yagi, K. J. and Chan, S. M. (2002). Function and cellular localization of farnesoic acid O-methyltransferase (FAMeT) in the shrimp, Metapenaeus ensis. *Eur J Biochem* 269, 3587–3595.

Hopkins, P. M. (2001). Limb Regeneration in the Fiddler Crab, Uca pugilator: Hormonal and Growth Factor Control. *Amer. Zool.* 41, 389–398.

Hopkins, P. M. (2012). General and Comparative Endocrinology. *General and Comparative Endocrinology* 175, 357–366.

Huxel, G. R. (1999). Rapid displacement of native species by invasive species: effects of hybridization. *Biological Conservation* 89, 143–152.

Inoki, K. and Guan, K.-L. (2006). Complexity of the TOR signaling network. *Trends in Cell Biology* 16, 206–212.

Inoki, K., Li, Y., Xu, T. and Guan, K.-L. (2003). Rheb GTPase is a direct target of TSC2 GAP activity and regulates mTOR signaling. *Genes Dev* 17, 1829–1834.

Jaenicke, E., Foll, R. and Decker, H. (1999). Spider Hemocyanin Binds Ecdysone and 20-OH-Ecdysone. *J. Biol. Chem.* 274, 34267–34271.

Johnson, D. I. (1999). Cdc42: An essential Rho-type GTPase controlling eukaryotic cell polarity. *Microbiol Mol Biol Rev* 63, 54–105.

Kelley, A. L., de Rivera, C. E. and Buckley, B. A. (2011). Intraspecific variation in thermotolerance and morphology of the invasive European green crab,Carcinus maenas, on the west coast of North America. *Journal of Experimental Marine Biology and Ecology* 409, 70–78.

Kim, H. W. (2005). Three calpains and ecdysone receptor in the land crab Gecarcinus lateralis: sequences, expression and effects of elevated ecdysteroid induced by eyestalk ablation. *Journal of Experimental Biology* 208, 3177–3197.

Kim, H.-W., Batista, L. A., Hoppes, J. L., Lee, K. J. and Mykles, D. L. (2004). A crustacean nitric oxide synthase expressed in nerve ganglia, Y-organ, gill and gonad of the tropical land crab, Gecarcinus lateralis. *Journal of Experimental Biology* 207, 2845–2857.

Kim, H.-W., Lee, S. G. and Mykles, D. L. (2005). Ecdysteroid-responsive genes, RXR and E75, in the tropical land crab, Gecarcinus lateralis: Differential tissue expression of multiple RXR isoforms generated at three alternative splicing sites in the hinge and ligand-binding domains. *Molecular and Cellular Endocrinology* 242, 80–95.

Klassen, G. J., Locke, A., Oceans, C. D. O. F. A. and Canada, G. F. C. (2007). *A Biological Synopsis of the European Green Crab, Carcinus Maenas*.

Komarov, D. A., Slepneva, I. A., Glupov, V. V. and Khramtsov, V. V. (2005). Superoxide and hydrogen peroxide formation during enzymatic oxidation of DOPA by phenoloxidase. *Free Radic Res* 39, 853–858.

Kültz, D., Fiol, D., Valkova, N., Gomez-Jimenez, S., Chan, S. Y. and Lee, J. (2007). Functional genomics and proteomics of the cellular osmotic stress response in "non-model" organisms. *Journal of Experimental Biology* 210, 1593–1601.

Lachaise, F., Le Roux, A., Hubert, M. and Lafont, R. (1993). The molting gland of crustaceans: localization, activity, and endocrine control (a review). *Journal of Crustacean Biology*.

Layalle, S., Arquier, N. and Léopold, P. (2008). The TOR Pathway Couples Nutrition and Developmental Timing in Drosophila. *Developmental Cell* 15, 568–577.

Lee, K. J., Kim, H.-W., Gomez, A. M., Chang, E. S., Covi, J. A. and Mykles, D. L. (2007a). Molt-inhibiting hormone from the tropical land crab, Gecarcinus lateralis: Cloning, tissue expression, and expression of biologically active recombinant peptide in yeast. *General and Comparative Endocrinology* 150, 505–513.

Lee, S. G., Bader, B. D., Chang, E. S. and Mykles, D. L. (2007b). Effects of elevated ecdysteroid on tissue expression of three guanylyl cyclases in the tropical land crab Gecarcinus lateralis: possible roles of neuropeptide signaling in the molting gland. *Journal of Experimental Biology* 210, 3245–3254.

Lee, S. P., Hwang, Y. S., Kim, Y. J., Kwon, K. S., Kim, H. J., Kim, K. and Chae, H. Z. (2001). Cyclophilin a binds to peroxiredoxins and activates its peroxidase activity. *J. Biol. Chem.* 276, 29826–29832.

Leyens, G., Donnay, I. and Knoops, B. (2003). Cloning of bovine peroxiredoxins—gene expression in bovine tissues and amino acid sequence comparison with rat, mouse and primate peroxiredoxins. *Comp Biochem Physiol B Biochem Mol Biol* 136, 943–955.

Lovric, J. (2011). *Introducing Proteomics*. John Wiley & Sons.

López, J. L. (2007). Two-dimensional electrophoresis in proteome expression analysis. *J Chromatogr B Analyt Technol Biomed Life Sci* 849, 190–202.

Magdeldin, S., Enany, S., Yoshida, Y., Xu, B., Zhang, Y., Zureena, Z., Lokamani, I., Yaoita, E. and Yamamoto, T. (2014). Basics and recent advances of two dimensional- polyacrylamide gel electrophoresis. *Clinical Proteomics* 11, 16.

McDonald, A. A., Chang, E. S. and Mykles, D. L. (2011). Comparative Biochemistry and Physiology, Part A. *Comparative Biochemistry and Physiology, Part A* 158, 150–162.

McLaughlin, P. A. (2005). *Common and scientific names of aquatic invertebrates from the United States and Canada: crustaceans*. American Fisheries Society Special Publication.

Morrison, B. J., Hastie, M. L., Grewal, Y. S., Bruce, Z. C., Schmidt, C., Reynolds, B. A., Gorman, J. J. and Lopez, J. A. (2012). Proteomic Comparison of MCF-7 Tumoursphere and Monolayer Cultures. *PLoS ONE* 7, e52692.

Mykles D.L. (1997) Crustacean muscle plasticity: molecular mechanisms determining mass and contractile properties. *Comparative Biochemistry and Physiology* 117, 367-378.

Mykles, D. L. (2001). Interactions Between Limb Regeneration and Molting in Decapod Crustaceans. *Amer. Zool.* 41, 399–406.

Mykles, D. L. (2011). Ecdysteroid metabolism in crustaceans. *Journal of Steroid Biochemistry and Molecular Biology* 127, 196–203.

Mykles, D.L. (1980). The Mechanism of Fluid Absorption at Ecdysis in the American Lobster Homarus Americanus. *Journal of Experimental Biology* 84, 89-102.

Mykles, D. L., Adams, M. E., Gäde, G., Lange, A. B., Marco, H. G. and Orchard, I. (2010). Neuropeptide Action in Insects and Crustaceans*. *Physiol Biochem Zool* 83, 836–846.

Nagaraj, M. (1993). Combined effects of temperature and salinity on the zoeal development of the green crab, Carcinus maenas(Linnaeus, 1758)(Decapoda: Portunidae). *Scientia Marina(Barcelona)*.

Nakatsuji, T., Lee, C.-Y. and Watson, R. D. (2009). Crustacean molt-inhibiting hormone: Structure, function, and cellular mode of action. *Comparative Biochemistry and Physiology Part A: Molecular & Integrative Physiology* 152, 139–148.

Neumann, S. (2004). *Bruker ultreflex TOF/TOF Operator Manual*.

Nimitkul, S. (2011). *Feedback Regulation of Ecdysteroid Analog on Y-Organs of the Green Crab Carcinus Maenas*. Proquest, UMI Dissertation Publishing.

Nishioku, T., Dohgu, S., Koga, M., Machida, T., Watanabe, T., Miura, T., Tsumagari, K., Terasawa, M., Yamauchi, A. and Kataoka, Y. (2012). Cyclophilin A secreted from fibroblast-like synoviocytes is involved in the induction of CD147 expression in macrophages of mice with collagen-induced arthritis. *J Inflamm (Lond)* 9, 44–44.

Niwa, R., Namiki, T., Ito, K., Shimada-Niwa, Y., Kiuchi, M., Kawaoka, S., Kayukawa, T., Banno, Y., Fujimoto, Y., Shigenobu, S., et al. (2010). Non-molting glossy/shroud encodes a short-chain dehydrogenase/reductase that functions in the "Black Box" of the ecdysteroid biosynthesis pathway. *Development* 137, 1991–1999.

Obchoei, S., Wongkhan, S., Wongkham, C., Li, M., Yao, Q. and Chen, C. (2009). Cyclophilin A: potential functions and therapeutic target for human cancer. *Med Sci Monit* 15, RA221–RA232.

Pascoal, S., Creer, S., Taylor, M. I., Queiroga, H., Carvalho, G. and Mendo, S. (2009). Development and Application of Microsatellites in Carcinus maenas: Genetic Differentiation between Northern and Central Portuguese Populations. *PLoS ONE* 4, e7268.

Peterson, R. T., Beal, P. A., Comb, M. J. and Schreiber, S. L. (2000). FKBP12-Rapamycin-associated Protein (FRAP) Autophosphorylates at Serine 2481 under Translationally Repressive Conditions. *J. Biol. Chem.* 275, 7416–7423.

Pondeville, E., David, J.-P., Guittard, E., Maria, A., Jacques, J.-C., Ranson, H., Bourgouin, C. and Dauphin-Villemant, C. (2013). Microarray and RNAi Analysis of P450s in Anopheles gambiae Male and Female Steroidogenic Tissues: CYP307A1 Is Required for Ecdysteroid Synthesis. *PLoS ONE* 8, e79861.

Pringle, J. M., Blakeslee, A. M. H., Byers, J. E. and Roman, J. (2011). Asymmetric dispersal allows an upstream region to control population structure throughout a species' range. *Proceedings of the National Academy of Sciences of the United States of America* 108, 15288–15293.

Queiroga, H., Costlow, J. D. and Moreira, M. H. (1997). Vertical migration of the crab Carcinus maenas first zoea in an estuary: implications for tidal stream transport. *Oceanographic Literature …*.

Rabilloud, T. (1998). Use of thiourea to increase the solubility of membrane proteins in two-dimensional electrophoresis. *Electrophoresis* 19, 758–760.

Rabilloud, T. (2002). Two-dimensional gel electrophoresis in proteomics: old, old fashioned, but it still climbs up the mountains. *Proteomics* 2, 3–10.

Reiber, C. L. and McGaw, I. J. (2009). A Review of the "Open" and 'Closed' Circulatory Systems: New Terminology for Complex Invertebrate Circulatory Systems in Light of Current Findings. *International Journal of Zoology* 2009, 1–8.

Reid, D. G., Abelló, P., Kaiser, M. J. and Warman, C. G. (1997). Carapace Colour, Inter-moult Duration and the Behavioural and Physiological Ecology of the Shore Crab Carcinus maenas. *Estuarine* 44, 203–211.

Rodríguez-López, J. N., Fenoll, L. G., Peñalver, M. J., García-Ruiz, P. A., Varón, R., Martínez-Ortíz, F., García-Cánovas, F. and Tudela, J. (2001). Tyrosinase action on monophenols: evidence for direct enzymatic release ofo-diphenol. *Biochim Biophys Acta* 1548, 238–256.

Roman, J. (2006). Diluting the founder effect: cryptic invasions expand a marine invader's range. *Proceedings of the Royal Society B: Biological Sciences* 273, 2453–2459.

Roman, J. and Darling, J. A. (2007). Paradox lost: genetic diversity and the success of aquatic invasions. *Trends Ecol Evol* 22, 454–464.

Roman, J. and PALUMBI, S. R. (2004). A global invader at home: population structure of the green crab, Carcinus maenas, in Europe. *Mol Ecol* 13, 2891–2898.

Rusnak, F. and Mertz, P. (2000). Calcineurin: form and function. *Physiol Rev* 80, 1483–1521.

Satoh, K., Godo, S., Saito, H., Enkhjargal, B. and Shimokawa, H. (2014). Dual roles of vascular-derived reactive oxygen species--with a special reference to hydrogen peroxide and cyclophilin A. *J Mol Cell Cardiol* 73, 50–56.

Satoh, K., Nigro, P., Matoba, T., O'Dell, M. R., Cui, Z., Shi, X., Mohan, A., Yan, C., Abe, J.-I., Illig, K. A., et al. (2009). Cyclophilin A enhances vascular oxidative stress and the development of angiotensin II-induced aortic aneurysms. *Nat Med* 15, 649–656.

Savigny, P., Evans, J. and McGrath, K. M. (2007). Cell membrane structures during exocytosis. *Endocrinology* 148, 3863–3874.

Skinner, D. M. (1962). The structure and metabolism of a crustacean integumentary tissue during a molt cycle. *Biol Bull* 123, 635.

Skinner, D. M. (1966). Breakdown and reformation of somatic muscle during the molt cycle of the land crab, Gecarcinus lateralis. *Journal of Experimental Zoology*.

Skinner, D. M. (1985a). Interacting factors in the control of the crustacean molt cycle. *Amer. Zool.*

Skinner, D. M. (1985b). Molting and regeneration. *The biology of Crustacea*.

Skinner, D. M. and Graham, D. E. (1972). Loss of limbs as a stimulus to ecdysis in Brachyura (true crabs). *Biol Bull*.

Smagghe, G. (2009). *Ecdysone: Structures and Functions*. (ed. Smagghe, G. Dordrecht: Springer.

Spees, J. L., Chang, S. A., Mykles, D. L., Snyder, M. J. and Chang, E. S. (2003). Molt cycle-dependent molecular chaperone and polyubiquitin gene expression in lobster. *Cell Stress Chaperones* 8, 258–264.

Spindler, K.-D., Hönl, C., Tremmel, C., Braun, S., Ruff, H. and Spindler-Barth, M. (2009). Ecdysteroid hormone action. *Cell. Mol. Life Sci.* 66, 3837–3850.

Steinmann, B., Bruckner, P. and Superti-Furga, A. (1991). Cyclosporin A slows collagen triple-helix formation in vivo: indirect evidence for a physiologic role of peptidyl-prolyl cis-trans-isomerase. *J. Biol. Chem.* 266, 1299–1303.

Sugumaran, M. (1991). Molecular mechanisms for mammalian melanogenesis:Comparison with insect cuticular sclerotization 1 1 Presented at the International Workshop on Melanogenesis — Its Chemistry as a Therapeutic Strategy in Melanoma held at Paterson Institute in Manchester, England during March 17–20, 1991. *FEBS Letters* 295, 233–239.

Suzuki, J., Jin, Z.-G., Meoli, D. F., Matoba, T. and Berk, B. C. (2006). Cyclophilin A is secreted by a vesicular pathway in vascular smooth muscle cells. *Circ Res* 98, 811–817.

Tepolt, C. K., Darling, J. A., Bagley, M. J., Geller, J. B., Blum, M. J. and Grosholz, E. D. (2009). European green crabs (Carcinus maenas) in the northeastern Pacific: genetic evidence for high population connectivity and current-mediated expansion from a single introduced source population. *Diversity and Distributions* 15, 997–1009.

Terwilliger, N. B. and Ryan, M. C. (2006). Functional and Phylogenetic Analyses of Phenoloxidases from Brachyuran (Cancer magister) and Branchiopod (Artemia franciscana, Triops longicaudatus) Crustaceans. *Biol Bull* 210, 38–50.

Terwilliger, N. B. N., Dangott, L. L. and Ryan, M. M. (1999). Cryptocyanin, a crustacean molting protein: evolutionary link with arthropod hemocyanins and insect hexamerins. *Proc Natl Acad Sci U S A* 96, 2013–2018.

Terwilliger, N. B., Ryan, M. C. and Towle, D. (2005). Evolution of novel functions: cryptocyanin helps build new exoskeleton in Cancer magister. *Journal of Experimental Biology* 208, 2467–2474.

Thongboonkerd, V., Klein, E. and Klein, J. B. (2004). Sample preparation for 2-D proteomic analysis. *Contrib Nephrol* 141, 11–24.

Todd, P. A., Briers, R. A., Ladle, R. J. and Middleton, F. (2005). Phenotype-environment matching in the shore crab (Carcinus maenas). *Marine Biology* 148, 1357–1367.

Tomanek, L. (2011). Environmental Proteomics: Changes in the Proteome of Marine Organisms in Response to Environmental Stress, Pollutants, Infection, Symbiosis, and Development. *Annu. Rev. Marine. Sci.* 3, 373–399.

Tomanek, L. and Zuzow, M. J. (2010). The proteomic response of the mussel congeners Mytilus galloprovincialis and M. trossulus to acute heat stress: implications for thermal tolerance limits and metabolic costs of thermal stress. *J. Exp. Biol.* 213, 3559–3574.

Tovar-Méndez, A., Matamoros, M. A., Bustos-Sanmamed, P., Dietz, K.-J., Cejudo, F. J., Rouhier, N., Sato, S., Tabata, S. and Becana, M. (2011). Peroxiredoxins and NADPH-dependent thioredoxin systems in the model legume Lotus japonicus. *Plant Physiol* 156, 1535–1547.

Trendelenburg, A. U., Meyer, A., Rohner, D., Boyle, J., Hatakeyama, S. and Glass, D. J. (2009). Myostatin reduces Akt/TORC1/p70S6K signaling, inhibiting myoblast differentiation and myotube size. *Am J Physiol Cell Physiol* 296, C1258–C1270.

Ueno, M., Bidmon, H. J. and Stumpf, W. E. (1992). Ecdysteroid binding sites in gastrolith forming tissue and stomach during the molting cycle of crayfishProcambarus clarkii. *Histochemistry* 98, 1–6.

Uzogara, S. G. (2000). The impact of genetic modification of human foods in the 21st century: a review. *Biotechnol Adv* 18, 179–206.

VanHook, A. M. and Patel, N. H. (2008). Crustaceans. *Curr Biol* 18, R547–R550.

Vertical migration and selective tidal stream transport in the megalopa of the crab Carcinus maenas (1998). *Developments in Hydrobiology* 132 137–149.

Walton, W. C., MacKinnon, C., Rodriguez, L. F., Proctor, C. and Ruiz, G. M. (2002). Effect of an invasive crab upon a marine fishery: green crab,Carcinus maenas, predation upon a venerid clam,Katelysia scalarina, in Tasmania (Australia). *Journal of Experimental Marine Biology and Ecology* 272, 171–189.

Wang, W., Scali, M., Vignani, R., Spadafora, A., Sensi, E., Mazzuca, S. and Cresti, M. (2003). Protein extraction for two-dimensional electrophoresis from olive leaf, a plant tissue containing high levels of interfering compounds. *Electrophoresis* 24, 2369–2375.

Wang, Y. H. and LeBlanc, G. A. (2009). Interactions of methyl farnesoate and related compounds with a crustacean retinoid X receptor. *Molecular and Cellular Endocrinology* 309, 109–116.

Watson, J. D. and Crick, F. H. C. (1953). Molecular Structure of Nucleic Acids: A Structure for Deoxyribose Nucleic Acid. *Nature* 171, 737–738.

Weaver, W. (1970). Molecular biology: origin of the term. *Science* 170, 581–582.

Yamada, S. B. and Gillespie, G. E. (2008). Will the European green crab (Carcinus maenas) persist in the Pacific Northwest? *ICES Journal of Marine Science* 65, 725–729.

Yamada, S. B., Dumbauld, B. R., Kalin, A., Hunt, C. E., Figlar-Barnes, R. and Randall, A. (2005). Growth and persistence of a recent invader Carcinus maenas in estuaries of the northeastern Pacific. *Biol Invasions* 7, 309–321.

Yates, J. R., Ruse, C. I. and Nakorchevsky, A. (2009). Proteomics by mass spectrometry: approaches, advances, and applications. *Annu Rev Biomed Eng* 11, 49–79.

Yu, X., Chang, E. S., & Mykles, D. L. (2002). Characterization of limb autotomy factor-proecdysis (LAF(pro)), isolated from limb regenerates, that suspends molting in the land crab Gecarcinus lateralis. *The Biological Bulletin* 202(3), 204–212.

Zoncu, R., Efeyan, A. and Sabatini, D. M. (2011). mTOR: from growth signal integration to cancer, diabetes and ageing. *Nat Rev Mol Cell Biol* 12, 21–35.

Appendix A. All significant detected proteins.